EVALUATION OF THE EFFECTIVENESS OF ALKALINE-EARTH METAL OXIDES IN INHIBITING VANADIUM-INDUCED HOT CORROSION OF YTTRIA-STABILIZED ZIRCONIA THERMAL BARRIER COATINGS (TBCs)

BY

GBADAMOSI ALIYU ARISEKOLA

A Thesis Presented to the
DEANSHIP OF GRADUATE STUDIES

KING FAHD UNIVERSITY OF PETROLEUM & MINERALS
DHAHRAN, SAUDI ARABIA

In Partial Fulfillment of the
Requirements for the Degree of

MASTER OF SCIENCE

In

MECHANICAL ENGINEERING

December, 2013

KING FAHD UNIVERSITY OF PETROLEUM & MINERALS

DHAHRAN 31261, SAUDI ARABIA

DEANSHIP OF GRADUATE STUDIES

This thesis, written by Gbadamosi, Aliyu Arisekola under the direction of his thesis advisor and approved by his thesis committee, has been presented to and accepted by the Dean of Graduate Studies, in partial fulfillment of the requirements for the degree of **MASTER OF SCIENCE in MECHANICAL ENGINEERING**

Thesis Committee

Dr Zuhair M. Gasem (Advisor)

Prof. A.F.M. Arif (Member)

Dr. S.S. Akhtar (Member)

Dr. Zuhair M. Gasem

Department Chairman

Dr. Salam A. Zummo

Dean of Graduate Studies

6/1/14

Date

DEDICATED

TO MY BELOVED PARENTS,

GRANDPARENTS, WIFE,

SIBLINGS AND MY EXTENDED

FAMILY

ACKNOWLEDGEMENTS

All praise to Almighty Allah for his mercy upon us and guiding us towards the right path. My immense appreciation goes to my mother; Mrs. M.I. Gbadamosi for her support. My siblings, Abimbola, Afolake and Abisola have also been wonderful in their support guiding me since cradle. My wife; Mrs. Bilikis Gbadamosi level of support cannot also be quantified. I also extend my gratitude to my friends, in-laws, immediate and extended families for their support. May Allah also blessed the soul of my Daddy, Mr. S.A. Gbadamosi, my granny; Mama Halimatu Busari and all the dead ones who have also contributed positively in one way or the other to my growing up before their demise.

My appreciation also goes to my thesis advisor, Dr. Zuhair M. Gasem for taking out of his tight schedule time to contribute immensely to my success in the MSc. programme. Likewise my thesis committee members, Prof. A.F.M. Arif and Dr. S.S. Akhtar contribution is unquantifiable. My appreciation also goes to Dr. Khaled Alathel and Dr. Jafar Albinmousa who also contributed to the success of my research work.

Words can't also quantify the contribution of Nigeria community, African and Asian communities in KFUPM; and also my friend in all walks of life.

Thank you all. Allah will bless you abundantly.

TABLE OF CONTENTS

LIST OF FIGURES

LIST OF TABLES

THESIS ABSTRACT (ENGLISH)

NAME: **GBADAMOSI ALIYU ARISEKOLA**

TITLE: **Evaluation of the Effectiveness of Alkaline-earth metal oxides in Inhibiting Vanadium-induced Hot Corrosion of Yttria-stabilized Zirconia Thermal Barrier Coatings (TBCs)**

MAJOR FIELD: MECHANICAL ENGINEERING

DATE: **December, 2013**

Vanadium-induced hot corrosion is an accelerated high temperature corrosion of yttria stabilized zirconia (YSZ) ceramic topcoat in Thermal Barrier Coatings (TBCs) of gas turbine engines. It occurs due to YSZ interaction with fused vanadium salt that results from the usage of fuel contaminated with vanadium. The hot corrosion causes spallation and degradation of the topcoat due to reaction of yttria stabilizer (Y_2O_3) with the vanadium salt based on Lewis-acid mechanism and presence of molten acidic salts; and transformation of the yttria stabilized zirconia from tetragonal zirconia phase to monoclinic.

The use of alkaline earth-metal oxides (MgO and CaO) to inhibit vanadium-induced hot corrosion of YSZ has been investigated experimentally using powder and as-sprayed samples. Samples with alkaline-metal/vanadium-oxide molar concentrations of 1, 2, 3 and 5 were subjected to 900^{o}C isothermal heating for up to 100hrs and subsequent cooling in laboratory air.

Characterizations by colour spectrum, XRD, SEM, EDS and X-ray mapping analyses were carried out to estimate the phase distribution. Samples with low molar concentrations of 1 and 2 indicated degradation and destabilization of the 8YSZ within short period of heating while those with high molar concentration ratios showed inhibition effect of vanadium-induced hot corrosion. CaO showed better inhibition when compared to MgO of the same molar concentration to V_2O_5. Samples with MgO/V_2O_5=5, CaO/V_2O_5=3 and CaO/V_2O_5=5 molar concentrations displayed high inhibition efficiencies. The mechanism of inhibition is found to be consistent with Lewis-acid mechanism.

Master of Science Degree

King Fahd University of Petroleum and Minerals

Dhahran, Saudi-Arabia

December, 2013

THESIS ABSTRACT (ARABIC)

ملخص الرسالة

الاسم: عليو اريسكولا جباداموسى

عنوان الرسالة :تقييم فاعلية اكاسييد المعادن الارضية القلوية فى تثبيط التاكل للطلاء المقاوم للحرارة المصنع من الزركونيا المستقر بالياتيريا

المجال الرئيسى :الهندسة الميكانيكية

تاريخ الدرجة: سبتمبر 2013

التاكل المستحث بالفاناديوم يعجل التاكل (عندرجات الحرارة العالية) لطلاء السيراميك المصنع من الزركونيا المستقر بالياتيريا للطلاء المقاوم للحرارة فى تربينات المحركات الغازية.

وهذا يحدث نتيجة الى تداخل الزركونيا المستقر بالياتيريا مع مصهوراملاح الفاناديوم الناتجة عن استخدام وقود يحتوى على الفاناديوم . يسبب التاكل انفصال وتدهور الطلاء العلوى ويرجع ذلك الى تفاعل اكسيد الياتيريا مع املاح الفاناديوم والقائم على الية حمض لويز ووجود مصهور املاح الاحماض : وتحول الزركونيا المستقر بالياتيريا من الزركونيا رباعى البلورة الى الزركونيا احادى البلورة.

تم دراسة استخدام الاكاسييد المعادن الارضية القلوية (اكسيد الماجنييزيوم واكسيد الكالسيوم) لتثبيط التاكل المحث بالفاناديوم للزركونيا المستقر بالياتيريا معمليا باستخدام البودرة كعينات منتشرة . العينات مع معادن قلوية/اكسيد الفاناديوم بتركيزات

1و2و3و4و5 مول تم تعريضها لحرارة 900 مئوية لمدة مائة ساعة ثم تم التبريد فى الهواء داخل المعمل . تم عمل توصيف باستخدام طيف الوان واشعة اكس المجهر الالكترونى و تحليل العناصر لحساب توزيع الاطوار .

اظهرت العينات ذات التركيز المولى الاقل 1و2 تاكل و عدم استقرار الزركونيا المستقر بالياتيريا خلال مدة زمنية قصيرة من التسخين . بينما العينات ذات التركيز المولارى العالى اظهرت تثبيط جيد للتاكل المستحث بالفاناديوم . ايضا اظهرت النتائج ان اكسيد الكالسيوم له تثبيط جيد مقارنة باكسيد الماجنيزيوم لنفس التركيز من اكسيد الفاناديوم . اظهرت نتائج العينات بتركيز مولى(اكسيد الماحنسيوم للاكسيد الفاناديوم)بنسبة 5 ونسية اكسيد الكالسيوم للاكسيد الفاناديوم بنسبة 3 والكسيد الكالسيوم للاكسيد الفاناديوم بنسبة 5 اظهرت كفائة تثبيط عالية . وتم التوصل الى ان الية التثبيط متوافقة مع الية حمض لويس.

درجة الماجستير فى العلوم

جامعة الملك فهد للبترول والمعادن

الظهران , المملكة العربية السعودية

ديسمبر 2013

CHAPTER 1

INTRODUCTION

1.1 Coatings

Coatings are defined as any protective films applied to the surface of a material. McGraw-Hill Dictionary of Scientific and Technical dictionary defines coatings as thin films of material bonded to metals in order to add specific surface properties, such as corrosion or oxidation resistance, color, attractive appearance, wear resistance, optical properties, electrical resistance and thermal protection. It can be inferred from various definitions, that coatings are used to improve the aesthetic, impermeability, wetability and adhesion properties of a substrate. It also improves corrosion, wear and scratch resistance of a substrate. A substrate is a parent or base material that is designed for a particular function in a system on which surface a coating is applied. Coatings are majorly used for protecting the substrate to elongate its life span.

1.2 Types of Coatings

Coatings are classified into various groups based on the following criteria, which includes operating temperature of the system, mechanism of coating deposition and coating materials etc.

(i). Temperature of the System

Birks et al. [1] classified coatings into ambient temperature coatings and high temperature coatings. Ambient temperature coatings include paints for car corrosion protection and those for jewelry aesthetic appearance; they are specifically for systems operating within room

temperature. High temperature coatings include diffusion coatings, overlay coatings and thermal barrier coatings (TBCs) that are used in systems operating at high temperature.

(ii). Method of Coatings

Coatings are classified as overlay or diffusion coatings based on their bonding interaction with the substrate. Overlay coatings are those that are deposited on the substrate while diffusion coatings are those which diffuse into the substrate forming chemical bonds [1, 2]. Diffusion coatings diffuse into the substrate during deposition to form part of the substrate. It includes aluminide, chromized and silicide coatings obtained from elements of aluminum, chromium and silicon, respectively. The major disadvantage of diffusion coatings is the limitation in elements that can be used as diffusion coatings. However overlay coatings give better versatility in the number of elements that can be part of the coatings. It does not form bond with the substrate but forms a layer on top of the substrate. It is often an alloy of metals and includes Ni-Cr-Al and Co-Cr-Al base coating alloys.

(iii). Coating Materials

Roberge [3] classified coatings into three general types namely organic, metallic and inorganic coatings based on the coating material. Figure 1.1 shows various types of coatings based on their parent material composition.

(iv). Coating Applications

Coatings are also classified based on purpose of application on a substrate. Aesthetic coatings are used for aesthetic purpose like improving the facial appearance of the substrate by making it more appealing and beautiful. It includes coatings for jewelries and enameling for ceramics.

Paints for automobiles and buildings can also be classified as aesthetic coatings. Wear, corrosion and scratch coatings are the major applications of coatings; such coatings protect the substrate from the effects of wear, scratch and corrosion. It includes TBCs in hot section of gas turbine engines and boilers, galvanize steel, paints in automobiles and marines

Other applications of coatings are fire proof, water proof, anti-foulings and sound proof applications.

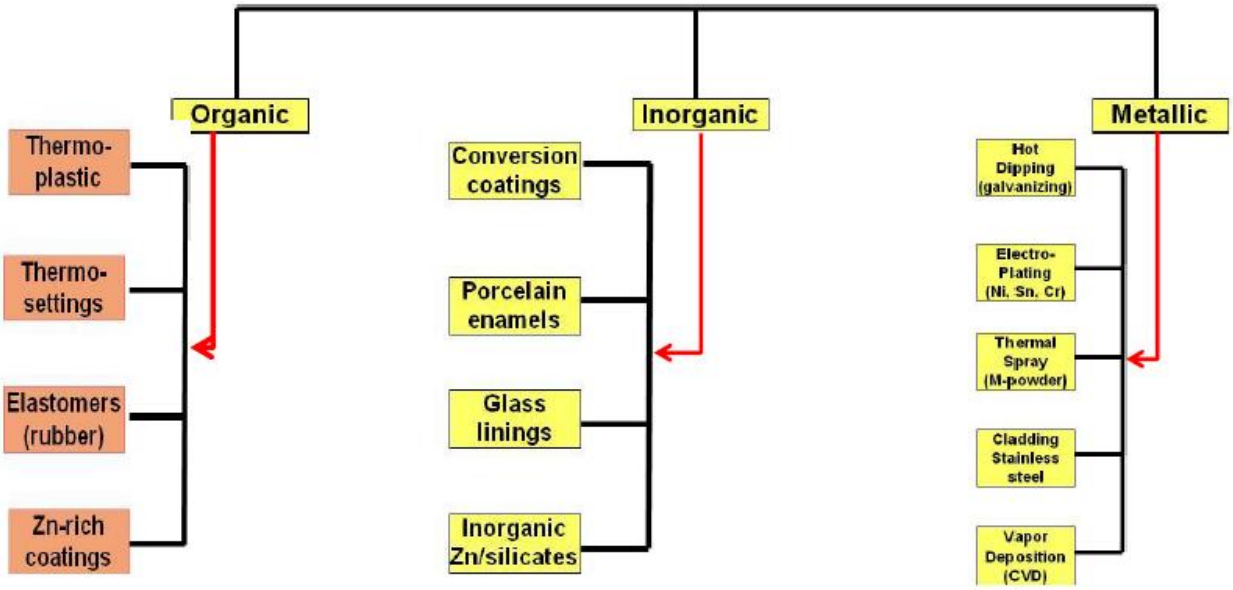

Figure 1.1: Types of Coatings [4]

1.3 Thermal Barrier Coatings (TBCs)

Thermal barrier coatings (TBCs) are protective coatings for thermal insulation in high temperature applications [1, 2] because TBCs can achieve temperature gradient reduction of between 150^{o}C to 175^{o}C across the coating [1, 5]. TBCs find applications in gas turbine engine blades, vanes, seals and combustor chambers of aircraft, marines and land base power generation plants; and in boilers [1, 5-7]. Engine components in high temperature applications e.g. gas

turbines engines and boilers, are mostly made from metal alloys that have temperature limits. Aside the metal alloys temperature limits, engines are also subjected to higher operating temperature due to required high efficiency; this necessitates the use of thermal barrier coatings to protect these metal alloy substrates. A good example is the gas turbine engine blades that are made from nickel based alloys which are designed for strength but have high temperature limits. The TBCs in conjunction with internal air cooling provide an optimum operating temperature for nickel based alloy blades in gas turbine engines as shown in Fig. 1.2 [1, 6, 7]. TBCs consist of a ceramic topcoat and metal alloy bondcoat [1, 2, 5, 8]. The ceramic topcoat provides the insulative protection for the substrate [1, 2, 7, 8]. Although historically the earlier forms of ceramic topcoats in TBCs were alumina, calcium oxide stabilized zirconia and magnesium oxide stabilized zirconia [1], insulative ceramic topcoat presently used in TBCs is yttria stabilized zirconia (YSZ) [1, 5, 9, 10]. Zirconia compound constitute larger composition of the present generation of ceramic topcoat used in TBCs due to high thermal coefficient of expansion comparable to substrate metal alloys and low thermal conductivity properties which made it an ideal ceramic topcoat material [2, 11]. The property of zirconia also includes its existence in different crystal structures, at room temperature as monoclinic and at higher temperature as tetragonal and cubic zirconia [7]. The existence of different phase of zirconia makes it undergo phase transformation phenomenon when temperature changes from high to room temperature and vice versa. The most commonly referenced transformation of zirconia compounds is that of transforming from the tetragonal phase to monoclinic phase which is accompanied with 3-5% increase in volume of the zirconia compound [11]. Yttria (Y_2O_3) like other oxides is used to stabilize the zirconia compound to hinder this transformation with temperature variation; in which 7-8 wt.% yttria has been proven as an ideal stabilizer for tetragonal zirconia in TBCs [1, 5,

7, 9, 10]. Fig.1.3 shows the phase diagram of ZrO_2 and Y_2O_3. The bondcoat which is either cobalt or nickel based alloys; MCrAlY, (M=Ni, Co) protects the substrate from high temperature oxidation by forming a thermally grown oxide (TGO) layer of Al_2O_3 [1, 2, 7, 8]. Al_2O_3 is a known stable oxide at high temperature; the bondcoat also provides a good adherence of the ceramic topcoat with the substrate [1, 2, 12].

1.4 Methods of TBCs Deposition

There are two major methods of depositing YSZ-TBCs on the substrate. Bondcoat and ceramic topcoat are deposited by either air plasma spray (APS) or electron beam physical vapour deposition (EB-PVD) [1, 2, 7, 8, 13]. APS has been seen as a simple technique and it gives the ceramic topcoat a splat-like structure with high porosity. EB-PVD unlike APS produces a columnar structures [1, 13]. EB-PVD topcoat has smoother surface finish, longer thermal cycle lifetime, better surface finish retention and superior erosion resistance when compared to APS topcoat. Fig. 1.4 shows YSZ ceramic topcoat deposited by APS and EB-PVD methods.

1.5 Hot Corrosion

Hot corrosion is defined as an accelerated high temperature corrosion caused by reaction of corrosive molten salts of sodium (Na), vanadium (V), sulphur (S) and phosphorus (P) at high temperature with metal alloys and ceramics [14]. Hot corrosion in TBCs is associated with the use of low grade fuels, that contain contaminant elements of vanadium (V), sodium (Na), sulphur (S) and phosphorus (P) [8, 9, 15-18]. Low grades of marine distillate fuels are allowed up to 0.05 weight percent ash which contains appreciable amounts of 17 wt % sodium, up to 2 wt.% sulfur and up to 100 ppm vanadium [19]. Table 1.1 also shows the composition of a 310CST utilities type of low grade fuel from ARAMCO with 200ppm vanadium composition. However despite

the impending danger of hot corrosion; there has been increase in the use of low grade fuels to power gas turbine due to its relative availability and low cost. This is buttress by facts like, the present crude oil world reserve indicates that only about 25% is low vanadium crude oil and there is tendency that vanadium-free fuels will become increasing expensive in the future [20]. Gasem and Khalid [8] also reported increase in inclination in the use of low grade fuels to power land base gas turbine in Saudi-Arabia due to its readily availability and relatively lower cost. The use of low grade fuels to power gas turbines makes it prone to hot corrosion from molten salts formed from the contaminants.

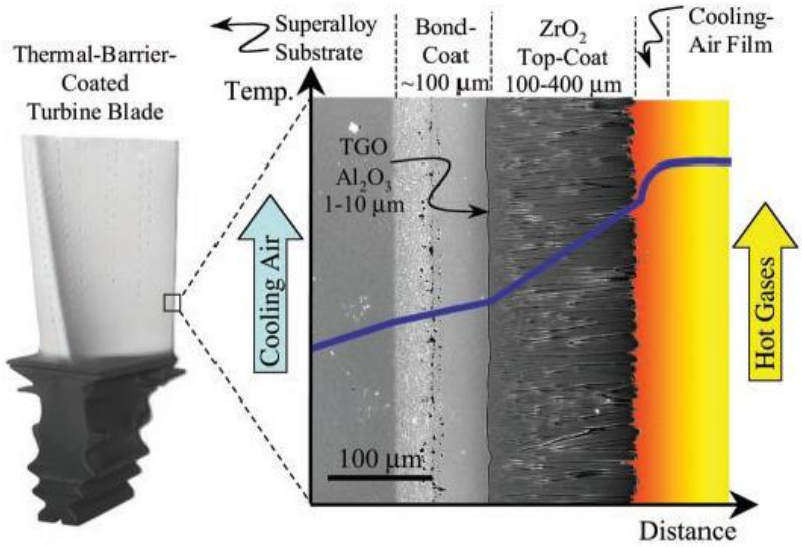

Figure 1.2: Thermal Barrier Coatings [7]

The combustion of these contaminants produce molten salts of V_2O_5, NaCl, Na_2SO_4 and P_2O_5 that initiate and cause hot corrosion of the TBCs [8]. The 8YSZ ceramic topcoat and alloy bondcoat are subjected to degradation due to hot corrosion from these molten salts. The extent of hot corrosion degradation depends on the type of molten salt formed by fuel contaminants

present, operating temperature, thermal cycle, mass composition of the molten corrosive salt, time and presence of other forms of impurities in the environment [1].

1.5.1 Hot corrosion of 8YSZ in the Presence of P_2O_5 contaminant

Mohan et al. [16] reported the destabilization of an APS 8YSZ on a steel substrate in the presence of P_2O_5 molten salt. The degradation occurs at lower and higher temperature due to the reaction of the contaminant with the zirconia compound forming ZrV_2O_7 as shown in reaction 1.1. Mohan et al. [16] also reported that the hot corrosion mechanism involves the contaminant leaching out the zirconia compound from the stabilized ceramic topcoat. The leaching effect consequentially led to increase in mass composition of the stabilizer in the ceramic topcoat that causes transformation of the zirconia phase, thus degradation occurred.

$$ZrO_2\,(s)\ (\text{in YSZ}) + P_2O_5(l) \longrightarrow ZrP_2O_7(s) + \text{c-}ZrO_2(s)(\text{yttria rich}) \qquad (1.1)$$

1.5.2 Hot corrosion of 8YSZ in the Presence of Na_2SO_4 contaminant

Na_2SO_4 as a contanminant doesn't cause the destabilization of the 8YSZ ceramic topcoat. Mohan et al. [16] reported the stability of the tetragonal zirconia phase of an APS 8YSZ after hot corrosion test at 900^{o}C after 1hr in the presence of Na_2SO_4 molten salt. Hiroshi et al. [21] also reported zero degradation of an APS 8YSZ ceramic topcoat in the presence of Na_2SO_4 +NaCl as contaminants when the ceramic topcoat was subjected to 1273^{o}C isothermal corrosion test after 3hrs.

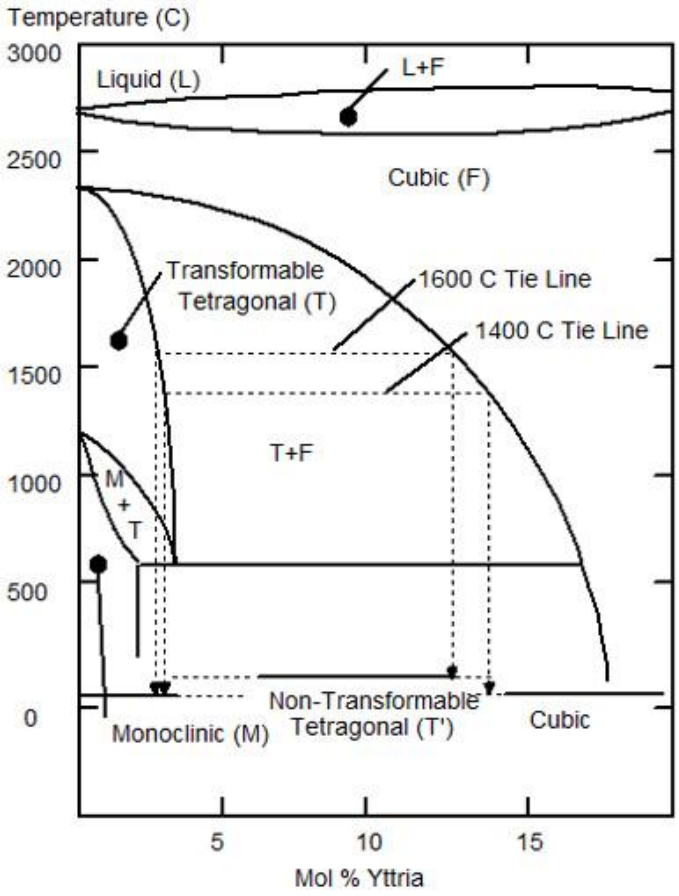

Figure 1.3: ZrO_2-Y_2O_3 phase diagram [22]

1.5.3 Hot corrosion of 8YSZ in the Presence of Na_2SO_4+V_2O_5 contaminants

8YSZ ceramic topcoat however undergoes destabilisation with Na_2SO_4 contanminant in the presence of V_2O_5. The destabilsation of an as-sprayed 8YSZ topcoat was recorded in the presence of 50% Na_2SO_4 + 50% V_2O_5 [16] , 75% wt. Na_2SO_4 + 25% wt. V_2O_5 [8] , 85% V_2O_5+15% Na_2SO_4 and 15% V_2O_5 + 85% Na_2SO_4 [21]. The reason was associated with the formation of acidic sodium vanadate compound from the molten salts as shown in reaction 1.2 and Fig. 1.5. The sodium vanadate which is an acidic compound reacts with the yttria stabilizer and causes transformation of the tetragonal to monoclinc zirconia as depicted in reaction 1.3 [8,

16]. The growth of YVO_4 compound is also seen as part of the hot corrosion products that causes the degradation of the topcoat.

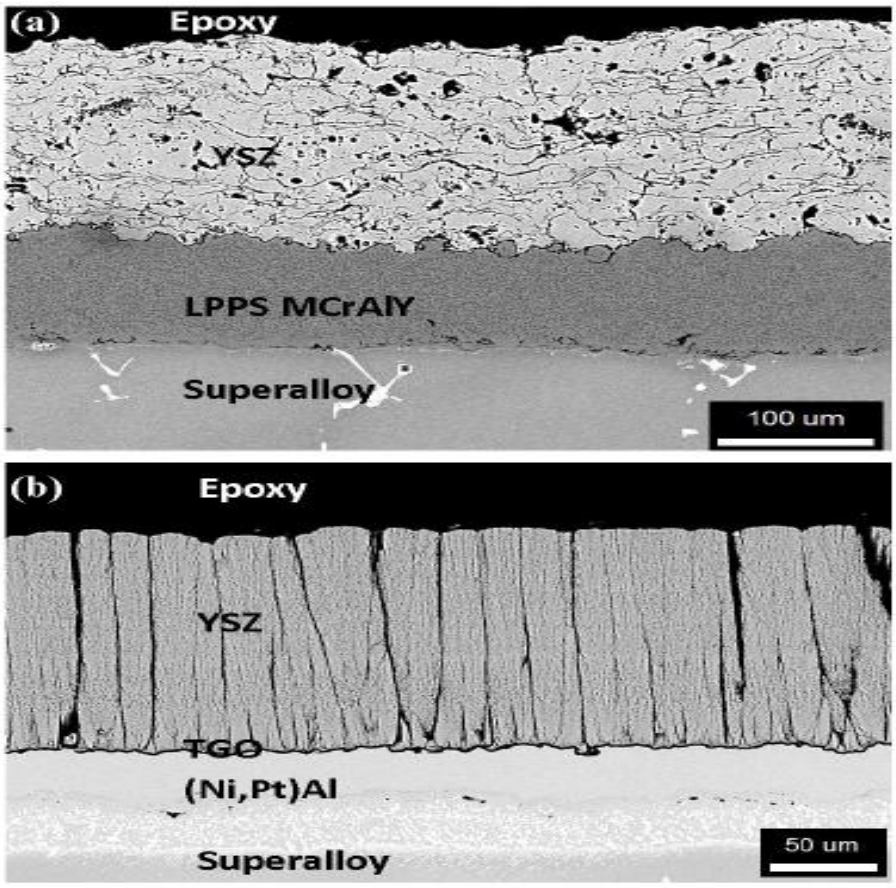

Figure 1.4: SEM micro-structural micrographs. (a) APS YSZ,(b) EB-PVD YSZ [23]

$$Na_2SO_4\ (ss) + V_2O_5\ (ls) \longrightarrow 2NaVO_3 + SO_3 \qquad (1.2)$$

$$t\text{-}ZrO_2\ (Y_2O_3)\ (ss) + 2NaVO_3\ (ls) \longrightarrow YVO_4 + m\text{-}ZrO_2 + Na_2O \qquad (1.3)$$

The formation of the sodium vanadate corrosive salt can also occurs via chemical reaction shown in reaction 1.4.

$$Na_2O\ (base) + V_2O_5\ (acid) \longrightarrow 2NaVO_3 \qquad (1.4)$$

Table 1.1: Utilities fuel oil 310CST product specification [ARAMCO]

TEST	GUARANTEE	METHOD
Aluminum	Less than 5	(Note a,c)
Sodium	Max 20	(Note a)
Nickel	Max 20	(Note a)
Vanadium, ppm	Max 200	(Note a)
Sulphur, wt%	Max 3.7	ASTM D-4294 ASTM D-1552
Ash, wt%	Max 0.10	ASTM D-482
Carbon Residue, wt%	Max 16	ASTM D-189

Yugeswaran et al. [24] in Fig. 1.6 shows XRD analysis of hot corrosion test of a gas tunnel plasma sprayed 8YSZ ceramics topcoat in 40% wt. V_2O_5 + 60% wt. Na_2SO_4 after 5hrs of isothermal heating at 1173K. The XRD analysis showed YVO_4 and transformation of tetragonal to monoclinic zirconia as the hot corrosion products. The degradation mechanism also follows reactions 1.2 and 1.3. Ahmaniemi et al. [25] also reported the same hot corrosion products in the same type of corrosive salt after 200hrs of isothermal heating of an APS 8YSZ at 650^oC.

Habibi et al. [6] reported the destabilization of air plasma sprayed 8YSZ with bondcoat on a nickel alloy substrate at 1050^oC sprayed with 20mg/cm^2 salt solution of V_2O_5 + Na_2SO_4. The degradation occurred via chemical reaction, with formation of YVO_4 due to high mobility of Y^{3+} ion and its reaction with the V ion. Habibi et al. [6] reported that the reaction was accompanied with 3-5% increase in volume of the 8YSZ topcoat due to transformation of the tetragonal zirconia to monoclinic zirconia.

Habibi et al. [6] also reported increase in hot corrosion rate of the 8YSZ in V_2O_5+ Na_2SO_4 with increase in the quantity of the salt deposition in the experiment due to availability of more corrosive salt.

Habibi et al. went further to show the dependence of hot corrosion on thermal cycling in hot corrosion test of 8YSZ at 1050^oC isothermal heating in molten salt of V_2O_5+ Na_2SO_4. Major spallation and destabilization of the 8YSZ ceramic was recorded after 20hrs for 5-4hrs thermal cycle.

An air plasma sprayed 8YSZ indicates cracking at the topcoat/bond coat after 400hrs but excessive spallation in the topcoat after 700hrs at 900^oC isothermal heating when subjected to a molten salts of 75% wt. Na_2SO_4 +25% wt. V_2O_5 purely oxidizing air environment [8]. The growth of YVO_4 and transformation of the zirconia phase were reported as the hot corrosion products that accompanied the degradation.

Unlike others, Hiroshi et al. [21] reported the presence of YVO_4 and $Y_8V_2O_{17}$ as corrosion products of 1273^oC isothermal heating of 8YSZ in 85% wt. V_2O_5 + 15% wt. Na_2SO_4 after 3hrs. The presence of strong concentration of cubic zirconia, medium concentration of tetragonal zirconia and weak presence of monoclinic zirconia were also indicated as corrosion products. Minor attack of the 8YSZ topcoat occurred when the corrosive salt was a mixture of 15% wt. V_2O_5 + 85% wt. Na_2SO_4 after 3hrs [21].

Nakaira et al. [21] monitored the hot corrosion destabilization of the ceramic topcoat with an AE signal. AE signals were generated at beginning of 1273^oC isothermal heating of 8YSZ in molten corrosive salts of pure V_2O_5, 85% wt. V_2O_5+15% wt. Na_2SO_4 and15% wt. V_2O_5+85% wt.

Na_2SO_4 hot corrosion tests. Fig.1.7 shows the AE signals comparison between 8YSZ without corrosive salt, with corrosive salt of 85% wt. V_2O_5+15% wt. Na_2SO_4 and unstabilized zirconia ceramic topcoat. The unstabilized zirconia indicates high AE count due to large destabilization of the zirconia phase and the 8YSZ without corrosive show the least count due to less transformation of the zirconia compound.

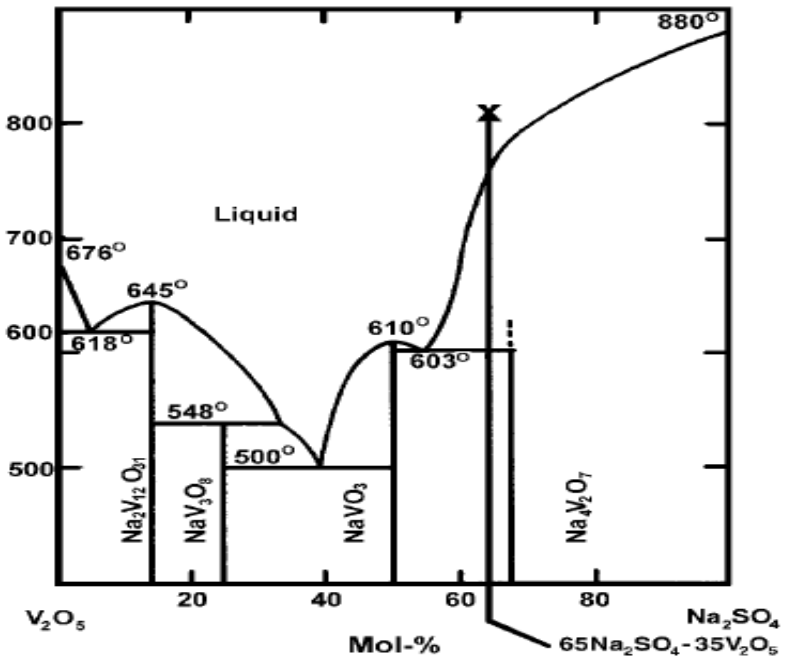

Figure 1.5: V_2O_5-Na_2SO_4 phase diagram [25]

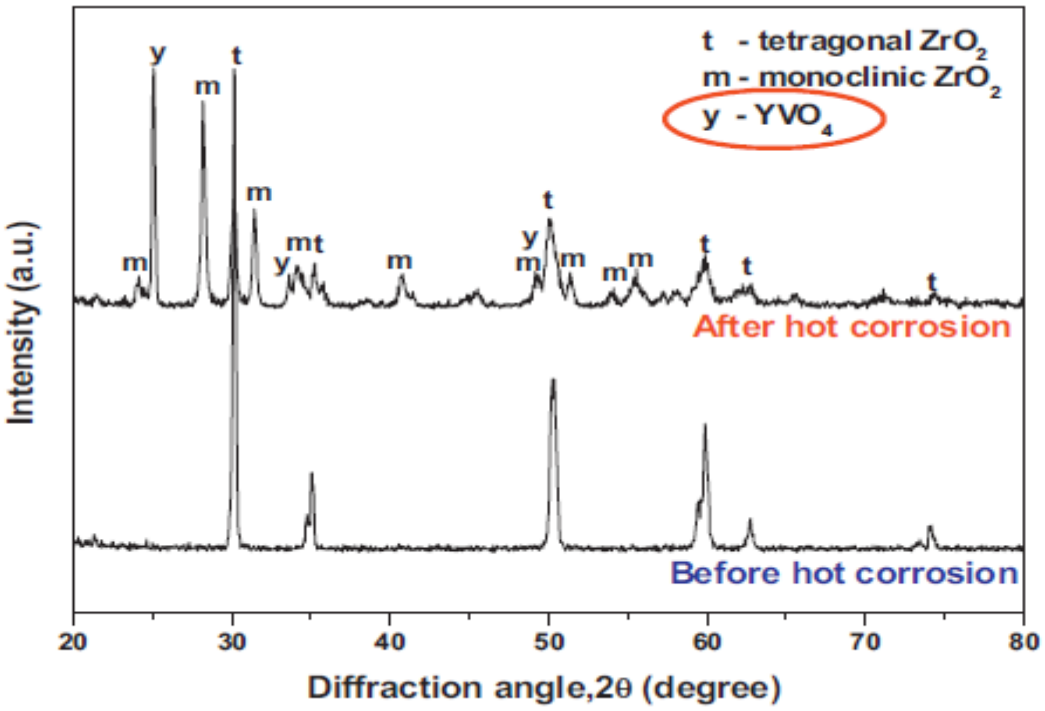

Figure 1.6: Hot corrosion of 8YSZ in the presence of Na_2SO_4+V_2O_5[24]

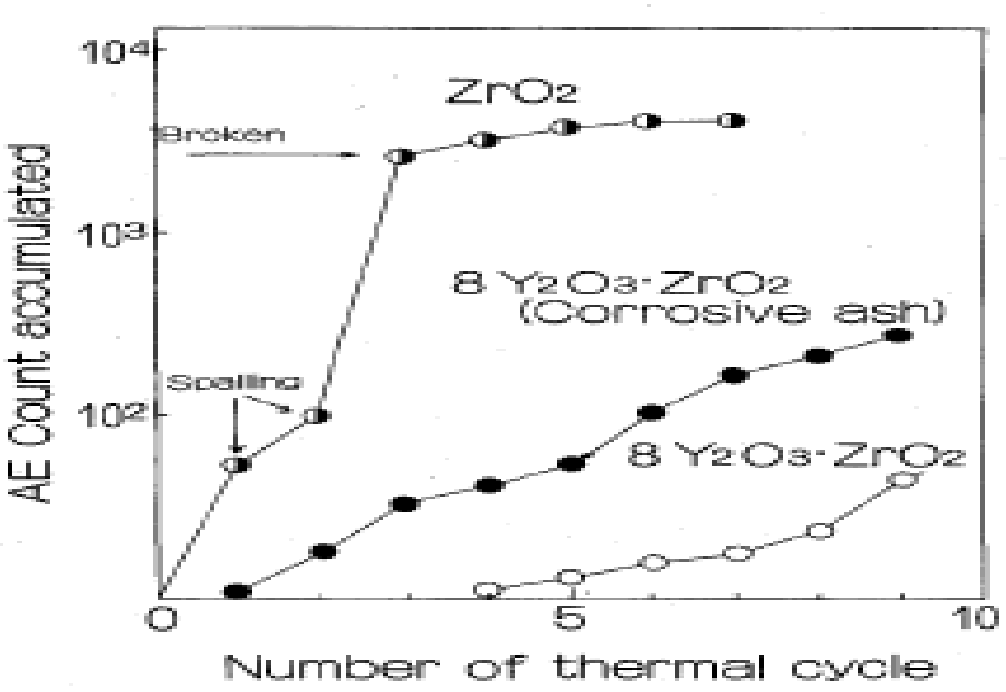

Figure 1.7: AE signal monitoring of destabilization of ceramic topcoat[21]

1.5.4 Hot corrosion of 8YSZ in the presence of V_2O_5 contaminant

Vanadium contaminant in low grade fuels oxidizes to V_2O_5 salt at high temperature that causes vanadium-induced hot corrosion in YSZ-TBCs. V_2O_5 has melting point of 698^oC which makes it to be in molten form at high operating temperature in gas turbine engines. Its presence in molten form in gas turbine expedites its infiltration into the porous ceramic layer TBCs to initiate and cause vanadium-induced hot corrosion. Fig. 1.8 shows the TGA and DSC plots for V_2O_5 showing its melting point. Vanadium-induced hot corrosion of YSZ ceramic topcoat in TBCs occurs via dissolution, chemical reaction and infiltration [11]. The hot corrosion mechanism involves dissolution and chemical reaction in the planar reaction zone (PRZ) which is the top layer of the ceramic topcoat where the molten salt deposits [11]. The mechanism via dissolution-chemical reaction and infiltration occurs in the melt infiltration reaction zone (MIRZ) which is in-depth of the ceramic topcoat [11]. Fig. 1.9 shows various zones in ceramic topcoat of YSZ TBCs.

Likewise stabilized zirconia reaction mechanism due to vanadium-induced hot corrosion occurs via chemical reaction or mineralization depending on the zirconia stabilizing oxide [13]. CeO_2 and In_2O_3 stabilized zirconia ceramic topcoat vanadium-induced hot corrosion occur via mineralization. The hot corrosion products via mineralization mechanism are the stabilizing oxide itself and the monoclinic zirconia phase. Vanadium-induced hot corrosion of YSZ and Sc_2O_3 stabilized zirconia occur via chemical reaction of the stabilizer with the V_2O_5 molten salt. Vanadium-induced hot corrosion via chemical reaction is based on Lewis acid mechanism [10, 20], where there is preferential reaction between strong acid and strong alkaline in presence of other weak acids and bases. In 8YSZ ceramic topcoat, vanadium-induced hot corrosion involves the contaminant V_2O_5; the acid leaching out the Y_2O_3 stabilizer that is of high basicity compared

to the ZrO_2 compound. The leaching of the stabilizer brings forth the transformation of the tetragonal zirconia phase to monoclinic phase and formation of YVO_4 compound. The zirconia phase transformation causes about 3-5% increase in its volume that initiates cracks and spallation of the topcoat. Reaction 1.5 shows the vanadium-induced hot corrosion reaction equation for 8YSZ ceramic topcoat in TBCs.

$$t\text{-}ZrO_2\ (Y_2O_3)\ (ss) + V_2O_5\ (ls) \longrightarrow YVO_4 + m\text{-}ZrO_2 \qquad (1.5)$$

Zun Chen et al. [10] showed that products of vanadium-induced hot corrosion of an APS yttria stabilized zirconia depend on the isothermal heating temperature and time. In-situ XRD monitoring of phase evolution of YSZ topcoat at 700^{o}C and 750^{o}C in the presence of V_2O_5 indicates the presence of ZrV_2O_7 and YVO_4 phases at initial stage of heating. Zun Chen et al. [10] reported the transformation of the ZrV_2O_7 to monoclinic zirconia after some minutes of isothermal heating at these temperatures due to instability nature of the ZrV_2O_7 compound. At 800^{o}C and 900^{o}C, the corrosion products from the beginning of the experiment were the YVO_4 and m-ZrO_2 due to transformation of the t-ZrO_2 [10]. Figure 1.10 shows phase evolution against time at different temperatures for the in-situ XRD monitoring of vanadium-induced corrosion of 7% wt. Y_2O_3-ZrO_2. Reactions 1.6 to 1.8 show the reaction equations and corrosion products of vanadium-induced hot corrosion of the 7% wt. Y_2O_3-ZrO_2 topcoat at different temperatures.

$$t\text{-}ZrO_2\ (Y_2O_3)\ (ss) + V_2O_5\ (ls) \longrightarrow YVO_4 + m\text{-}ZrO_2 \qquad (1.6)$$

$$ZrO_2\ (\text{in } t\text{-}ZrO_2) + V_2O_5\ (\text{liquid}) \longrightarrow ZrV_2O_7 \qquad (1.7)$$

$$Y_2O_3\ (\text{in } t\text{-}ZrO_2) + V_2O_5\ (\text{liquid}) \longrightarrow YVO_4 \qquad (1.8)$$

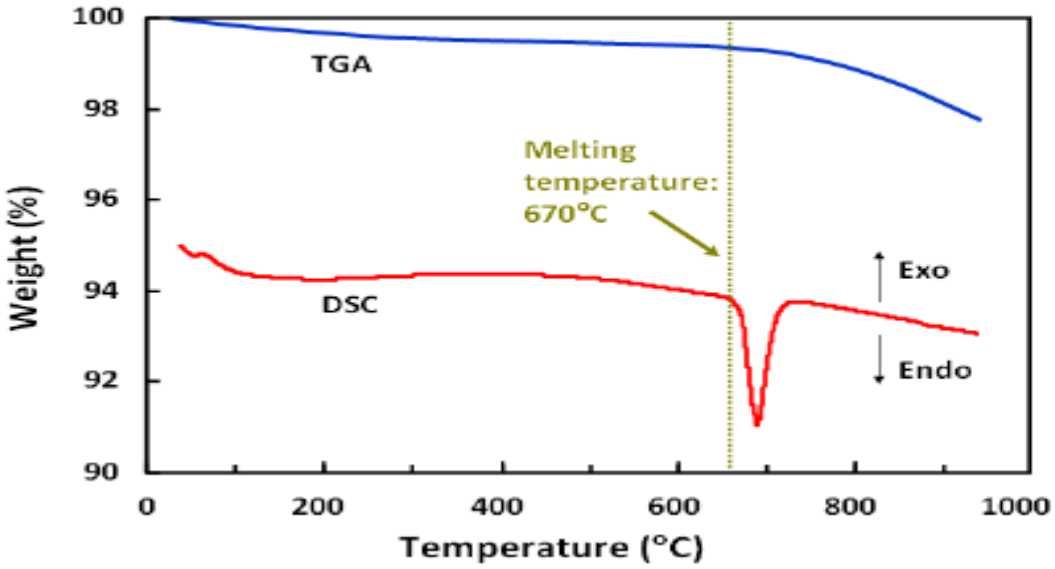

Figure 1.8: TGA and DSC plot for V_2O_5[26]

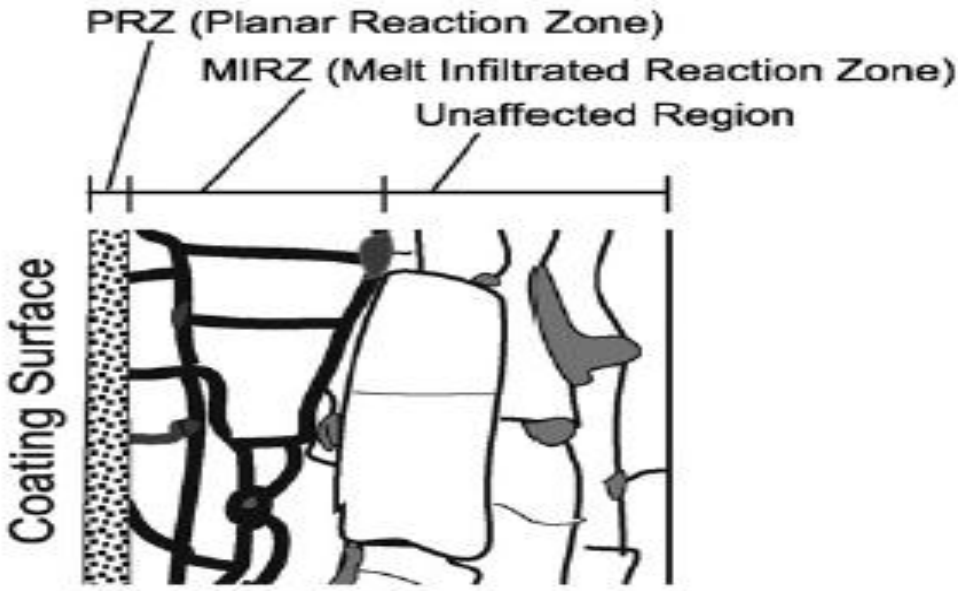

Figure 1.9: Hot corrosion zones in TBCs[11]

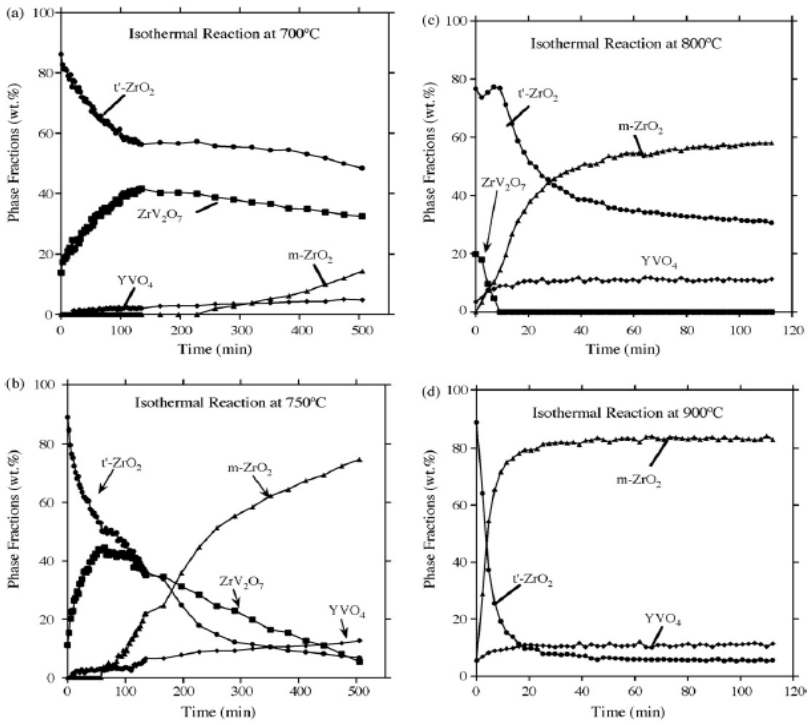

Figure 1.10: Phase evolution versus time plot for vanadium oxide hot corrosion of 7YSZ ceramic topcoat [10]

Nakira et al. [21] like [10] reported the degradation of an APS 8YSZ on a 304 type stainless steel substrate after 3hr-1273^{o}C isothermal heating in V_2O_5. The degradation occurred via growth of YVO_4 and transformation of the zirconia which is a similitude of the destabilization of 7YSZ at intermediate temperature of 900^{o}C reported by [10].

Mohan et al. [16] also validates the fact that products of vanadium-induced hot corrosion of 8YSZ ceramic topcoat are dependent on the temperature. At temperature above 747^{o}C the mechanism of destabilization is the leaching of the stabilizer to form YVO_4 and transformation of the zirconia phase as shown in reaction 1.5. The hot corrosion products below this temperature are mixture of ZrV_2O_7 and t-ZrO_2 as shown in reaction 1.9.

$$ZrO_2\,(\text{in YSZ}) + V_2O_5 \longrightarrow ZrV_2O_7 + \text{t-}ZrO_2\,(\text{YSZ}) \qquad (1.9)$$

The mass composition of V_2O_5 also determines the rate of destabilization of YSZ ceramic topcoat. The rate of evolution of monoclinic zirconia from tetragonal zirconia for an APS 7YSZ sprayed with 1% wt. V_2O_5 is greater when compared to 0.1% wt. V_2O_5 added as corrosive salt [10].

Kondos [27] showed the effect of different concentration of vanadium oxide on the rate of destabilization of 8YSZ using powder samples. Kondos [27] showed that larger concentration of vanadium oxide contaminant hastens the rate of vanadium-induced hot corrosion and produced large destabilization of the ceramic compound. Table 1.2 gives summary of peak intensities of the tetragonal zirconia, monoclinic zirconia and YVO_4 phase with different concentration of V_2O_5.

Table 1.2: Peak Intensities of phases in vanadium induced hot corrosion of 8YSZ powder sample[27]

V_2O_5 %wt	(111) C, Peak (counts)	($\bar{1}$11) M, Peak (counts)	(200) Y, Peak (counts)	Reaction time (hours)
1	11485	643	350	168
3	8878	1591	729	168
5	7044	1949	1262	168
7	2964	5004	1995	168
10	0	6982	2601	100

The ultimate effect of hot corrosion of YSZ topcoat that arises as a result of change in volume of the zirconia compound due to transformation are spallation, cracks and degradation of the ceramic topcoat.

1.6 Reaction of Calcium oxide (CaO) and Magnesium oxide (MgO) with V_2O_5

CaO and MgO are oxides of alkaline earth metals of calcium (Ca) and magnesium (Mg) respectively. Alkaline earth metals occupies group 2 in the period table. Mg occupies period 3 on the periodic table; it has atomic mass and number of 24.305 and 12 respectively. Ca occupies period 4, it has atomic mass and number of 40.078 and 20 respectively. MgO is a white hydroscopic solid with melting point and boiling point of 2852^{o}C and 3600^{o}C respectively. It has a spinel crystal structure and density of 3.58g/cm^3. CaO also referred to as quicklime is also a white hydroscopic solid with melting point and boiling point of 2572^{o}C and 2850^{o}C respectively. It has a density of 3.35g/cm^3. The reactions between the oxides of calcium and magnesium with vanadium oxide give metallic vanadate compounds. The vanadate compounds formed depend on the molar concentration of the reacting oxides and temperature as shown in the phase diagram in Figs. 1.11 and 1.12. High molar concentration of the alkaline oxide reaction with vanadium oxide i.e. 3:1 molar concentration ratio; yields vanadate compounds with high melting point, $Mg_3V_2O_8$ and $Ca_3V_2O_8$ as depicted in the phase diagrams. MgV_2O_6 and CaV_2O_6 are reaction products when lower molar concentration of the alkaline oxides reacts with vanadium oxide. The reaction of intermediate molar concentration of the alkaline oxides produces $Mg_2V_2O_7$ and $Ca_2V_2O_7$ respectively as shown in the phase diagrams.

Clark and Morley [28] carried out an experimental research on solid-to-solid reaction of MgO and V_2O_5 with different molar concentration of MgO. The mixture were heated at 1010^{o}K,

870°K and 770°K for 14hrs in a furnace and characterized with DTA and XRD. Table 1.3 shows various vanadate compounds formed from different molarity combinations of MgO-V_2O_5 solid reaction at 1010°K. The chart indicates the formation of two phases of $Mg_2V_2O_7$, namely alpha-$Mg_2V_2O_7$ and beta-$Mg_2V_2O_7$ which are not mentioned in the MgO-V_2O_5 phase diagram.

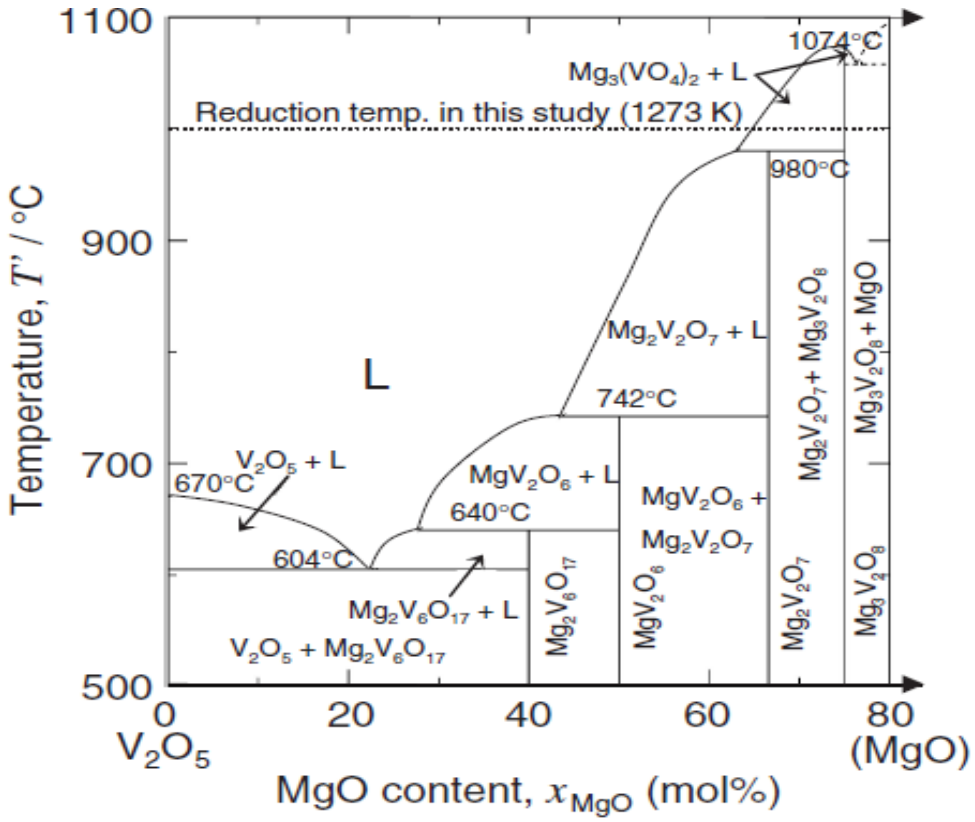

Figure 1.11: MgO-V_2O_5 phase diagram [29]

Said and Wahab [30] reported the formation of $Mg_3V_2O_8$ in the reaction between the products from decomposition of $Mg(OH)_2$ and ammonium metavanadate calcined at 400°C,500°C and 700°C respectively. Said and Wahab [30] reported MgO and V_2O_5 as the initial products formed from the decomposition of the two compound which reacts to give magnesium vanadate compounds as the final product. $Mg_3V_2O_8$ formed when the molar concentration of ammonium

vanadate is between 20% to 30% but MgV_2O_6 formed when the its molar concentration reaches 50% in the reaction.

Miyauchi et al. [29] in the production of vanadium metal by Preform Reduction Process produced $Ca_2V_2O_7$ and $Mg_2V_2O_7$ by mixing slurry mixtures of V_2O_5-CaO and V_2O_5-MgO respectively as initial reaction products. Metal vanadates compound of $CaVO_4$ and $MgVO_4$ were final products from the initial vanadate compounds after reduction with Ca and Mg vapour respectively.

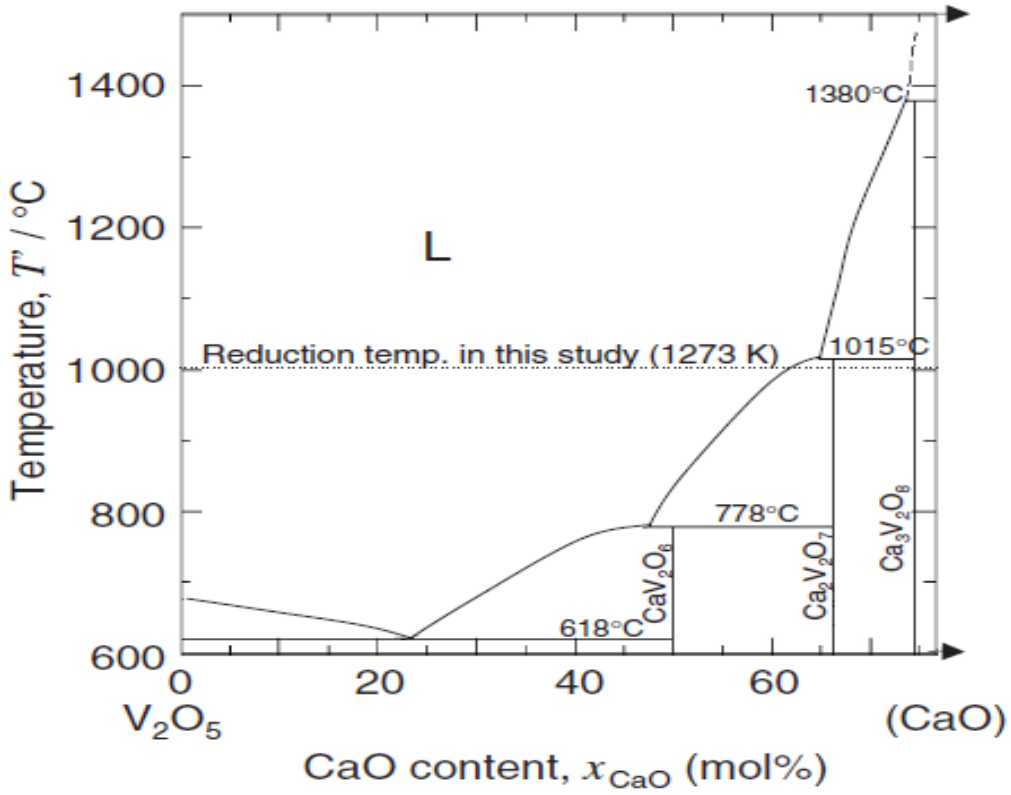

Figure 1.12: CaO-V_2O_5 phase diagram [29]

1.7 Motivation and Objective

1.7.1 Motivation

The motivation for this research arose due to increase in inclination for the use of low grade fuels in land base gas turbine in Saudi Arabia. Low grade fuels are readily available and cheap. Based on the literature reviewed, fuel additives method appeared to be the easiest, less costly and most suitable alternative for inhibiting vanadium-induced hot corrosion in gas turbines. Most literature have worked on fuel additives for inhibiting vanadium-induced hot corrosion in metal alloys with little or none on TBCs. This research is meant to delve into the suitability of using oxide additives in inhibiting vanadium-induced hot corrosion of yttria stabilized zirconia topcoat in TBCs of turbine engines. Most of the methods proposed to inhibit the hot corrosion haven't been hundred percent effective and these methods are complex to incorporate into the TBCs. The use of oxide additives will be the most viable option in inhibiting vanadium-induced hot corrosion of TBCs considering its simplicity and cost. MgO and CaO which are the proposed inhibitors are readily available and cheap; aside this is the simplicity behind the technology of achieving the inhibition goal.

1.7.2 Objective

To evaluate and compare the effectiveness of magnesium oxide (MgO) and calcium oxide (CaO) as additives to inhibit vanadium-induced corrosion of 8YSZ in Thermal Barrier Coatings (TBCs).

Table 1.3: Products Obtained from $MgO-V_2O_5$ solid reaction at 1010^oK [28]

Molar concentration ratio of $MgO:V_2O_5$/Magnesium Vanadate compounds	7:2	3:1	5:2	2:1	3:2	1:1	2:3
$Mg_3V_2O_8$	1	1	1				
α- $Mg_2V_2O_7$							
β- $Mg_2V_2O_7$		3	1	1	1		
MgV_2O_6					1	1	1
MgO	2						
V_2O_5							2

Key to symbols: 1, major constituent; 2, minor constituents (>10%); 3, trace constituents (<10%)

CHAPTER 2

LITERATURE REVIEW

Inhibition of vanadium-induced hot corrosion of 8YSZ ceramic topcoat in TBCs involves different methodologies which are basically aimed at preventing the acid-base reaction and transformation of the stabilized zirconia associated with temperature change. The methods include seeking alternative stabilizers that are less reactive with the vanadium oxide to stabilize the zirconia compound. Methods of preventing infiltration of the molten salts into the ceramic topcoat by sealing mechanism and sacrificial overlay coating have been examined; and the use of alternative ceramic topcoat such as pyrochlores has also been explored. The use of additives for inhibiting vanadium-induced hot corrosion has also been reported extensively for metal alloys at high temperature, though its use for ceramic topcoat has received less attention.

2.1 Alternative Stabilizers for zirconia compound

Vanadium-induced hot corrosion of YSZ topcoat occurs via Lewis acid mechanism, which necessitates the technology of seeking alternate stabilizers that are of less basicity compared to yttria. This is aimed at retarding the acid-zirconia stabilizer reaction thereby hindering the destabilization of zirconia; phase transformation reduces if the leaching of zirconia stabilizer by reaction with V_2O_5 is hindered. CeO_2, Ta_2O_5 and Sc_2O_3 etc. have been found as better alternatives to yttria because they are of lesser basicity. This reduces their affinity and reaction with the acidic vanadate salts, hence hot corrosion of the topcoat is reduced. Some of these alternate stabilized zirconia ceramics are commercially available, while some are not; but their vanadium-induced hot corrosion resistances have been evaluated:

2.1.1Ta_2O_5-stabilized Zirconia

Ta_2O_5 is an oxide of tantalum that has either hexagonal or orthorhombic crystal structure and has a melting point of 1872^oC. The hot corrosion resistant of Ta_2O_5 stabilized zirconia has been quantified by using a tetragonal phase $YTaO_4$-ZrO_2 obtained from 10% mol Y_2O_3 and 10% mol Ta_2O_5; and an orthorhombic Ta_2O_5-ZrO_2 (14TZ) obtained from 14% mol Ta_2O_5 [31]. $YTaO_4$-ZrO_2 like YSZ has low thermal conductivity, better phase stability at elevated temperature, comparable co-efficient of thermal expansion, lower elastic modulus and ability to be deposited by plasma spray, while 14TZ has low thermal conductivity [31].

In pure V_2O_5 environment isothermal heating, at lower and intermediate temperature above the melting point of V_2O_5; 700^oC and 900^oC using powder samples, 14TZ powder showed resistance to hot corrosion. $YTaO_4$-ZrO_2 however under the same condition undergoes degradation due to leaching of yttria and corresponding precipitation of 14TZ rather than mass growth of the monoclinic zirconia [31].

In pure $NaVO_3$ contaminant, under the same experimental conditions $YTaO_4$-ZrO_2 powder undergoes little or minute degradation with weak signal of YVO_4, monoclinic zirconia and $NaTO_3$. This was deduced to reduction in activity and diffusibility of Y^{3+} ion due to presence of Ta^{5+} in the stabilized zirconia. 14TZ in the same contaminant at 700^oC showed resistance to degradation like $YTaO_4$-ZrO_2, but at 900^oC it undergoes destabilization forming monoclinic zirconia and sodium tantalite [31].

The hot corrosion resistance of the two forms of tantalum oxide stabilized zirconia at 700^oC and 900^oC in $NaVO_3$ and V_2O_5 molten salt compared to the YSZ is presented in the Table 2.1. The result indicates the two forms of tantalum stabilized zirconia are more resistant to hot corrosion

to vanadium salts than YSZ, but $YTaO_4$-ZrO_2 is more resistant to $NaVO_3$ out of the two; while is vice versa for resistant to V_2O_5.

Table 2.1: Hot corrosion of YSZ, $YTaO_4$-ZrO_2 and Ta_2O_5-ZrO_2 in $NaVO_3$ and V_2O_5 at 700°C and 900°C isothermal heating [31]

Chemistry	Temperature (°C)	100% $NaVO_3$	100% $NaVO_3$ to 40% $NaVO_3$ + 60% V_2O_5	40% $NaVO_3$ + 60% V_2O_5 to 100% V_2O_5
YSZ	700	X	X	X
	900	X	X	X
20$YTaO_4$SZ	700	√	X	X
	900	√	X	X
14TZ	700	√	√	√
	900	X	√	√

2.1.2 Sc_2O_3- stabilized Zirconia (SSZ)

Scandia (Sc_2O_3) is an amphoteric white solid oxide of scandium with melting point of 2485°C. Scandia has a stable oxidation state of 3+, is the most acidic of the rare earth oxides and 5% scandia is sufficient to stabilize tetragonal zirconia [20]. Thermo gravimetric study of scandia oxide powder reaction at 800°C with molten $NaVO_3$ under SO_3 partial pressure showed it to be a promising hot corrosion resistant zirconia stabilizer. It showed growth of $ScVO_4$ at higher SO_3 partial pressure compared to the growth of YVO_4 with Y_2O_3 at lower partial pressure under the same experimental conditions [32].

In furtherance to this, the reactions of scandia powder with $NaVO_3$ and V_2O_5 at 700°C and 900°C, characterized with XRD show formation of $ScVO_4$ with the two melt at 700°C, but was only evident with V_2O_5 melt at 900°C [20]. The study shows the suitability of scandia as an

alternate stabilizer for zirconia that will be of better resistance than yttria to hot corrosion from fuel impurities of vanadium, sulphur and sodium.

Jones [20] showed the superiority of scandia stabilized zirconia to yttria stabilized zirconia using 5%wt. scandia stabilized zirconia pellet subjected to isothermal heating at lower and intermediate temperature above the melting point of V_2O_5. At 700^oC with thin film of $NaVO_3$; SSZ depicts no transformation of phase present in the as-received pellet sample while YSZ undergoes transformation and YVO_4 evolving from the process under the same test condition [20]. SEM micrograph after 475hrs of 700^oC isothermal heating is shown in Fig. 2.1. It indicates the formation of rod-like structure YVO_4 in YSZ, unlike SSZ that shows no formation of new phases. XRD characterization analysis of SSZ pellet after 160hrs of 900^oC isothermal heating in vapour deposition of $NaVO_3$ is shown in Fig. 2.2 compared with that of YSZ pellet under the same test conditions. The SSZ pellet maintains its structure of SSZ at 900^oC after 160hrs isothermal heating compared to the YSZ pellet which has its yttria leached out to form YVO_4 and has transformed from tetragonal zirconia to monoclinic zirconia as shown in the XRD analysis [20].

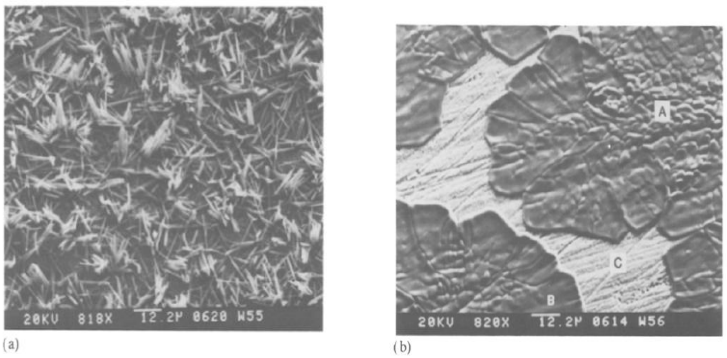

Figure 2.1: SEM micrograph of YSZ and SSZ after 475 hrs isothermal heating at 700^oC. (a) YSZ, (b) SSZ [20]

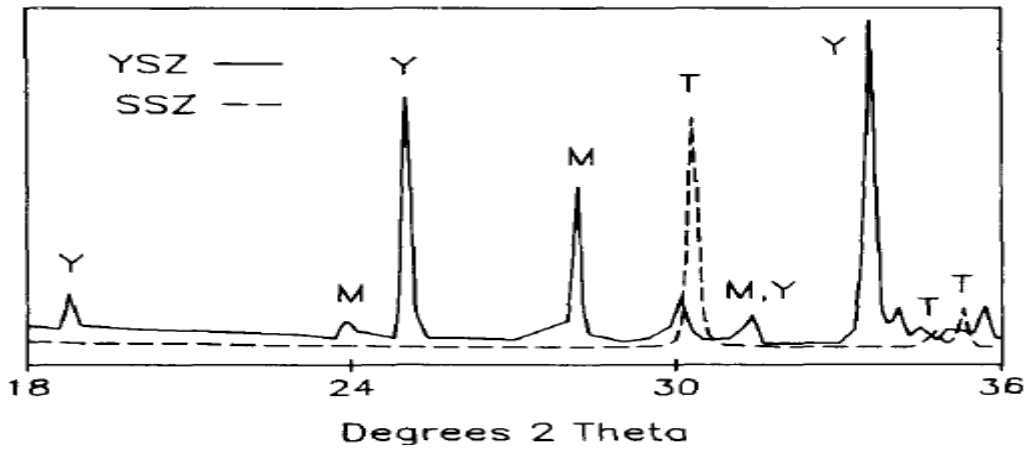

Figure 2.2: XRD analysis of YSZ and SSZ after 160 hrs isothermal heating at 900^{o}C [20]

2.1.3 MgO-stabilized Zirconia (MSZ)

Magnesium oxide stabilized zirconia (MSZ) is one of the earliest insulative ceramic topcoats in TBCs [1]. It is commercially available presently from Sulzer Company. Like YSZ with between 7-8% wt. yttria stabilizer, MgO stabilized zirconia with these compositions have been reported 22%wt. MgO-ZrO_2 [25], 7.6%wt. MgO-ZrO_2 [21] and 15-30%wt. MgO-ZrO_2 (Sulzer Company).

Jones [32] performed thermo gravimetric analysis of MgO as a stabilizer for zirconia at 800^{o}C with molten $NaVO_3$ under SO_3 partial pressure. The result obtained was formation of $MgSO_4$ and $Mg_3V_2O_8$ as weight gain at lower SO_3 partial pressure, which was similar to formation of YVO_4 for Y_2O_3 stabilizer also at lower SO_3 partial pressure. The reaction for MgO and Y_2O_3 occurred at lower partial pressure compare to formation of $ScVO_4$ and $InVO_4$ from Sc_2O_3 and In_2O_3 respectively at higher SO_3 partial pressure under the same experimental conditions. This study portrays MgO as similar to Y_2O_3 when used to stabilize zirconia which was further proven by other hot corrosion researches on magnesium oxide stabilized zirconia.

Jones [13] reported that the reaction equations for degradation of magnesia stabilized zirconia in a burner rig test at 800^{o}C with a fuel doped with various levels of vanadium, phosphorus, sodium, calcium, iron and magnesium etc. follow reactions 2.1 and 2.2.

$$ZrO_2\,(MgO) + SO_3\,(g) \longrightarrow ZrO_2\,(\text{monoclinic}) + MgSO_3 \qquad (2.1)$$

$$ZrO_2\,(MgO) + V_2O_5\,(l) \longrightarrow ZrO_2\,(\text{monoclinic}) + Mg_3V_2O_8 \qquad (2.2)$$

The reaction in equation 2.1 represents the destabilization of the magnesia stabilized zirconia when magnesium is presence in the fuel why that of equation 2.2 represents the reaction occurring when magnesium is absent in the fuel. Like yttria stabilizer, MgO stabilizer was leached out by the vanadium oxide and sulphur oxide contaminant to form magnesium vanadate and magnesium sulphate respectively and is accompanied by phase transformation of the zirconia compound to m-ZrO_2.

Ahaminiemi et al. [25] carried out an experimental test on destabilization resistance of an as sprayed magnesium oxide stabilized zirconia in the presence of 60% Na_2SO_4 + 40% V_2O_5 at 650^{o}C isothermal heating for 200hrs. XRD analysis of the hot corrosion sample indicates large presences of m-ZrO_2 peaks as a result of the transformation of the cubic 22%wt. MgO-ZrO_2 as-spayed specimen.

At higher temperature Nakira et al. [21] reported the attack of APS 7.6MgO-ZrO_2 on a 304 type stainless steel substrate subjected to 1273^{o}C isothermal heating in the presence of vanadium oxide for 3hrs. The specimen showed spallation and cracks after the hot corrosion test.

Although thermgravimetric analysis by Jones [32] indicates similarity between MgO and yttria stabilizer, but the probable superiority of magnesia stabilized zirconia to YSZ in vanadium oxide was presented in the reaction in eq. 2.3 by [13].

$$ZrO_2\ (Y_2O_3) + Mg_3V_2O_8\ (l) \longrightarrow ZrO_2\ (\text{monoclinic}) + MgO + YVO_4 \qquad (2.3)$$

2.1.4 CeO_2-stabilized Zirconia (CSZ)

CeO_2 is an oxide of rare earth metal of cerium. It has a melting point and boiling point of 2400^{o}C and 3500^{o}C respectively. It has a density of 3.75g/cm^3. CSZ is cerium oxide stabilized zirconia, its tetragonal in crystal structure, it has a much lower thermal conductivity and a higher thermal expansion coefficient than YSZ [33]. CSZ is commercial available from Sulzer Company.

Cerium stabilized zirconia has been proven to have better resistant to hot corrosion compare to YSZ. The hot corrosion resistant of ceria-stabilized zirconia was evaluated using CSZ stabilized with 10%, 12.5% and 15% mol of CeO_2 [34]. The test was conducted at 950^{o}C isothermal heating with Na_2SO_4 and a mixture of Na_2SO_4 plus 2% mol of V_2O_5 as the molten salt respectively. Table 2.2 summarizes what was observed after different hours of isothermal heating at 950^{o}C from the XRD characterization of phase that evolved from the test. The result indicates higher transformation of tetragonal zirconia to monoclinic zirconia when 2% mol of V_2O_5 is contained in the molten salt compare to pure Na_2SO_4 and the higher the ceria composition the lower the transformation. It also confirms that ceria stabilized zirconia destabilize in the presence of V_2O_5.

Park et al. [33] investigated hot corrosion resistance of zirconia stabilized with 25% wt. CeO_2 and 2.5% wt.Y_2O_3[CYSZ]. The as-sprayed CSYZ on a Ni-alloyed substrate was subjected to

900^{o}C isothermal heating for 300hrs after adding salt sample of $NaVO_3$ to the specimens. XRD and SEM characterization methods indicate mineralization of CeO_2 and consequential growth of the monoclinic zirconia and YVO_4 phase after 70hrs of heating. At 300hrs of isothermal heating, $CeVO_4$ phase developed and complete transformation of the tetragonal phase to monoclinic phase accompanied with cracks and spallation due to volume change occurred. Figure 2.3, shows XRD analysis of hot corrosion test of the CYSZ specimen.

Table 2.2: Hot corrosion resistant of ceria-stabilized zirconia [34]

Molten salt		10%CeO_2-ZrO_2	10%CeO_2-ZrO_2	12.5%CeO_2-ZrO_2	12.5%CeO_2-ZrO_2	15%CeO_2-ZrO_2	15%CeO_2-ZrO_2
		% m-ZrO_2	% t-ZrO_2	% m-ZrO_2	% t-ZrO_2	% m-ZrO_2	% t-ZrO_2
As-sintered CeO_2-ZrO_2		2	98	1	99	2	98
Na_2SO_4	20hrs	7	93	3	97	1	99
Na_2SO_4+2%mol V_2O_5	5hrs	75	25	25	75	10	90

Transformation of tetragonal zirconia to monoclinic zirconia, mineralization of CeO_2 to form $CeVO_4$ and leaching of yttria to form YVO_4 was also the result of the hot corrosion test of CeO_2/Y_2O_3 stabilized zirconia in Na_2SO_4 +V_2O_5 environment [35].

Nakahira et al. [21] also reported attack of an as sprayed 15% CeO_2-ZrO_2 in the presence of V_2O_5 when subjected to 1273^{o}K isothermal heating for 3hrs. In the presence of

85%V_2O_5+15%Na_2SO_4 under the same test condition, minor attack of the ceramic topcoat was observed.

The tests all depict CeO_2-ZrO_2 is of higher hot corrosion resistant when compare with a full YSZ because the CeO_2 stabilizer is more acidic than yttria and based on Lewis acid mechanism; the V_2O_5 reaction with CeO_2 is slower compared to its leaching effect on yttria.

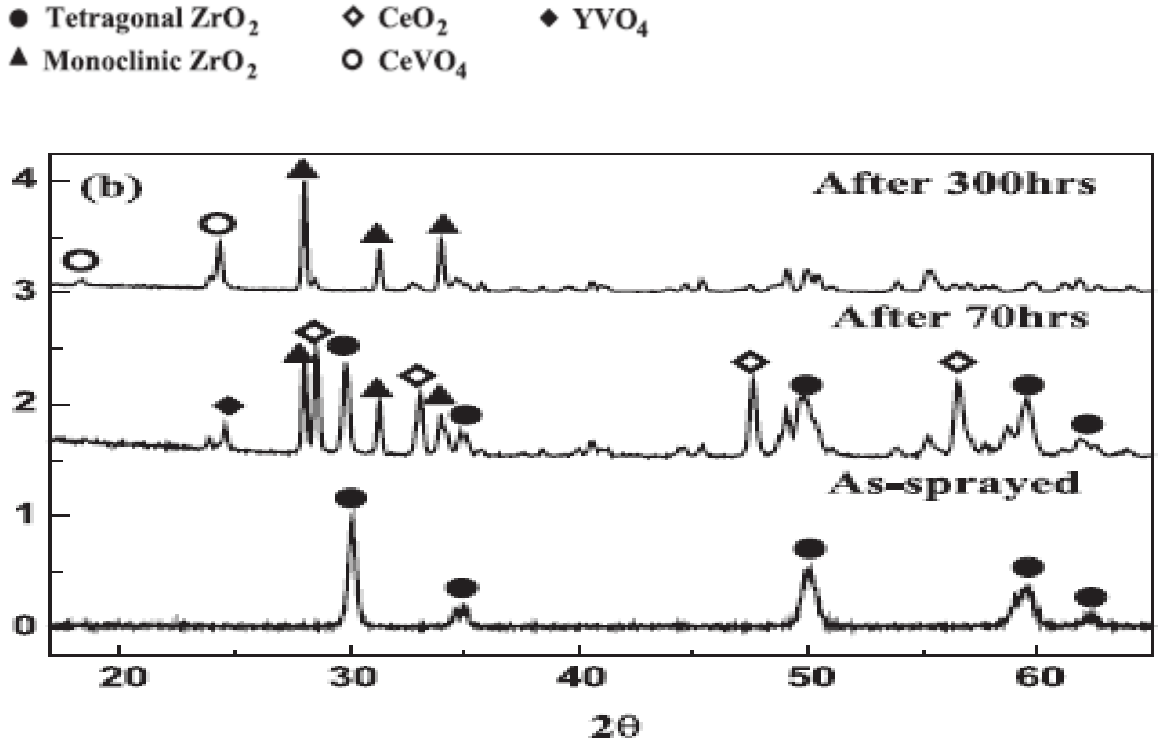

Figure 2.3: XRD analysis of hot corrosion test of zirconia stabilized with 25% wt. CeO_2 and 2.5% wt. Y_2O_3[33]

2.1.5 CaO-stabilized zirconia (CaO-ZrO_2)

CaO stabilized zirconia (CaO-ZrO_2) like MgO-ZrO_2 was one of earliest stabilized form of zirconia topcoats in TBCs [1] and it is commercially available from Sulzer Company. Like 7-8YSZ, calcium oxide stabilized zirconia with 10CaO-ZrO_2 composition was reported by [21].

$CaO\text{-}ZrO_2$ resistant to vanadium-induced hot corrosion is lesser when compared to YSZ because it is of more basicity than Y_2O_3, the CaO stabilizer reacts easily with the molten salt of vanadium.

Nakahira et al. [21] reported cracks and spallation features in an as-sprayed $10CaO\text{-}ZrO_2$ on steel substrate subjected to1273^oC isothermal heating for 3hrs in the presence of V_2O_5 only and $85\%V_2O_5+15\%Na_2SO_4$. Spallation and broken features appeared under the same test condition for the same as-sprayed calcium oxide stabilized zirconia but in the presence of $15\%V_2O_5+85\%Na_2SO_4$ and $90\%Na_2SO_4+10\%NaCl$ respectively. Figure 2.4 shows the features observed for the $CaO\text{-}ZrO_2$ in different corrosive molten salt.

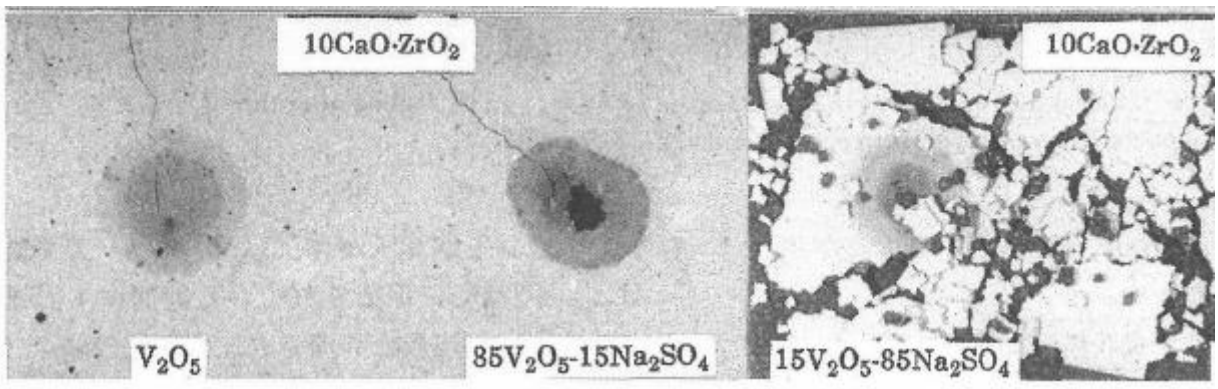

Figure 2.4: SEM micrograph of Hot Corrosion of $10CaO\text{-}ZrO_2$ in molten fuel contaminant salts [21]

2.1.6 In_2O_3-stabilized zirconia

India (In_2O_3) is an amphoteric oxide of indium with melting point of 1910^oC and it has cubic crystal structure. In_2O_3 has high vapour pressure that makes it vaporizes out of zirconia when deposited on substrate by APS; but EB PVD deposition of 3.5-11% mol In_2O_3 stabilized cubic zirconia was reported [36].

In_2O_3 like Sc_2O_3 in thermo gravimetric study of stabilizing oxides of zirconia reactions at 800^oC with molten $NaVO_3$ in SO_3 partial pressure atmosphere indicates formation of $InVO_4$ compound at higher SO_3 partial pressure [32]. Both oxides showed higher hot corrosion resistant trend when compared to that of reaction between the molten salt and yttria oxide to form YVO_4 [32].

Vanadium-induced hot corrosion resistant of india stabilized zirconia powder was tested in an environment of $NaVO_3$ with various amount of V_2O_5 melts [36]. The 3.9% In_2O_3-ZrO_2 powder undergoes destabilization in pure environment of $NaVO_3$ with less composition of V_2O_5 melt forming In_2O_3, but formation of $InVO_4$ was observed with higher concentration of V_2O_5 melt. It was concluded that destabilization occurs by mineralization at lower concentration of V_2O_5 melts but by chemical reaction at higher concentration, though proved to be better when compared to YSZ [36].

2.1.7 SnO_2-stabilized zirconia

Tin oxide (SnO_2) is a white powder with melting point of 1630^oC and it has tetragonal crystal structure. Though tin oxide stabilized zirconia is not commercially available, but it has been seen as a promising ceramic topcoat with better resistance to hot corrosion. SnO_2 is inert to Na_2O-V_2O_5-SO_3 attack [36]. XRD characterization of reaction between tin dioxide with probable oxides composition of impure fuel containing S, V and Na in a combustible environment; at 700^oC and 800^oC indicates no new phases emerging [19]. This confirm the non-reactivity of tin oxide with these fuel contaminant molten salts at high temperature and depicts tin oxide either as a component or been alloy with other compound will resist hot corrosion of molten salts. These properties of tin oxide also prove tin oxide to be an excellent material for stabilizing zirconia for

hot corrosion resistant [19, 36], hence tin oxide stabilized zirconia will be more hot corrosion resistant at lower temperature [36].

2.1.8 TiO_2-stabilized zirconia

Titania (TiO_2) is a white solid oxide of titanium with melting point of 1842^oC and boiling point of 2972^oC. TiO_2 can exists in form of rutile, anatase which both has tetragonal crystal structure and it also exists in orthorhombic and monoclinic crystal forms [18]. Like tin oxide, titania oxide has also been seen as a promising zirconia stabilizer, though titania stabilized zirconia is not commercially available. TiO_2 is a moderate acidic, it neither reacts with $NaVO_3$ nor V_2O_5 but undergoes mineralization like CeO_2, changing from anatase to rutile structure but it reacts with Na_2SO_4 easily forming $NaTiO_3$ and SO_3 [36]. The transformation of tetragonal or cubic structure to monoclinic phase due to mineralization was observed for ceramic mixture of TiO_2-ZrO_2 in a vanadate corrosion test [36].

2.1.9 Yb_2O_3 stabilized Zirconia (Yb_2O_3-ZrO_2)

Ytterbia is an oxide of ytterbium; it is white solid with melting point of 2355^oC. It is more acidic when compared to yttria and can be use effectively to stabilized zirconia [36]. The activity of V_2O_5 at 900^oC using thermodynamic data required to form $YbVO_4$ is $9.3X10^{-10}$ which is higher than that required to form YVO_4 ($8X10^{-11}$) but much more less when compare to that required to form $ScVO_4$ [36]. Yb_2O_3 stabilized zirconia resistance to vanadate will not have much difference when compared to that of YSZ [13].

The alternate stabilized zirconias haven't been proven to be the best alternative to yttria stabilized zirconia in mitigating vanadium-induced hot corrosion. The alternate stabilized

zirconias that are commercially available though retard the degradation but still undergo degradation in the presence of molten salts. Others which have promising better resistant are only available on paper not in practice.

2.2 Pyrochlores

Pyrochlores (Rare earth zirconates) are composite compound of zirconia and lanthanide metals with chemical formular $M_2Zr_2O_7$, where M represents the lanthanide metal. Pyrocholores have been seen as an alternative to 8YSZ as ceramic topcoat in TBCs due to its better resistance to hot corrosion and other desirable properties. Pyrochlore has low thermal conductivity, high temperature stability, high thermal co-efficient of expansion and better stability to accommodate defects [6].

Sa Li et al. [37] evaluated the hot corrosion resistant of rare earth zirconates of ytterbium,$Yb_2Zr_2O_7$ in V_2O_5. The plasma sintered pyrochlore undergoes destabilization at 600^oC isothermal heating at both 2hrs and 8hrs forming compounds of $YbVO_4$ and ZrV_2O_7. $Yb_2Zr_2O_7$ at 700^oC formed $YbVO_4$ with either m-ZrO_2 or $ZrVO_7$ after 8hrs and 2hrs respectively. $YbVO_4$ and m-ZrO_2 formed mainly both after 2hrs and 8hrs isothermal heating at 800^oC due to instability of the $ZrVO_7$ at higher temperature.

Yugeswaran et al. [24] evaluated $La_2Zr_2O_7$ pyrochlore hot corrosion resistant in molten salt of 40%V_2O_5+60%Na_2SO_4 at 1173^oK isothermal heating after 5hrs. $La_2Zr_2O_7$ is rare earth zirconate of lanthanum. The gas tunnel plasma sprayed lanthanum zirconate gave a better hot corrosion compared to 8YSZ, though it undergoes destabilization forming $LaVO_4$ and tetragonal-monoclinic zirconia.

$Gd_2Zr_2O_7$ hot corrosion resistance in molten salt mixture of Na_2SO_4 and V_2O_5 was evaluated by Habibi et al. [6]. An APS $Gd_2Zr_2O_7$ subjected to 1050^oC isothermal heating developed spallation and cracks after 9cycles of 4hrs of heating. The pyrochlore hot corrosion products are $GdVO_4$ and m-ZrO_2. An APS 8YSZ under the same test condition suffered spallation and cracks after 5cycles.

Like the alternate stabilized zirconias, the use of pyrochlores has also been seen not to provide hundred percent mitigation of hot corrosion. It only retards the phenomenon of hot corrosion in the ceramic topcoat in presence of molten salts.

2.3 Ceramic Composites

Ceramic composite topcoats in TBCs are made from mixing together two promising ceramic topcoat materials aimed at achieving a desirable property i.e. better hot corrosion resistant. 8YSZ that is the most prominent ceramic topcoat material is often mixed with other ceramic materials like alumina and pyrochlore for improved hot corrosion resistant. Hot corrosion resistant of such ceramic topcoat composites have also been evaluated as a means of achieving a durable ceramic topcoat. Yugeswaran et al. [24] carried out an experiment to evaluated plasma spray composite ceramic topcoat of 50% 8YSZ+50% $La_2Zr_2O_7$ hot corrosion resistant in $NaVO_3$ at 1173^oK isothermal heating for 5hrs. The formation of flake like $LaVO_4$ inhibits formation of YVO_4 that made the hot corrosion resistance of composite better compared to 8YSZ ceramic topcoat.

Habibi et al. [6] also evaluated composite mixture of $Gd_2Zr_2O_7$ +8YSZ hot corrosion resistant. It showed better resistance compared to 8YSZ which undergoes destabilization after 5cycles of 4hrs isothermal heating. $GdVO_4$ growth from the composite inhibits the formation of YVO_4

which prolongs the spallation time of the composite till after 9cycles of 4hrs heating at 1050^{o}C isothermal heating.

Afrasiabi et al. [9] showed that the rate of transformation of tetragonal zirconia to monoclinic zirconia in an APS YSZ is greater than when having APS composite mixture of 60% wt.YSZ+40%wt.Al_2O_3. In the presence of $NaVO_3$, after 40hrs of hot corrosion test carried out at 1050^{o}C; APS YSZ indicates the presence of 66% m-ZrO_2 while the composite indicates 20% m-ZrO_2. Although both indicate spallation and cracks; that of the composite is less severe compared to the APS YSZ. Fig. 2.5 shows the volumetric monoclinic zirconia in different types of APS ceramic topcoats.

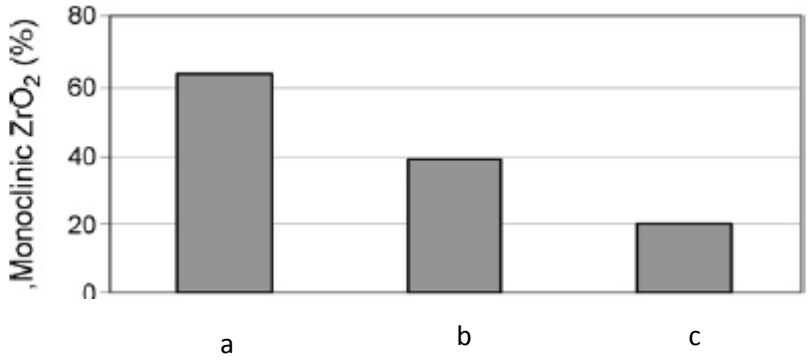

Figure 2.5: Volume fraction of monoclinic zirconia in the coatings after hot corrosion test, (a) YSZ, (b) YSZ+Al_2O_3, (c) YSZ/Al_2O_3[9]

2.4 Overlay coating

The use of overlay coatings which are often sacrificial layers have also been employed to mitigate hot corrosion problem in TBC. Alumina based composites have been the major forms of overlay coatings used for protecting TBC. Xiaolong et al. [38] evaluated the effectiveness of an overlay coating alumina composite to mitigate hot corrosion in TBCs. $LaMgAl_{11}O_{19}$ coating on

an APS 8YSZ was subjected to 900^{o}C isothermal heating in the presence of V_2O_5. Its resistant was evaluated and compared to an APS 8YSZ under the same experimental conditions. Characterization of the overlay coating TBCs specimen after 50hrs indicates the growth of YVO_4 which is the same for the free APS 8YSZ specimen at 20hrs. The overlay coating undergoes destabilization to protect the ceramic topcoat by hindering infiltration of the molten salt into it. 8YSZ layer of the overlay coated specimen showed longer destabilization life span since it is not in direct contact with the contaminant compared to the free APS 8YSZ specimen that comes in contact with V_2O_5 directly.

Afrasiabi et al. [9] showed that the presence of an APS alumina layer on an APS YSZ on nickel alloy substrate offered greater resistance to destabilization in $NaVO_3$. The hot corrosion test XRD analysis after 40hrs at 1050^{o}C isothermal heating indicates the presence of considerable amount of t-ZrO_2 compared to that of an APS YSZ tested under the same experimental conditions. The better resistant offered by the APS YSZ with alumina overlay coat is attributed to the reduction in the infiltration of molten salt into it by the alumina layer.

Mohammadreza et al. [39] obtained lesser degradation of an APS YSZ when protected with a nano-Al_2O_3 structure as an overlay coating in presence of V_2O_5+Na_2SO_4 molten salt. The transformation of the zirconia phase and growth of YVO_4 after 52hrs heating at 1000^{o}C was reduced when compared with that of an APS YSZ under the same test conditions. The nano-Al_2O_3 covered YSZ gave a better hot corrosion resistance due to the nano-Al_2O_3 overlay hindering the infiltration of the contaminant into the topcoat hence reduces its accelerated corrosion.

Z. Chen at al. [40] also reported the reduction in destabilization of an APS 8YSZ topcoat covered with an EB-VPD alumina layer. The growth of YVO_4 and transformation of the zirconia phase reduced when compare with an APS 8YSZ in direct contact with molten salt of $95\%Na_2SO_4+5\%V_2O_5$ heated at 950^oC between 10mins to 100hrs. The rate of the destabilization of the TBCs was calculated using equation 2.4, where M and T represents the intensity of the monoclinic (-111) and tetragonal (111) zirconia peaks from XRD analysis. Figure 2.6 shows the comparison between the two topcoats, with the YSZ/alumina system showing less destabilization out of the two; though both portray increase in destabilization with time. The alumina layer reduces the infiltration of the molten salt into 8YSZ ceramic topcoat, hence making it more resistance to hot corrosion.

$$D\% = \frac{M}{T+M} \times 100 \qquad (2.4)$$

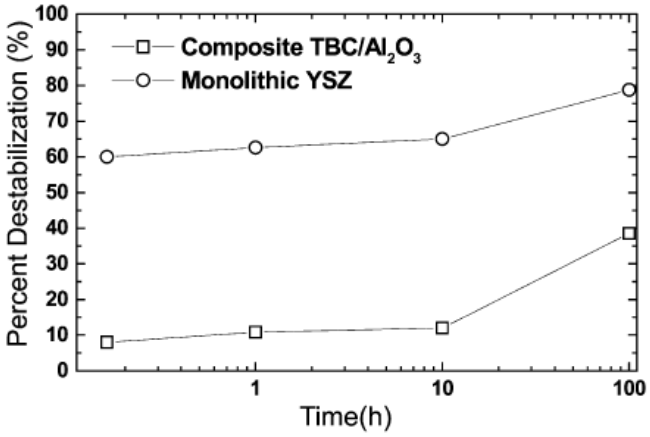

Figure 2.6: Rate of Destabilization versus time plot of as sprayed ceramic topcoat[40]

Canumalla et al. [41] evaluated the effectiveness of three forms of overlay coating in protecting the TBCs against hot corrosion of molten salt of Na_2SO_4. The alumina composites include mullite ($3Al_2O_3.2SiO_2$) and BAS ($BaO.Al_2O_3.2SiO_2$), while the third is calcium silicate compound ($1.8CaO.SiO_2$). The overlay coatings were air plasma sprayed on an APS 8YSZ TBC and all the specimens subjected to 900^oC isothermal hot corrosion test in molten Na_2SO_4. Their hot corrosion resistant were compared to that of an APS 8YSZ under the same experimental condition. Although the contaminant doesn't react with YSZ but its solidification after infiltration caused destabilization of the topcoat. Mullite proved to be best out of the overlay coatings neither does it reacts nor allows the infiltration of the molten salt. The 8YSZ for the calcium silicate coatings undergoes destabilization due to reaction of the calcium silicate with the contaminant forming a new compound. The formation of new compound generates stress mismatch between the YSZ/overlay coating boundary which initiates the destabilization of the topcoat, though still portrays more resistant than free 8YSZ.

2.5 Surface Sealing

Hot corrosion of 8YSZ especially APS type, is hasten due to infiltration of molten salt into the in-depth of the ceramic topcoat through the porosity. Hindering the infiltration of the molten salt through various methods has been seen as an alternative way to mitigate hot corrosion of 8YSZ ceramic topcoat in TBCs often by laser glazing.

Batista et al. [42] carried out an experimental analysis on mitigation of hot corrosion in ceramic topcoat with laser glazing. Nd-YAG and CO_2 laser glazed APS 8YSZ on a steel substrate resistant to hot corrosion from V_2O_5+Na_2SO_4 contaminant was evaluated and compared with that of APS 8YSZ. The specimens were subjected to 1000^oC isothermal heating and subsequent

cooling in open air. The laser glazed specimens show no sign of destabilization up till 72hrs as compared to APS 8YSZ in V_2O_5 and combination of V_2O_5 and Na_2SO_4 contaminants, however the APS 8YSZ specimen shows the growth of YVO_4 within 24hrs of isothermal heating. Hot corrosion mitigation in the laser glazed specimens was attributed to reduced porosity of the ceramic which hinders infiltration of the contaminants. The little destabilization observed in the laser glazed was due to the infiltration of molten salt through the lateral pores created by the laser glazing operation. Fig. 2.7 shows the laser glazed surface with lateral pores and the unglazed ceramic topcoat with high level of porosity.

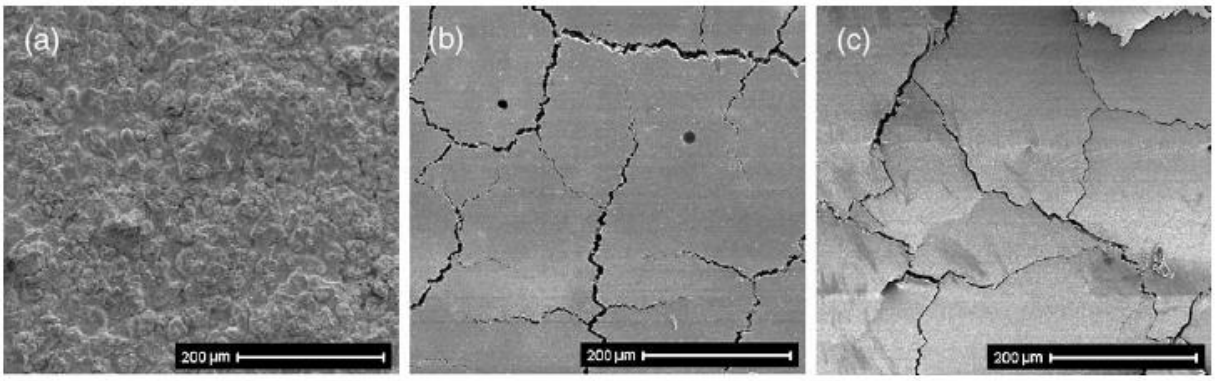

Figure 2.7: SEM surface morphology of ceramic topcoat before hot corrosion,(a) as sprayed ,(b) CO_2 laser glazed, (c) Nd-YAG laser glazed [42]

Ahmaniemi et al. [25] evaluated 60%Na_2SO_4+40%V_2O_5 molten salt hot corrosion resistant of different types of ceramic topcoat sealing methods. 8YSZ and 22MgO-ZrO_2 ceramic topcoats sealed by phosphate base sealant, Nd-YAG laser glazing and dense spraying using detonation gun hot corrosion resistant was compared to that of as-sprayed 8YSZ and 22MgO-ZrO_2 ceramic topcoats. The specimens were subjected to the same hot corrosion test of 650^oC isothermal heating for 200hrs and characterization with XRD, SEM after cooling in open air. Nd-YAG topcoat destabilization took longer hours compared to that of other sealed surfaces, but the

degradation is worst in the un-sealed ceramic topcoats. The MgO stabilized zirconia topcoat also posed higher hot corrosion resistant in the contaminant environment compared to the 8YSZ topcoat. The hot corrosion resistances of the sealed surfaces were attributed to reduction in the porosity of the topcoat which reduces the infiltration of the molten contaminant.

2.6 Fuel Additive Inhibitors

The use of fuel additives to mitigate vanadium-induced hot corrosion has been explored mostly for metal alloys, with little on ceramic topcoats in TBCs. It is the most favourable in term of cost and simplicity compared to other methodologies. Hot corrosion mitigation in metal alloys using fuel additives is also based on Lewis acid mechanism and Flood Lux acid mechanism, which define reaction between basic oxide and acidic oxide. The use of metal base compound of Mg, Ca, Y and Ni as the fuel additives to mitigate hot corrosion of metal alloy has been investigated and their effectiveness evaluated.

Barbooti et al. [43, 44] evaluated the efficiency of mitigating vanadic ash induced hot corrosion of three types of steel material with Mg base compound fuel additives; magnesium sterate and magnesium hydroxide. The inhibitive tests were conducted in the presence of vanadic ash with 67%wt. of V_2O_5 and 33%wt. of Na_2SO_4 composition in ratio 1:1, 1:2 and 1:3 to the Mg-base inhibitors at various temperatures between 550^oC and 950^oC. Maximum inhibiting efficiency was obtained at lower temperature of 550^oC and with inhibitor-vanadic ash molar ratio of 3:1. It was attributed to the formation of high melting point $Mg_3V_2O_8$ compound which peak was indicated in XRD characterization. Fig. 2.8 and Table 5 show the effect of the magnesium based fuel additives with different molar concentration in mitigating vanadium-induced hot corrosion of two different type of steel materials.

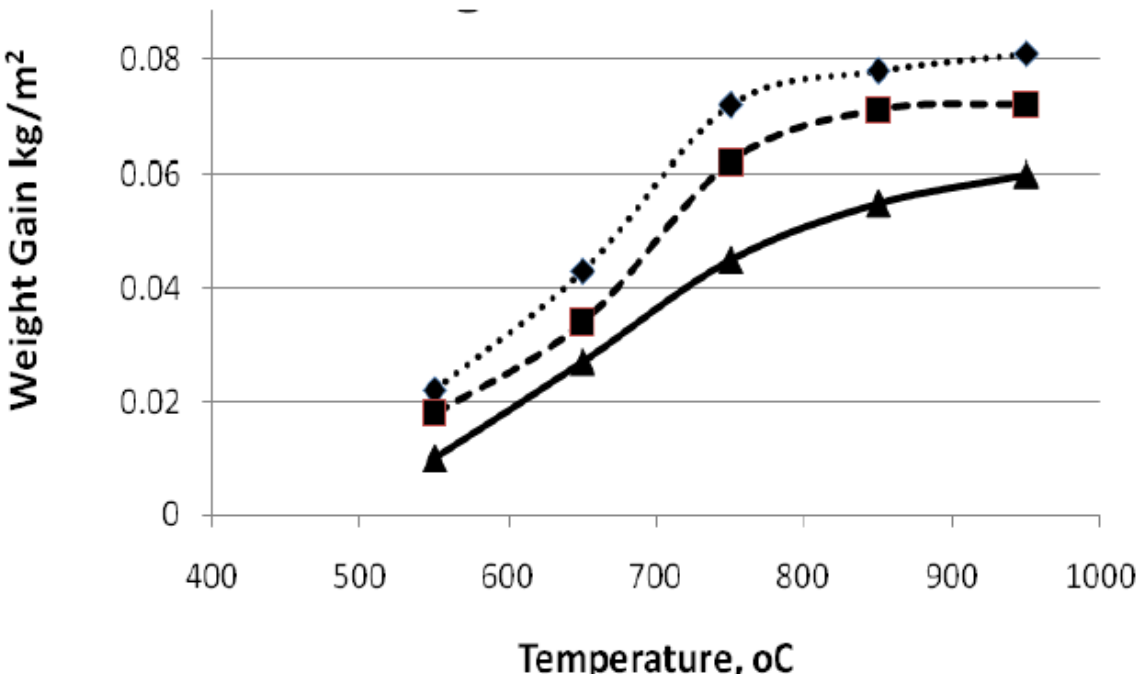

Figure 2.8: Action of Magnesium Stearate Addition on Weight gain for (213T1) steel at 1:1, dotted line; 2:1, dashed line and 3:1,solid [44]

Table 2.3: Inhibition Efficiency in the presence of $Mg(OH)_2$ for vanadium-induced hot corrosion of (SA-178) specimen [43]

$Mg(OH)_2$:Ash	Temperature, °C.				
	550	650	750	850	950
0:1	--	--	--	--	--
1:1	66	51	53	56	57
2:1	73	61	60	60	62
3:1	85	69	71	69	69

Chassagneux and Thomas [45] evaluated the protection of AISI 310 steel from V_2O_5 hot corrosion using Mg coating in molar concentration ratio of 3, 2 and 1 to 1 of vanadium respectively. Weight change for the coated specimen in which Mg/V=3 gave weight change

equal to that obtained from oxidized specimen without molten salt which is the best. In V_2O_5 environment, the AISI 310 recorded a weight gain of 2.77mg.cm^{-2} while in the environment with Mg/V=3, AISI 310 recorded a weight gain of 0.27mg.cm^{-2}. The coated specimen with Mg/V=2 and 1 gave a weight change which is 2 and 3.5 multiple that obtain for Mg/V=3 respectively. XRD characterization also shows the presence of $Mg_3V_2O_8$, $Mg_2V_2O_7$ and MgV_2O_6 for Mg/V equal to 3, 2 and 1, respectively.

Rhys-Jones et al. [17] evaluated the effectiveness of MgO additives in inhibiting vanadium-induced hot corrosion of Ni and Co alloy at 750^{o}C and 850^{o}C. The effectiveness of the additives to inhibit vanadium-induced hot corrosion of metal alloy in presence of SO_2/SO_3 in the system was also evaluated. The experiment involved samples of Ni and Co base alloys subjected to 100hrs; 850^{o}C and 750^{o}C isothermal heating with MgO/V_2O_5 molar concentration equals 3. The inhibitive effect was higher in the absence of the sulphur oxide due to the formation of high melting point of $Mg_3V_2O_8$. The presence of sulphur compound however reduces the inhibitive effect due to MgO inhibitor reacting with the sulphur compound. Figure 2.9 shows the weight change versus mass/area composition of the nickel alloy inhibitive hot corrosion test.

Rocca et al. [15] compared the effectiveness of fuel additives inhibitor oxides of Ni and Mg to mitigate vanadium- induced corrosion of metal alloy. The analysis involves weight measurement of nickel base alloy using in-situ thermogravemetric analysis subjected to isothermal heating test. The inhibitive effect of NiO was attributed to the formation high melting point $Ni_3V_2O_8$ similar to $Mg_3V_2O_8$ obtained for MgO in vanadium oxide environment. Figure 2.10, shows weight change of the nickel base alloy with NiO and MgO additives lowered than that without the inhibitors

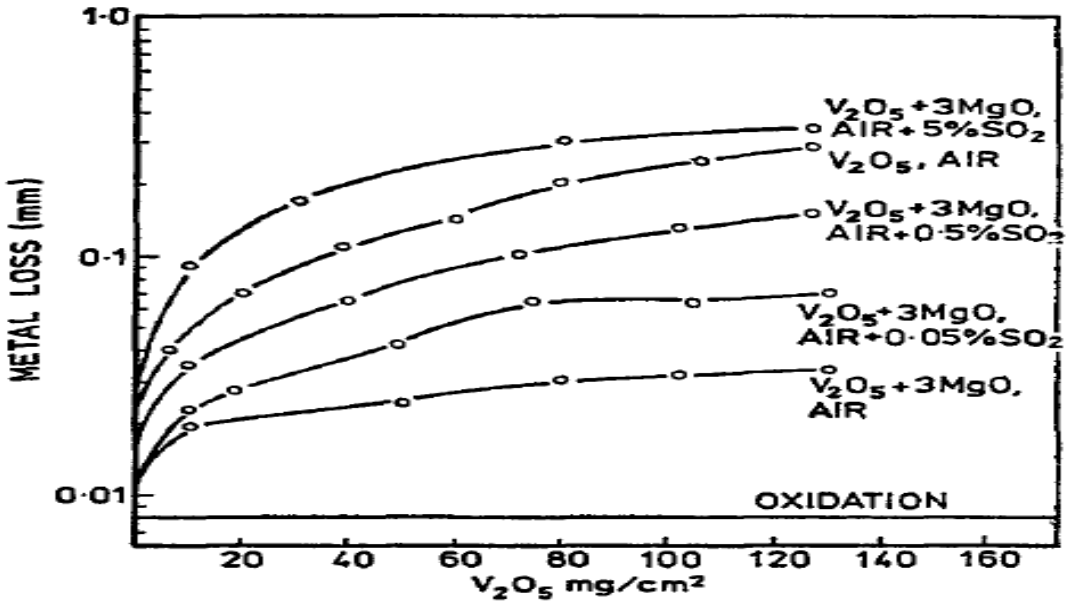

Figure 2.9: Effect of contaminants and inhibitor on high temperature corrosion of Nimonic 90 at 850^{o}C [17]

Singh et al. [18] used Y_2O_3 as an inhibitor for high temperature corrosion due to molten salt of Na_2SO_4 and V_2O_5 for Fe, Ni and Co base alloys. The alloys were subjected to 50cycles, 900^{o}C isothermal heating with 1hr heating and 20minutes cooling in open air and weight change measure during each cycle. The results showed weight change and spallation of alloy for inhibitive tests without inhibitor is more compared to those with inhibitor as seen in Fig 2.11.

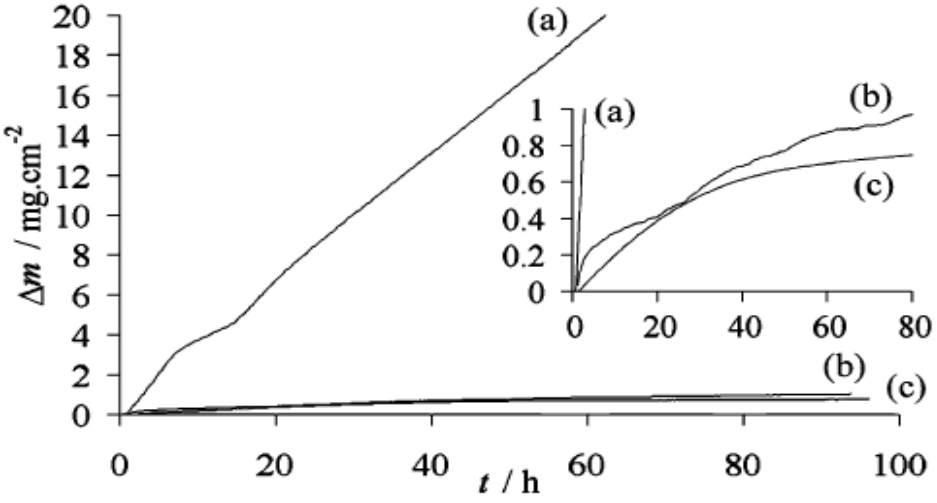

Figure 2.10: Weight change versus time (A) Na/V=1.5, (B) Na/V=1.5,Mg/V=3 and (c) Na/V=1.5,Ni/V=2.25 oxidation at 850^{o}C[15]

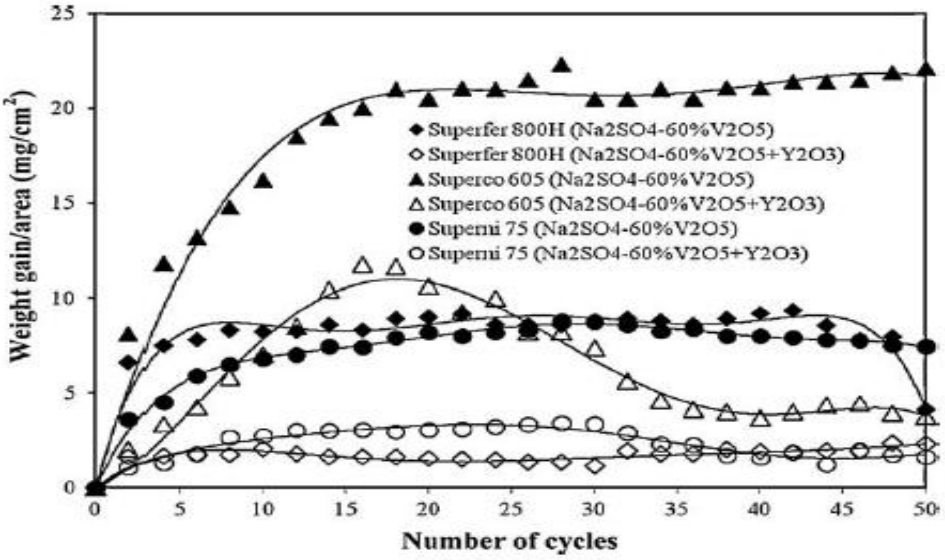

Figure 2.11: Weight change versus number of cycles [18]

CHAPTER 3

EXPERIMENTAL PROCEDURES

The use of as-sprayed YSZ (APS or EB-PVD) on metal alloy substrate specimens have been mostly reported from the literature in hot corrosion laboratory test of TBCs [8, 10]. The TBCs specimen is usually rectangular shaped TBCs on a metal alloy substrate coupon. The rectangular coupon is a replicate of the turbine blade which allows for laboratory experiments to depict the actual field experience in the gas turbine engines. Likewise the use of 8YSZ powder sample for hot corrosion experiment has also been reported, [27, 31] as an alternative to the as-sprayed specimen. The use of 8YSZ powder sample in hot corrosion experiment is simple and the easiest. It also provides a means of actually ensuring homogenous mixing of the 8YSZ powder with the contaminants and inhibitors. This gives a similitude of the molten salt infiltration in real field experience in gas turbine engines. The objective of this research was accomplished by carrying out an inhibitive isothermal hot corrosion experiments with powder samples and afterward using the APS 8YSZ coupons.

3.1 Materials

The materials used in the inhibitive hot corrosion research are 8YSZ (Metco 204NS), MgO, CaO and V_2O_5 powder samples. It also includes TBCs coupons; an APS 8YSZ-MCrAlY (Ni-22%Cr-10%Al-1%Y) TBCs on IN718 nickel super-alloy substrate. The choice of 8YSZ and V_2O_5 samples were based on simulating the actual field experience in the gas turbine engines where the topcoat is an as-sprayed 8YSZ and V_2O_5 is the molten salt formed from the combustion of

the vanadium contaminant at high temperature. Tables 3.1 and 3.2 below show the powder samples and their source; and the compositional property of the 8YSZ powder, respectively.

3.2 Equipment

The equipment used in the inhibitive hot corrosion research experiment are:

a) Phoenix AB 224 weighing Device: The equipment can measure up to four decimal figures. It was used to measure the required amount of powder samples for the experiments and weighing the APS TBCs specimens. This is shown in Fig. 3.1(a).

Table 3.1: Powder samples and their source.

Powder	Source
8YSZ (Metco 204NS)	Sulzer Company
MgO	Nano-scale Materials Inc.
CaO	Fisher Scientific Company
V_2O_5	Fluka 94720 Company

Table 3.2: Percentage weight compound composition of 8YSZ powder (Metco 204NS)

Compound	ZrO_2	Y_2O_3	Al_2O_3	Fe_2O_3	TiO_2	SiO_2	Monoclinic(max)
%wt. composition	Balance	7-9	0.2	0.2	0.2	0.7	10

b) Mortar, Alumina crucibles and Glass tubes: The powder samples were mixed to form homogenous samples by mixing in the glass tubes and grinding in the mortar. The alumina crucibles were used as containers for the portion samples of the homogenous powder samples

during heating in the furnace. The mortar, alumina crucibles and the glass tubes are shown in Fig 3.1(b).

c) Linderberg Blue-M Furnace: Hot corrosion in TBCs occurs at high temperature inside the gas turbine engines, the furnace was used to subject the samples to 900^{o}C isothermal heating for the stated heating period of between 10minutes to 100hrs.

3.3 Inhibitive Hot Corrosion Experiment

3.3.1 Inhibitive Hot Corrosion Experiment (Powder Samples)

The powder samples experimental design was meant to simulate the worst scenario that is obtainable in the field. This justifies the amount of the 8YSZ and V_2O_5 powders used in the experiments. Kondos [27] reported 90% of 8YSZ powder with 10% V_2O_5 powder gave the highest rate of degradation of the 8YSZ powder compared to those with lesser V_2O_5 concentration. The inhibitive tests entail varying the molar concentration ratio of the alkaline-earth metal oxide to vanadium oxide in the homogenous samples from 1 to 5 to determine the effective combination ratio of the powders. The powder samples inhibitive hot corrosion experimental procedure is as follows:

i) Measuring the desired amount of powder samples for the homogenous mixture.

ii) Homogenous mixing of the powder samples in the glass tube and mortar.

iii) Distributing the homogenous mixture in small portions into the alumina crucibles before putting it into the furnace for inhibitive hot corrosion test.

Tables 3.3 to 3.8 show the hot corrosion and inhibitive hot corrosion tests carried out with different composition of the powder samples.

3.3.2 Inhibitive Hot Corrosion Experiment (APS 8YSZ-TBCs Coupon Specimen)

The experimental procedure for inhibitive hot corrosion test of the as-sprayed samples entails firstly cleaning the APS 8YSZ specimens with an acetone-water mixture in a sonicator for 60minutes. This was subsequently followed with drying of the specimens in the furnace by heating at 200^{o}C for 15minutes and their weight measured. Homogenous slurry solutions of V_2O_5, MgO and CaO were prepared with the following molar concentration ratio, respectively; M_{MgO}/M_{V2O5} equals 3 and 5, respectively and M_{caO}/M_{V2O5} equals 3 and 5, respectively. This was based on those alkaline-earth metal oxide-vanadium oxide molar concentration ratios that portray good inhibitive results in the powder sample experiments. These slurry solutions were then applied on to the surface of the specimens and assigned as samples A to F. The slurry solutions were added gradually in each case in drops on to the surface of the as-sprayed specimen and dried by heating until the mass weight of the slurry on each specimen was 3-5 times that of the V_2O_5 powder on the vanadium-induced as-sprayed sample. The vanadium-induced as-sprayed sample has slurry of V_2O_5 up to 20mg/cm^2 on the surface of the specimen. The samples were then subjected to 900^{o}C isothermal heating for 100hrs in the furnace and subsequent cooling in the laboratory air. Table 3.9 shows the as-sprayed samples for the inhibitive hot corrosion experiment.

It is worthy to know that the following conditions were observed for the hot corrosion and inhibitive hot corrosion powder samples; and APS coupon experiments:

i) Isothermal heating at 900^{o}C

ii) Heating time was between 10minutes to 100hrs

iii) Vanadium contaminant was only considered (since it is the only contaminant that attacks the ceramic topcoat).

iv) Cooling of heated samples was done in laboratory air (except when testing for isothermal heating effect)

The powder samples experimental set-up with the alumina crucibles in the furnace is shown in Figure 3.2(a).

3.4 Characterization Methods

Characterizations of the samples were carried out after the inhibitive hot corrosion tests in order to explore the changes in the properties and characteristics of the samples. Characterization methods used include the following:

i) Colour Spectrum Analysis: The change in colour of the samples during the hot corrosion test was analyzed by visual appearance and taking pictures using camera. The use of Hunterlab device which measures colour scale of the powder samples was also employed. Fig. 3.2(b) shows the Hunterlab colour device.

ii) XRD analysis: XRD analysis as a method of characterization was used for phase analysis. The growth of the monoclinic zirconia due to phase transformation of the zirconia compound from hot corrosion was majorly monitored with the XRD analysis. Other phases of compound formed by elemental combination of vanadium, yttrium, magnesium, calcium and oxygen were also monitored with XRD analysis. The plot of phase intensity against 2θ was obtained from the XRD

analysis in which the chosen 2θ for the analysis ranges between 10^o to 80^o step 0.02^o. The XRD device used was a D8 XRD machine using a Cu $K\alpha_1$ target. The D8 XRD machine is shown in Fig. 3.3.

iii) Scanning Electron Microscopy (SEM): SEM analysis was used for morphology characterization of the powder samples. The powder samples SEM micrographs both before and after hot corrosion experiments were captured to monitor morphology change in the powder samples. TESCAN LYRA machine shown in Fig. 3.4(a) and JOEL JSM-6460LV machine in Fig. 3.4(b) were used to capture the SEM micrographs.

iv) Energy Dispersive Spectroscopy (EDS)/X-ray mapping: SEM micrographs depict only the morphology of the powder samples, but EDS and X-ray mapping analyses gave a better insight of the elemental distribution in the samples. In the inhibitive hot corrosion research, EDS and X-ray mapping characterizations were used for further analyses to determine the emerging compounds by elemental analysis. EDS analysis was carried out using the TESCAN LYRA machine like SEM while X-ray mapping was carried out using JOEL JSM-6460LV machine shown in Fig. 3.4(b).

Table 3.3: The effect of isothermal heating in hot corrosion test

Powder samples	Weight composition of V_2O_5	Molar concentration ratio of $CaO:MgO:V_2O_5$	900^oC isothermal heating time	Cooling Mechanism
8YSZ	N/A	N/A	2hrs	Cooling in the furnace and laboratory air

(a)

(b)

Figure 3.1: (a) Phoenix AB 224 weighing device , (b) Mortar, glass tube and alumina crucibles

Table 3.4: Vanadium-induced hot corrosion experiment with varying V_2O_5 concentration

Powder Samples	Weight composition of V_2O_5	900^oC isothermal heating time	Cooling Mechanism
8YSZ and V_2O_5	10% 8YSZ	10minutes-100hrs	Laboratory air
8YSZ and V_2O_5	0% 8YSZ	10minutes-100hrs	Laboratory air
8YSZ and V_2O_5	5% 8YSZ	10minutes-100hrs	Laboratory air
8YSZ and V_2O_5	2% 8YSZ	10minutes-100hrs	Laboratory air

Table 3.5: Inhibitive hot corrosion experiment with MgO powder inhibitor

Powder Samples	Weight composition of V_2O_5	Molar concentration ratio of MgO:V_2O_5	900^oC isothermal heating time	Cooling Mechanism
8YSZ, MgO and V_2O_5	10% 8YSZ	1:1	10minutes-100hrs	Laboratory air
8YSZ, MgO and V_2O_5	10% 8YSZ	2:1	10minutes-100hrs	Laboratory air
8YSZ, MgO and V_2O_5	10% 8YSZ	3:1	10minutes-100hrs	Laboratory air
8YSZ, MgO and V_2O_5	10% 8YSZ	5:1	10minutes-100hrs	Laboratory air

Table 3.6: Inhibitive hot corrosion experiment with CaO powder inhibitor

Powder Samples	Weight composition of V_2O_5	Molar concentration ratio of $CaO:V_2O_5$	900^oC isothermal heating time	Cooling Mechanism
8YSZ, CaO and V_2O_5	10% 8YSZ	1:1	10minutes-100hrs	Laboratory air
8YSZ, CaO and V_2O_5	10% 8YSZ	2:1	10minutes-100hrs	Laboratory air
8YSZ, CaO and V_2O_5	10% 8YSZ	3:1	10minutes-100hrs	Laboratory air
8YSZ, CaO and V_2O_5	10% 8YSZ	5:1	10minutes-100hrs	Laboratory air

Table 3.7: Inhibitive hot corrosion experiment with mixture of CaO and MgO powders as inhibitor

Powder Samples	Weight composition of V_2O_5	Molar concentration ratio of $CaO:MgO:V_2O_5$	900^oC isothermal heating time	Cooling Mechanism
8YSZ, MgO, CaO and V_2O_5	10% 8YSZ	1:1:1	10minutes-100hrs	Laboratory air
8YSZ, MgO , CaO and V_2O_5	10% 8YSZ	1:2:1	10minutes-100hrs	Laboratory air
8YSZ, MgO, CaO and V_2O_5	10% 8YSZ	2:1:1	10minutes-100hrs	Laboratory air

Table 3.8: Inhibitive hot corrosion experiment with lower V_2O_5 concentration

Powder Samples	V_2O_5 weight composition	CaO:MgO:V_2O_5 molar concentration	900^oC isothermal heating time	Cooling Mechanism
8YSZ, MgO and V_2O_5	5% 8YSZ	0:2:1	10minutes-100hrs	Laboratory air
8YSZ, MgO and V_2O_5	5% 8YSZ	0:3:1	10minutes-100hrs	Laboratory air
8YSZ, MgO and V_2O_5	5% 8YSZ	0:5:1	10minutes-100hrs	Laboratory air
8YSZ, CaO and V_2O_5	2% 8YSZ	1:0:1	10minutes-100hrs	Laboratory air
8YSZ, CaO and V_2O_5	2% 8YSZ	2:0:1	10minutes-100hrs	Laboratory air
8YSZ,CaO and V_2O_5	2% 8YSZ	3:0:1	10minutes-100hrs	Laboratory air

Table 3.9: APS 8YSZ-TBCs samples

Sample	Homogenous salt solution on the APS 8YSZ-TBCs specimen	Molar concentration ratio of powder samples in the salt solution (CaO:MgO:V_2O_5)
Sample A	N/A	N/A
Sample B	V_2O_5	N/A
Sample C	MgO + V_2O_5	0:3:1
Sample D	MgO + V_2O_5	0:5:1
Sample E	CaO + V_2O_5	3:0:1
Sample F	CaO + V_2O_5	5:0:1

(a)

(b)

Figure 3. 2: (a) Inhibitive Hot corrosion experimental set-up, (b) Hunterlab colour characterization device

Figure 3.3: D-8 XRD Machine

(a)

(b)

Figure 3. 4: (a) TESCAN LYRA Machine, (b) JOEL JSM 6460LV Machine

CHAPTER 4

RESULTS

The results are obtained from the characterization methods which include the colour spectrum, XRD, SEM, EDS and X-ray mapping elemental analyses. The results are both in qualitative and quantitative forms. Qualitative results include physical colour appearance, XRD spectra, SEM micrographs, EDS and X-ray mapping analyses. Quantitative results are colour scale measurement and amount of tetragonal zirconia phase transformation. The colour scale gives a measure of the degree of lightness or blackness which is represent by L*, the degree of redness or greenness; a* and the degree of yellowness and blueness; b* of the sample. The amount of tetragonal zirconia transformation to monoclinic zirconia depicts the extent of accelerated corrosion of the 8YSZ powder and APS 8YSZ topcoat; and is determine using equation 4.1. The equation measures the volume fraction of monoclinic zirconia in the 8YSZ using data from the XRD spectra [9, 38, 42, 46].

$$M\% = \frac{M_1 + M_2}{M_1 + M_2 + T} \qquad (4.1)$$

M% = volume fraction of monoclinic zirconia phase.

M_1 = intensity of monoclinic zirconia phase peak; (1 1 1) plane from the XRD spectrum

M_2 = intensity of monoclinic zirconia phase peak; ($\bar{1}$, 1, 1) plane from the XRD spectrum

T = intensity of the tetragonal zirconia phase peak; (1 0 1) plane from the XRD spectrum

M_1 and M_2 are intensities of monoclinic zirconia peaks at 2θ equal 28^o and 31.5^o respectively while T is that of tetragonal zirconia peak at 2θ equals 30^o.

4.1 Effect of Isothermal heating in Hot Corrosion Test

The effect of cooling rate in hot corrosion was evaluated with 8YSZ powder samples subjected to 900^oC isothermal heating for 2hrs and separately cooled in laboratory air and furnace. Fig. 4.1(i) shows the bar chart representation of monoclinic zirconia volume fractions in the samples and the as-received 8YSZ powder using Eqn. 4.1. The volume fractions of monoclinic zirconia for each sample of as- received 8YSZ powder, air cooled and furnace cooled appear almost the same. This indicates that the monoclinic zirconia from the transformation of the tetragonal zirconia is independent of the cooling rate.

The SEM micrographs for the samples are shown in Fig. 4.1(ii). The morphology of the powder samples in both case are the same. It shows powder samples with smooth-face spherical shaped particles. This further validates the earlier written statement that tetragonal zirconia transformation is independent of cooling rate.

4.2 Vanadium-induced Hot Corrosion of 8YSZ Powder

4.2.1 Colour Spectrum Analysis

The effect of varying amount of V_2O_5 concentration on colour spectrum of 8YSZ powder hot corrosion at 900^oC isothermal heating is shown in Fig. 4.2 and Tab. 4.1. The sample with 0wt.% V_2O_5 concentration; isothermal heated 8YSZ powder, Fig. 4.2(a) depicts a whitish colour at 100hrs, which is the same with the colour of the as-received 8YSZ powder. The whitish colour of the as-received 8YSZ powder however changes with increase in heating time for sample with

10wt.% V_2O_5 concentration, Fig 4.2(b-c). The white colour turns brownish after 10 minutes of heating, Fig. 4.2(b) and reddish after 50hrs of heating, Fig. 4.2(c). The hot corrosion products of samples with V_2O_5 concentration, 2% and 5% wt. 8YSZ indicate light yellowish and dark yellowish colour respectively throughout 100hrs heating time as shown in Fig. 4.2(d-e). The colour scale of the samples as shown in Tab. 4.1; has the 100hrs-900^{o}C isothermal heated 8YSZ powder as the reference sample. The scale shows that increasing the V_2O_5 concentration in the samples reduces the lightness and yellowness of the samples as shown with the isothermal heated 8YSZ sample having the highest L* and b* values while the sample with 10wt.% V_2O_5 shows the lowest colour scale value for lightness and yellowness out of all the samples. The redness of the samples however increases with increase in V_2O_5 concentration as shown in Tab. 4.1; sample with 10wt.% V_2O_5 has the highest a* value while the sample with 2wt.% V_2O_5 has the lowest. The isothermal heated 8YSZ sample portrays greenness with a negative measured a* value. The colour scale for powder sample with 10wt.% V_2O_5 also shows that with increase in isothermal heating time, there is reduction in lightness and yellowness of the sample but increase in redness of the sample. This is shown in the colour scale for the sample at 2hrs and 100hrs of isothermal heating.

4.2.2 XRD Analysis

Figures 4.3-4.4 show the XRD analysis of the effect of varying V_2O_5 concentration in vanadium-induced hot corrosion of 8YSZ powder sample subjected to 900^{o}C isothermal heating for 100hrs. Fig. 4.3(i) represents the XRD spectra of 900^{o}C isothermal heated 8YSZ powder; zero concentration of the V_2O_5. The spectra which are similar to that of the as-received 8YSZ powder spectrum Fig. 4.3(i-a), indicate the presence of only the monoclinic (PDF card number 01-037-

1484) and tetragonal (PDF card number 01-070-4431) zirconia phases identified with PDXL-2 software. The intensities of each phase peaks remain constant throughout the 100hrs isothermal heating period as shown in the spectra. Fig. 4.3(ii) shows the XRD spectra for hot corrosion test of 8YSZ powder in the presence of 2wt.% V_2O_5 concentration. The hot corrosion spectra unlike those of the isothermal heated 8YSZ powder sample, aside the zirconia peaks; indicate the presences of peaks corresponding to YVO_4 compound (PDF card number 01-074-1172). The sample indicates the presences of YVO_4 peaks and monoclinic zirconia peaks at 2θ values which are hitherto not in the as-received 8YSZ powder XRD spectrum within few minutes of isothermal heating. It also indicates major increment of the monoclinic zirconia peaks; (111) and ($\bar{1}$, 1, 1) planes and decrease in the tetragonal zirconia peak; (101) plane intensities within 2hrs, which remain almost constant throughout the remaining heating period. The XRD spectra for hot corrosion test sample with increased concentration of V_2O_5 (5% wt. 8YSZ) are shown in Fig. 4.4(i). It depicts the same trend with that of sample with 2wt.% V_2O_5; presence of the YVO_4 peaks and monoclinic zirconia peaks in new 2θ values but of higher intensities at early minutes of isothermal heating. The sample aside showing the new peaks, also shows increase in m-ZrO_2 peaks; (111) and ($\bar{1}$, 1, 1) planes intensities and corresponding decrease in that of t-ZrO_2 peak; (101) plane with the m-ZrO_2 peaks outgrowing the t-ZrO_2 peak at 100hrs. Fig. 4.4(ii) is the XRD spectra for 8YSZ powder sample with 10wt.% V_2O_5; it has almost exactly the same features with sample of 5wt.% V_2O_5 concentration. However unlike it, the t-ZrO_2 peak; (101) plane intensity reduces to zero at 50hrs of isothermal heating and has peaks of higher intensities.

Plots of m-ZrO_2 volumetric fraction against time for the samples using equation 4.1 are shown in Fig. 4.5. The values for M_1, M_2 and T are from the samples XRD spectra in Figs. 4.3-4.4. The

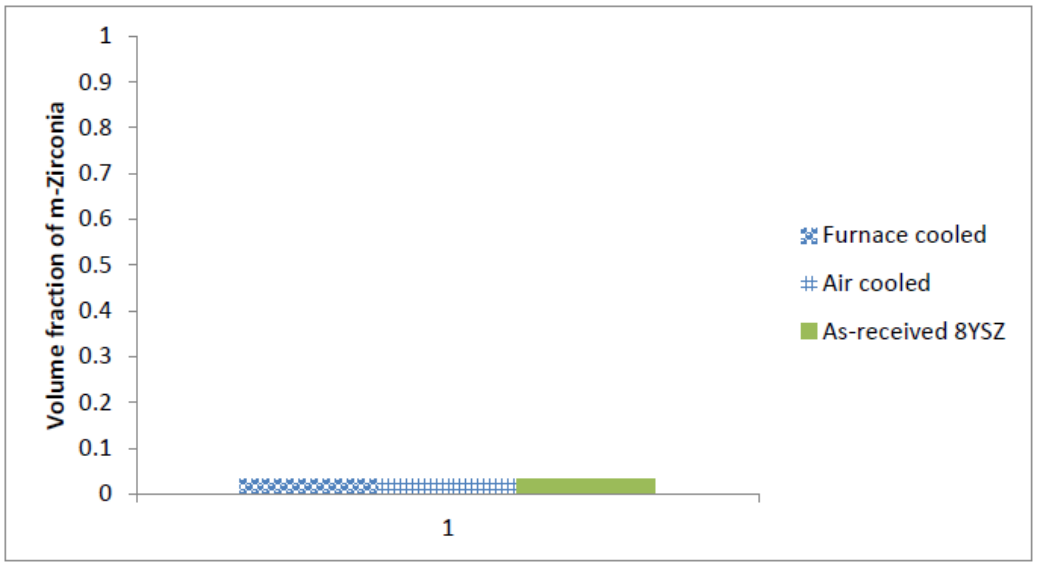

(i)

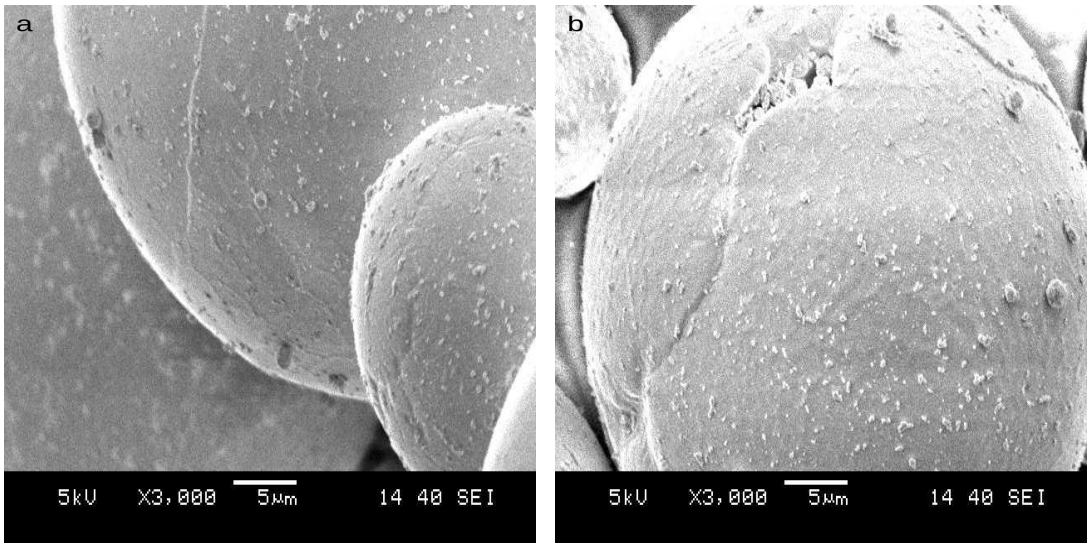

(ii)

Figure 4.1: (i) Monoclinic zirconia volume fraction bar chart on effect of isothermal heating on 2hrs-900^{o}C isothermal heated 8YSZ powder, (ii) SEM micrographs of 2hrs-900^{o}C isothermal heated 8YSZ powder. (a) Furnace cooled sample, (b) Laboratory air cooled sample .

graph indicates highest volume fraction of m-ZrO_2 in the sample with 10wt.% V_2O_5 throughout the heating period as compared to other samples. The 10wt.% V_2O_5 concentration sample shows huge m-ZrO_2 volume fraction within 2hrs of heating and attains a unit value at 50hrs isothermal heating. The isothermal heated 8YSZ powder sample shows the least volume fraction and those samples with intermediate V_2O_5 concentrations (2% wt. and 5% wt. 8YSZ) depicts m-ZrO_2 volume fraction which lies between these two extremes, with higher amount in the sample with 5wt.% V_2O_5. The plots show that major transformation of t-ZrO_2 phase occurred in the early isothermal heating time. The XRD spectra and rate of tetragonal zirconia transformation plots indicate that high V_2O_5 concentration produces huge degradation of the 8YSZ powder and that V_2O_5 causes vanadium-induced hot corrosion of 8YSZ ceramic topcoat in TBCs.

4.2.3 SEM and EDS Analyses

SEM micrographs of powder particles of the as-received 8YSZ and that of its 900^oC isothermal heated mixture samples with varying V_2O_5 concentration at 100hrs are shown in Fig. 4.6. Fig. 4.6(ii-a) shows smooth-face spherical shaped powder particles of the as-received 8YSZ powder. The dominant presence of these smooth-face particles in the as-received 8YSZ powder spectrum is shown in Fig. 4.6(i-a), which is an SEM of it taken at lower magnification. The SEM micrographs of the isothermal heated 8YSZ powder are shown in Figs. 4.6(i-b) and 4.6(ii-b); it is a resemblance of the as-received 8YSZ powder particles. It shows that no changes occurred in the morphology of the powder particles with isothermal heating of the 8YSZ powder for 100hrs in absence of V_2O_5 powder. The EDX analysis of the smooth-face spherical shaped powder particles is shown Fig.4.7. The spectra A, B and C indicate evenly elemental distribution of zirconium, oxygen and yttrium in the particles which is the expected elemental distribution for a

yttria-stabilized zirconia. Figs. 4.6i(c-e) and 4.6ii(c-e) represent the micrographs of the powder particles for vanadium-induced hot corrosion 8YSZ powder samples with varying concentration of V_2O_5; 2%, 5% and 10% wt. of 8YSZ respectively. It shows a complete transformation of the smooth-face spherical morphology of the as-received 8YSZ particles to rough-face spherical shaped particles; however the degree of roughness of the particles increases with increase in the V_2O_5 concentration. The rough-face particles comprise a mixture of an irregular and facet shaped structures as shown in Figure 4.6(c-e). The clearer composition of the rough-face spherical shaped particles; irregular and facet shaped structures are shown in the backscatter/secondary SEM micrograph taken at higher magnification as shown in Fig. 4.8(a). The analysis of these rough-face particles using the backscatter image and EDS analysis in Fig. 4.7; spectra F and G, indicate the irregular shape structures as zirconium and oxygen rich structures. The facet shaped structures indicate high presence of yttrium, vanadium and oxygen elements; spectrum D and E. The richness of the irregular shaped structures in zirconium and oxygen elements without yttrium which is different from the elemental distribution of the as-received 8YSZ powder particles portrays these structures as the monoclinic zirconia phase. However the presence of majorly the yttrium element with vanadium in the facet shaped structures depicts it as the YVO_4 compound formed from the reaction between Y_2O_3 and V_2O_5 as shown in the XRD spectra.

4.2.4 X-ray Mapping Analysis

X-ray mapping analysis of the rough-face spherical shaped particles in vanadium-induced samples is shown in Fig. 4.8(b). It shows elemental distribution of oxygen, zirconium, yttrium and vanadium in the particles. The evenly distribution of all the four element in these particles validates the XRD, SEM and EDS results that portray the rough-face particles as composition of

new phases formed from zirconium, yttrium, vanadium and oxygen elements. The monoclinic zirconia phase muddled up with YVO_4 compound.

4.3 MgO-inhibition of Vanadium-induced Hot Corrosion of 8YSZ Powder with V_2O_5 concentration (10% wt.8YSZ)

4.3.1 Colour Spectrum Analysis

The colour appearance of powder samples at 100hrs of 900^oC isothermal heating hot corrosion and MgO-inhibitive hot corrosion tests is shown in Fig. 4.9. The inhibitive hot corrosion samples are 8YSZ powder samples with varying molar concentration ratio of MgO to V_2O_5 powders (M_{MgO}/M_{V2O5}). The sample of M_{MgO}/M_{V2O5}=5, Fig. 4.9(g) looks whitish and is almost a resemblance of the isothermal heated 8YSZ sample, Fig. 4.9(a) while the sample of M_{MgO}/M_{V2O5}=3, Fig. 4.9(f) appears light yellowish in colour. The sample of M_{MgO}/M_{V2O5}=2, Fig. 4.9(e) portrays a dark yellowish appearance but not as dark yellowish as that of sample with M_{MgO}/M_{V2O5}=1, Fig. 4.9(d). The vanadium-induced hot corrosion sample, Fig. 4.9(b-c) looks brownish and is closer in colour appearance to the sample with M_{MgO}/M_{V2O5}=1. Thus the higher the M_{MgO}/M_{V2O5} in the sample the closer the sample colour to that of isothermal heated 8YSZ powder and the lower the M_{MgO}/M_{V2O5} the closer colour of the sample to that of vanadium-induced hot corrosion sample.

The colour scale for samples in Fig. 4.9 is shown in Tab. 4.2 with 100hrs-900^oC isothermal heated 8YSZ powder as the reference sample. The colour scale like in colour appearance shows the sample of M_{MgO}/M_{V2O5}=5 closer to the isothermal heated 8YSZ in terms of lightness, greenness and yellowness. The lightness and greenness of the samples however reduce with

reduction in M_{MgO}/M_{V2O5} but yellowness increases, thus sample of M_{MgO}/M_{V2O5}=3 is lighter and of less redness compared to sample with M_{MgO}/M_{V2O5}=2. Likewise the sample of M_{MgO}/M_{V2O5}=2 is lighter and of less redness compared to sample with M_{MgO}/M_{V2O5}=1. The colour scale also shows that the lower the M_{MgO}/M_{V2O5} in the sample the closer the lightness, redness and yellowness of the sample to that of vanadium-induced hot corrosion sample as shown in Tab. 4.2.

4.3.2 XRD Analysis

Figures 4.10-4.11 show the XRD analysis portraying the effectiveness of using MgO powder in mitigating vanadium–induced hot corrosion of 8YSZ powder mixture with V_2O_5 concentration (10% wt. 8YSZ). The spectra represent 900^oC isothermal heated samples of 8YSZ powder mixture samples with varying MgO/V_2O_5 molar concentration (M_{MgO}/M_{V2O5}). Fig. 4.10(i) shows the XRD spectra for sample of M_{MgO}/M_{V2O5}=1 between 2hrs to 100hrs. It further shows the inhibitive hot corrosion spectra peaks deviating from that of the as-received 8YSZ powder spectrum, with additional peaks indicating presence of YVO_4 and MgV_2O_6 compounds (PDF card number 00-034-0013). The sample spectra indicate the growth of YVO_4 and m-ZrO_2 in new 2θ positions in the early minutes of the inhibitive hot corrosion test as shown in spectrum for 2hrs. The sample likewise indicates consequential increase in the intensities of m-ZrO_2; (111) and ($\bar{1}$, 1, 1) plane peaks and that of t-ZrO_2; (101) plane peak growing vice versa. The spectra for sample with M_{MgO}/M_{V2O5}=2 are shown in Fig. 4.10(ii). It bears almost the same resemblance with that of Fig. 4.10(i), aside the presence of $Mg_2V_2O_7$ (PDF card number 01-070-1163) instead of MgV_2O_6 and reduced rate of change in intensities of m-ZrO_2 and t-ZrO_2 peaks. Figure 4.11(i) depicts XRD spectra for sample of M_{MgO}/M_{V2O5}=3, just like with earlier mentioned XRD

analysis; m-ZrO_2 and t-ZrO_2 peaks are present in the spectra. However unlike that of Fig. 4.10 inhibitive spectra, the presence of the YVO_4 peaks are only noticeable after 50hrs isothermal heating and its intensity is minute. The consequential change in m-ZrO_2; (111) and $(\bar{1}, 1, 1)$ and t-ZrO_2; (101) plane peaks intensities are also of minute magnitudes and $Mg_3V_2O_8$ compound (PDF card number 01-073-0207) peaks are present in the spectra as only the magnesium vanadate compound. $Mg_3V_2O_8$ compound is the expected magnesium vanadate compound from the reaction between MgO and V_2O_5 with M_{MgO}/M_{V2O5}=3. Figure 4.11(ii) depicts the spectra for sample of M_{MgO}/M_{V2O5}=5; it shows the presence of m-ZrO_2, t- ZrO_2 and $Mg_3V_2O_8$ phases only. The m-ZrO_2 and t-ZrO_2 peaks intensities also remain almost constant throughout the 100hrs isothermal heating process just like that of the as-received 8YSZ powder spectrum.

The amount of tetragonal zirconia transformation against time plots using equation 4.1 for the MgO-inhibitive hot corrosion, vanadium-induced hot corrosion and isothermal heated 8YSZ powder samples are shown in Fig.4.12. The MgO-inhibitive hot corrosion test plots contain that of 8YSZ mixture samples with M_{MgO}/M_{V2O5} equal 1, 2, 3 and 5 respectively. The data for the plots are obtained from the XRD spectra in Figs.4.10-4.11, 4.3(i) and 4.4(ii) respectively. The m-ZrO_2 volume fraction is highest in the plot for vanadium-induced hot corrosion 8YSZ sample which is closer to that of sample with M_{MgO}/M_{V2O5}=1 plot. The isothermal heated 8YSZ sample plot has the least volume fraction of m-ZrO_2 followed by that of sample of M_{MgO}/M_{V2O5}=5. The plots for samples with M_{MgO}/M_{V2O5} equal 2 and 3 fall in between that of samples with M_{MgO}/M_{V2O5} equal 1 and 5 respectively, with that of 3 next to 5 and that of 2 next to 1.

Figure 4.2: Colour appearance of vanadium-induced 8YSZ powder samples with varying concentration of V_2O_5 at 900^oC isothermal heating. (a) Isothermal heated 8YSZ at 100hrs, (b) 2hrs isothermal heated 8YSZ+10wt.%V_2O_5 powder sample, (c) 100hrs isothermal heated 8YSZ+10wt.%V_2O_5 powder sample, (d) 100hrs isothermal heated 8YSZ+2wt.%V_2O_5 powder sample, (e) 100hrs isothermal heated 8YSZ+5wt.%V_2O_5 powder sample

Table 4.1: Color scale of 8YSZ powder with varying V_2O_5 concentration hot corrosion samples at 900^oC isothermal heating

Powder samples with varying V_2O_5 concentration	L*	a*	b*	dL*	da*	db*
8YSZ at 100hrs	79.86	-2.74	13.49	79.86	-2.74	13.49
8YSZ+ V_2O_5 (10% wt. 8YSZ) at 2hrs	42.98	10.32	17.44	-36.88	13.05	3.95
8YSZ + V_2O_5 (10% wt. 8YSZ) at 100hrs	42.02	17.99	11.43	-37.84	20.73	-2.06
8YSZ + V_2O_5 (5% wt. 8YSZ) at 100hrs	60.03	6.23	38.79	-19.83	8.96	25.30
8YSZ + V_2O_5 (2% wt. 8YSZ) at 100hrs	65.61	4.73	39.78	-14.25	7.47	26.29

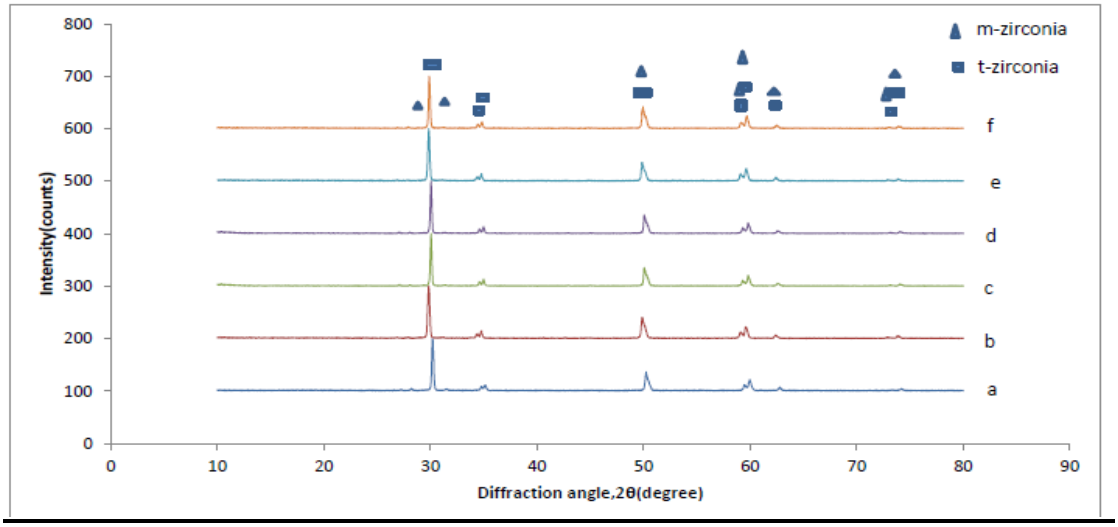

(i)

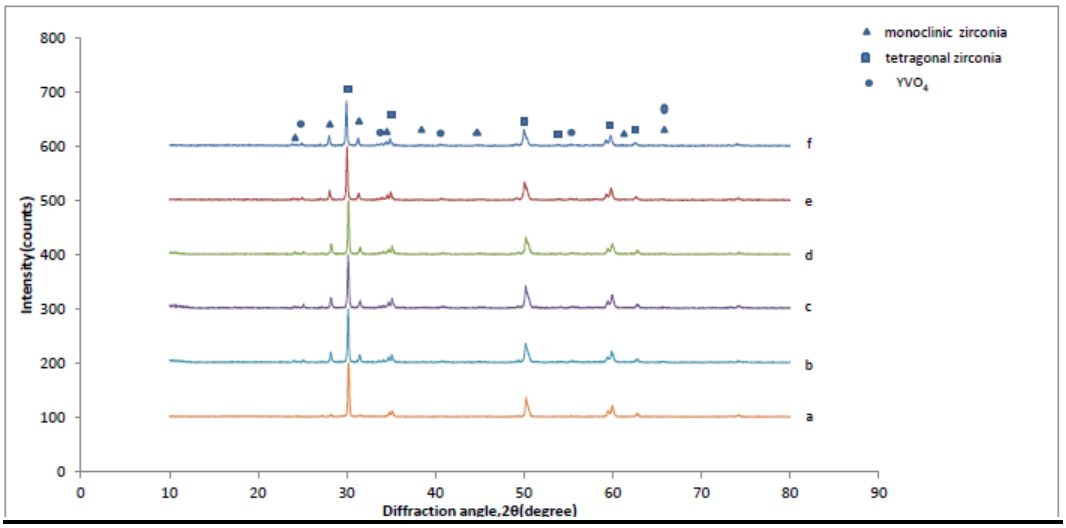

(ii)

Figure 4.3: XRD analysis spectra (i) 900^{o}C isothermal heated 8YSZ, (ii) 900^{o}C isothermal heated 8YSZ powder sample with V_2O_5 concentration (2% wt. 8YSZ). (a) As-received 8YSZ, (b) 2hrs isothermal heating, (c) 5hrs isothermal heating, (d) 20hrs isothermal heating , (e) 50hrs isothermal heating, (f) 100hrs isothermal heating

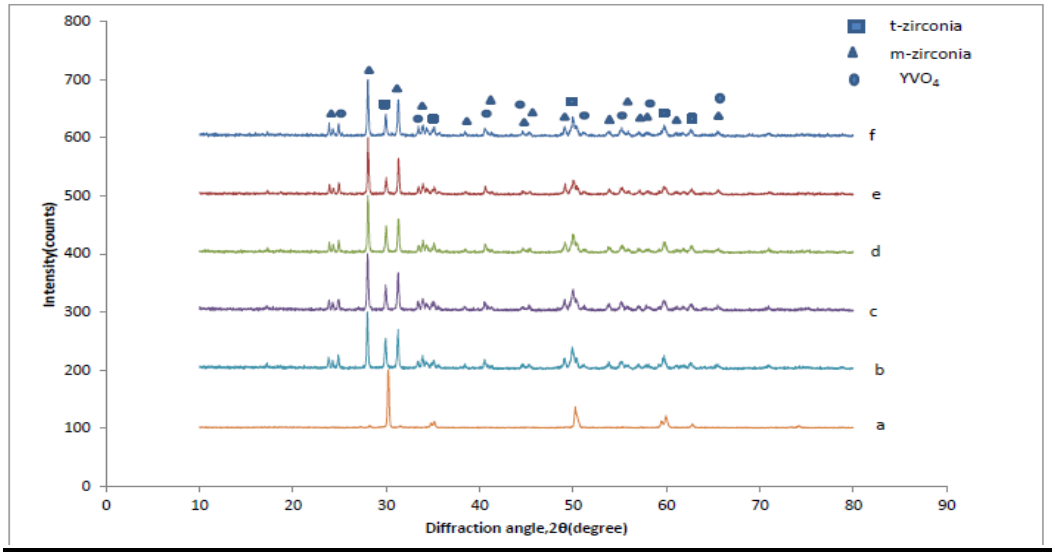

(i)

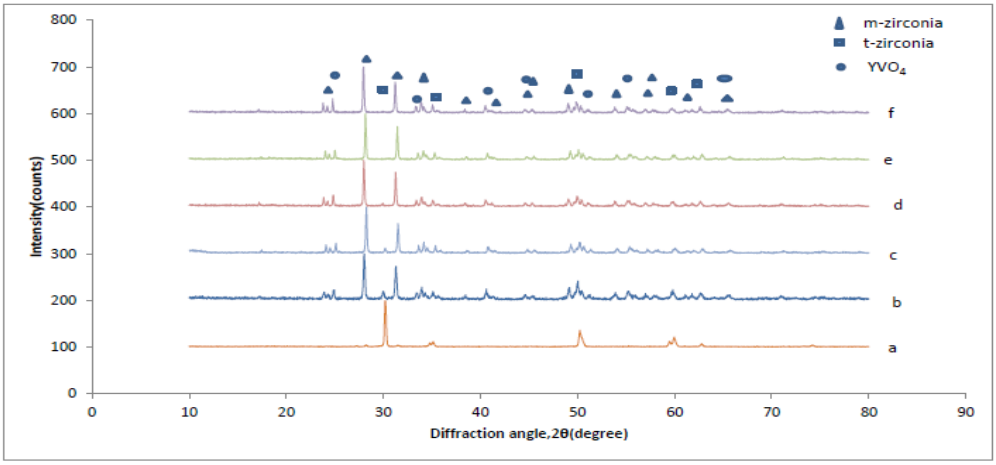

(ii)

Figure 4.4: XRD analysis spectra (i) 900^{o}C isothermal heated 8YSZ powder sample with V_2O_5 concentration (5% wt. 8YSZ), (ii) 900^{o}C isothermal heated 8YSZ powder sample with V_2O_5 concentration (10% wt. 8YSZ). (a) As-received 8YSZ, (b) 2hrs isothermal heating, (c) 5hrs isothermal heating, (d) 20hrs isothermal heating, (e) 50hrs isothermal heating, (f)100hrs isothermal heating

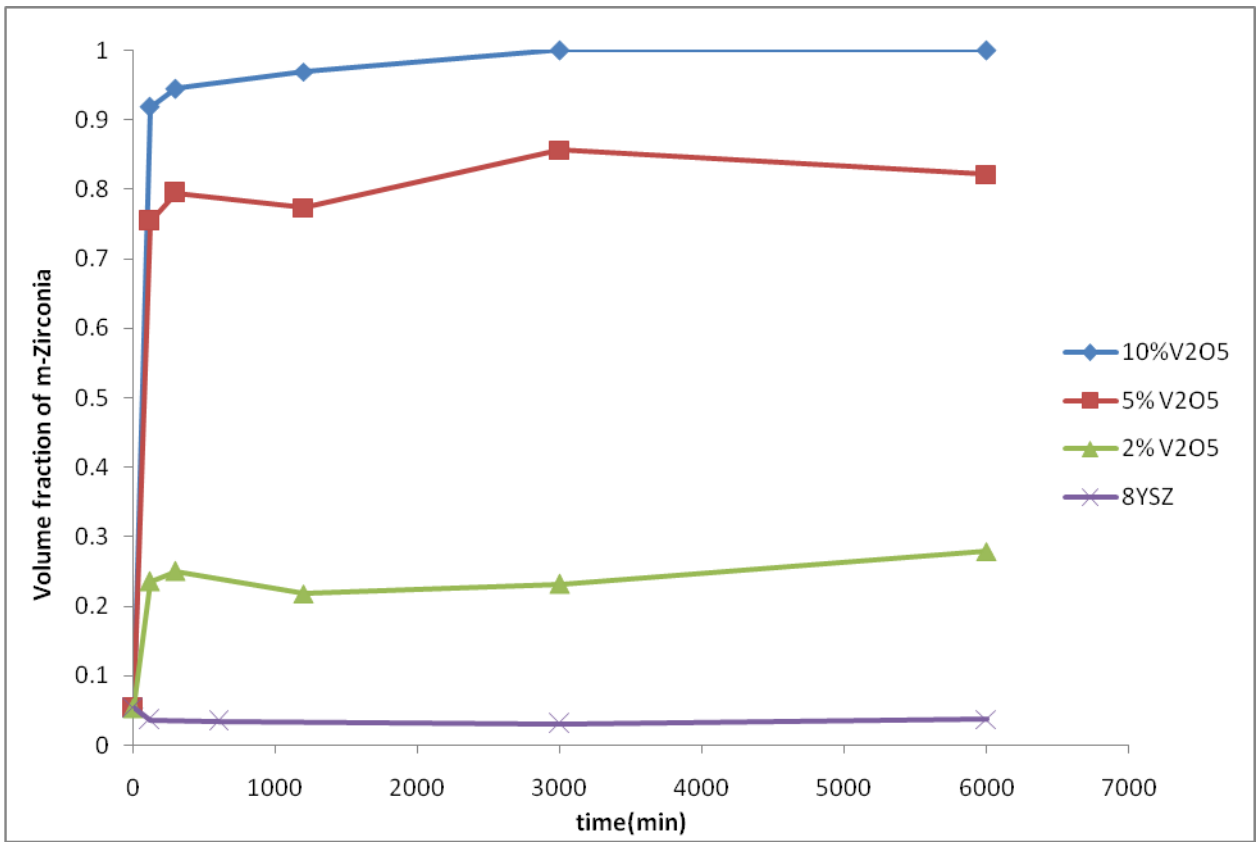

Figure 4.5: Amount of tetragonal-zirconia phase transformation against time for vanadium-induced hot corrosion 8YSZ powder samples with varying V_2O_5 concentration at 900^{o}C isothermal heating. (8YSZ) 8YSZ powder, (2% V2O5) 8YSZ+V_2O_5 (2% wt. 8YSZ) powder sample, (5%V2O5) 8YSZ+V_2O_5 (5% wt. 8YSZ) powder sample , (10%V2O5) 8YSZ+V_2O_5(10% wt. 8YSZ) powder sample

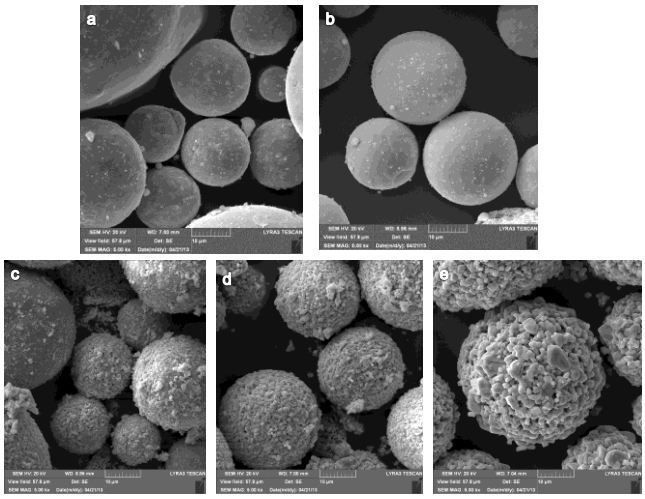

(i)

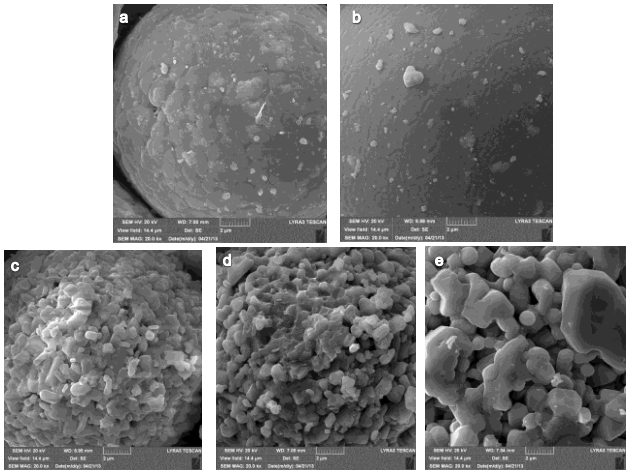

(ii)

Figure 4.6: SEM micrographs of 100hrs-900^{o}C isothermal heated as-received 8YSZ powder and its mixture samples with varying concentration of V_2O_5. (i) Lower Magnification, (ii) Higher Magnification. (a) As-received 8YSZ, (b) Isothermal heated 8YSZ, (c) 8YSZ+V_2O_5 (2% wt. 8YSZ), (d) 8YSZ+V_2O_5 (5% wt. 8YSZ), (e) 8YSZ+V_2O_5 (10% wt. 8YSZ)

a

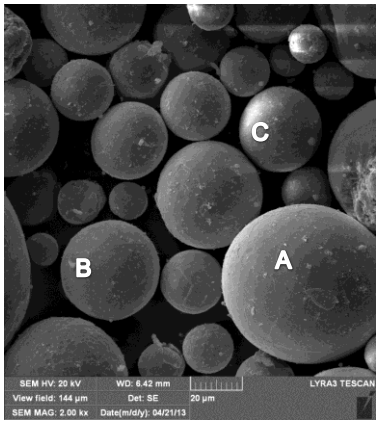

b

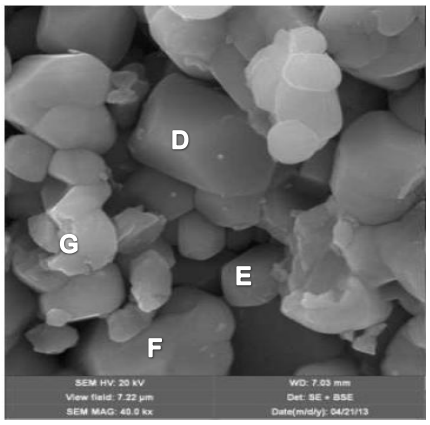

Spectrum	O	Y	V	Zr	Total
A	22.9	3.7	0.0	73.4	100.0
B	26.1	4.7	0.0	69.2	100.0
C	18.6	5.3	0.0	76.1	100.0
D	11.3	37.3	29.2	22.2	100.0
E	20.9	25.3	32.3	21.5	100.0
F	21.7	0.0	1.1	77.2	100.0
G	31.9	0.0	1.9	66.2	100.0

Figure 4.7: EDS analysis. (a) Smooth-face spherical shaped powder particles, (b) Rough-face spherical shaped powder particles

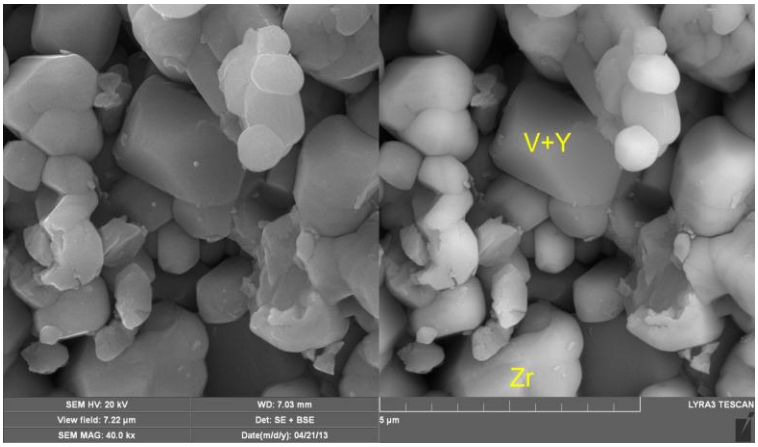

(a)

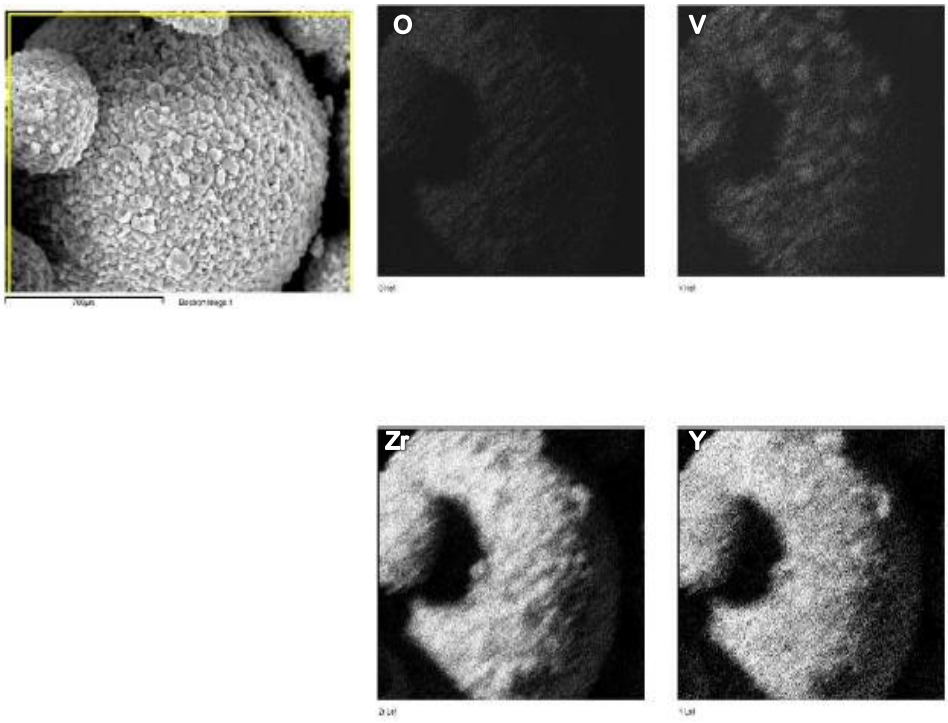

(b)

Figure 4.8: (a) Backscatter/Secondary SEM micrograph of rough-face spherical shaped powder particles, (b) X-ray mapping analysis of rough-face spherical shaped powder particles (Vanadium-induced hot corrosion sample)

4.3.3 SEM Analysis

Figure 4.13(i-ii) are SEM micrographs of powder particles for 900^{o}C isothermal heating of 8YSZ powder, vanadium-induced hot corrosion 8YSZ powder with 10wt.% V_2O_5 and MgO-inhibitive hot corrosion 8YSZ powder samples at 100hrs. The micrographs in Fig. 4.13-ii(a-b) show isothermal heated 8YSZ and vanadium-induced hot corrosion 8YSZ powder samples at 100hrs respectively. Figs. 4.13-i(a) and 4.13-ii(c) represent micrographs for the inhibitive test sample with M_{MgO}/M_{V2O5}=1. It shows the smooth-face spherical shaped particles of the as-received 8YSZ powder have turned into rough-face spherical particles; a mixture of bar-shape and irregular structures, Fig. 4.14. The micrographs in Fig. 4.13-i(b) and 4.13-ii(d) represent the inhibitive test sample with M_{MgO}/M_{V2O5}=2. It shows the presence of the rough-face and few smooth-face spherical shaped particles. Although the rough-face spherical shaped particles in this sample are similar to those in the sample of M_{MgO}/M_{V2O5}=1, however the dominance of these particles in the sample is lesser as shown in Fig. 4.13-ii(b). Ridge-face spherical shaped particles are what the as-received 8YSZ powder particles changed to in inhibitive test samples with M_{MgO}/M_{V2O5} equal 3 and 5 at 100hrs. This is shown in Fig. 4.13-ii(e-f) and its dominant presence in the samples is shown in Fig. 4.13-i(c-d). Aside these spherical shaped particles, lump-shaped structures either attached to the surface of the spherical particles or not; also appear in the SEM micrographs of the inhibitive test samples with M_{MgO}/M_{V2O5} equal 2, 3 and 5 respectively.

4.3.4 EDS Analysis

Elemental distribution analysis in the powder particles for MgO-inhibitive hot corrosion powder samples using EDS are shown in Figures 4.14-4.15. The bar shaped structures in the rough-face

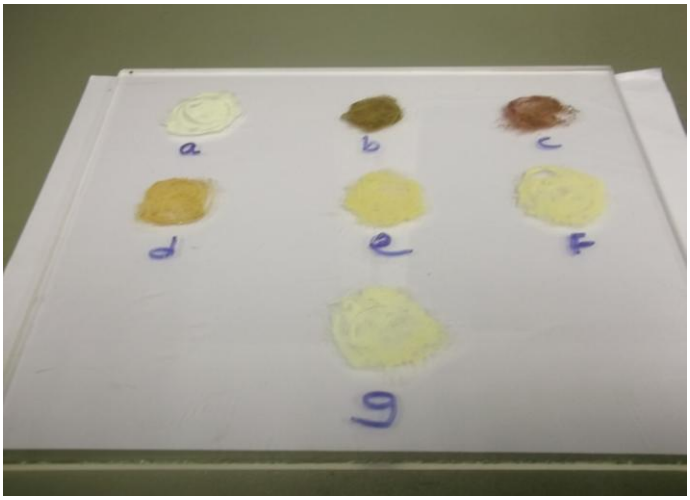

Figure 4.9: MgO-inhibitive vanadium-induced hot corrosion 8YSZ powder samples with varying MgO/V_2O_5 molar concentration (M_{MgO}/M_{V2O5}) colour spectrum at 900^oC isothermal heating. (a) Heated 8YSZ at 100hrs, (b) Vanadium-induced hot corrosion 8YSZ at 2hrs, (c) Vanadium-induced hot corrosion 8YSZ at 100hrs, (d) 8YSZ mixture sample of M_{MgO}/M_{V2O5}=1 at 100hrs, (e) 8YSZ mixture sample of M_{MgO}/M_{V2O5}=2 at 100hrs, (f) 8YSZ mixture sample of M_{MgO}/M_{V2O5}=3 at 100hrs, (g) 8YSZ mixture sample of M_{MgO}/M_{V2O5}=5 at 100hrs

Table 4.2: Colour scale of MgO-inhibitive vanadium-induced hot corrosion 8YSZ powder samples with varying MgO/V_2O_5 molar concentration (M_{MgO}/M_{V2O5}) at 100hrs-900^oC isothermal heating

Powder sample particles at 100hrs	L*	a*	b*	dL*	da*	db*
8YSZ	78.97	-3.17	16.17	78.97	-3.17	16.17
8YSZ + V_2O_5 (10% wt. 8YSZ)	34.19	22.14	22.19	-44.78	25.31	6.02
8YSZ +MgO (M_{MgO}/M_{V2O5} =1) + V_2O_5 (10% wt. 8YSZ)	57.11	15.09	39.61	-21.87	18.26	23.44
8YSZ+ MgO (M_{MgO}/M_{V2O5} =2) + V_2O_5 (10% wt. 8YSZ)	69.75	6.73	38.30	-9.22	9.91	22.13
8YSZ + MgO (M_{MgO}/M_{V2O5} =3) + V_2O_5 (10% wt. 8YSZ)	73.90	1.40	28.99	-5.07	4.57	12.82
8YSZ + MgO (M_{MgO}/M_{V2O5} =5) + V_2O_5 (10% wt. 8YSZ)	78.32	-1.70	16.44	-0.65	1.47	0.27

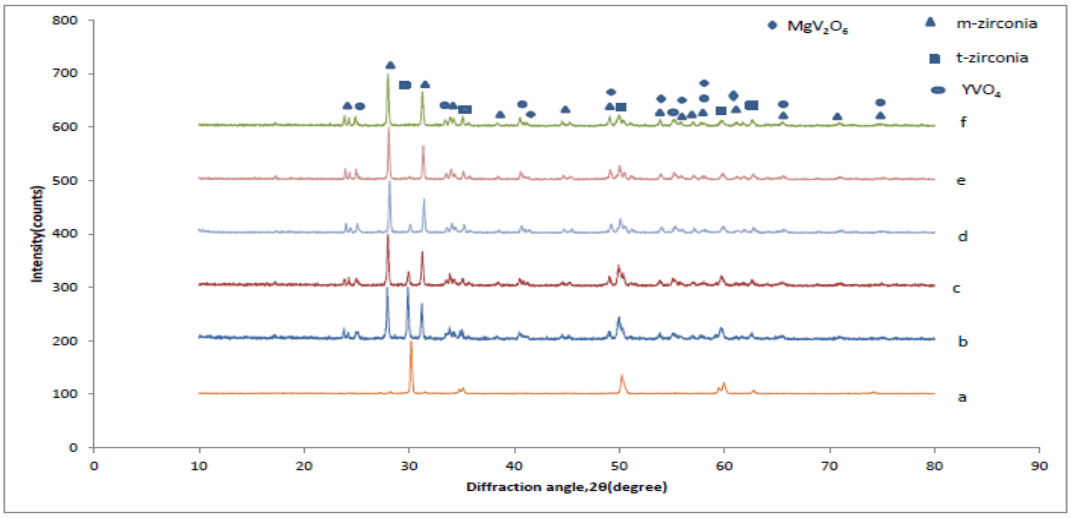

(i)

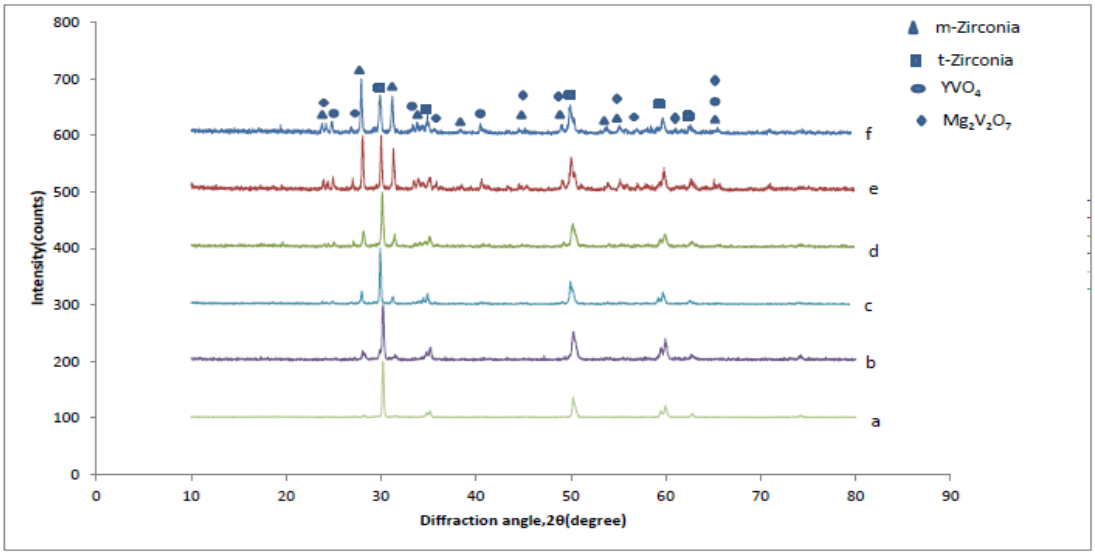

(ii)

Figure 4.10: (i) XRD analysis of MgO-inhibitive vanadium-induced hot corrosion 8YSZ powder sample with MgO/V_2O_5 molar concentration (M_{MgO}/M_{V2O5}) equals 1 at 900^{o}C isothermal heating, (ii) XRD analysis of MgO-inhibitive vanadium-induced hot corrosion 8YSZ powder sample with MgO/V_2O_5 molar concentration (M_{MgO}/M_{V2O5}) equals 2 at 900^{o}C isothermal heating. (a) As-received 8YSZ, (b) 2hrs heating, (c) 5hrs heating, (d) 20hrs heating, (e) 50hrs heating, (f) 100hrs heating

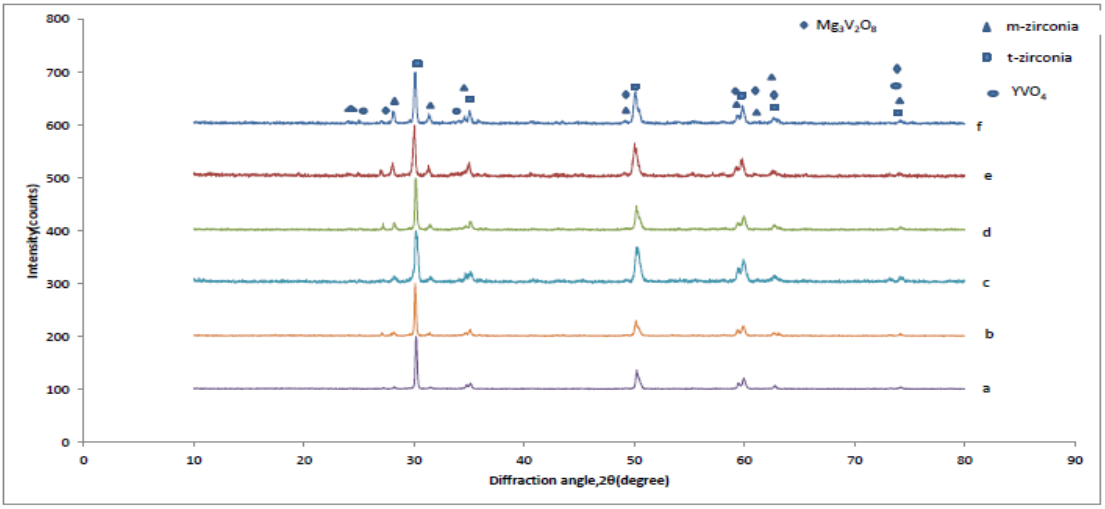

(i)

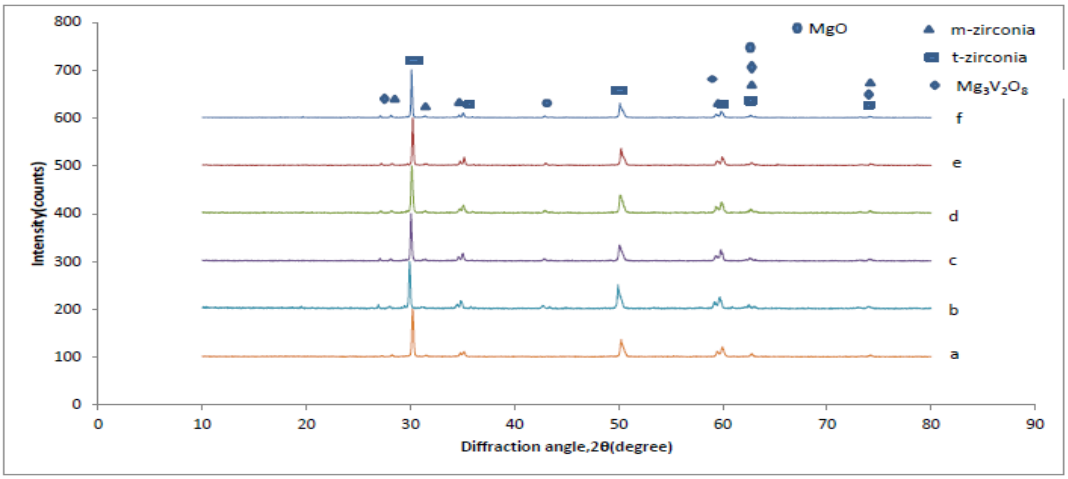

(ii)

Figure 4.11:(i) XRD analysis of MgO-inhibitive vanadium-induced hot corrosion 8YSZ powder sample with MgO/V_2O_5 molar concentration (M_{MgO}/M_{V2O5}) equals 3 at 900^{o}C isothermal heating, (i) XRD analysis of MgO-inhibitive vanadium-induced hot corrosion 8YSZ powder sample with MgO/V_2O_5 molar concentration (M_{MgO}/M_{V2O5}) equals 1 at 900^{o}C isothermal heating. (a) As-received 8YSZ, (b) 2hrs heating, (c) 5hrs heating, (d) 20hrs heating, (e) 50hrs heating, (f) 100hrs heating

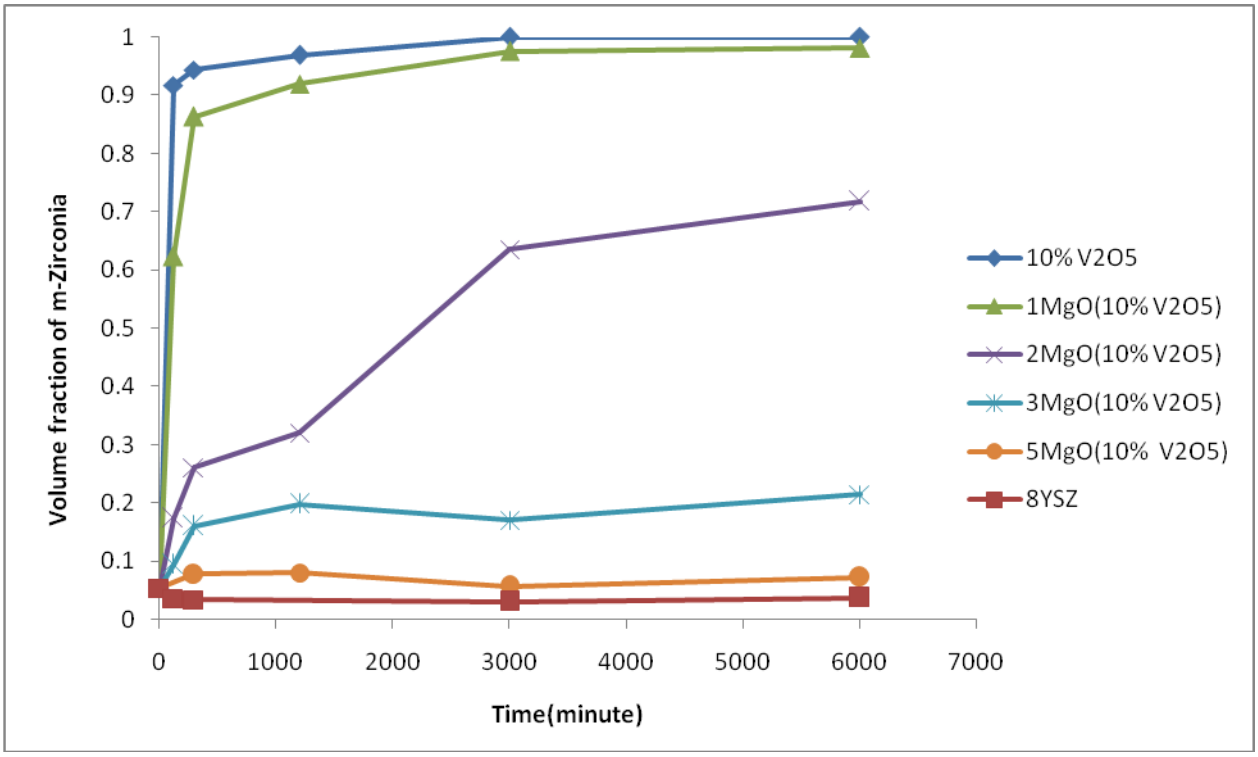

Figure 4.12: Amount of tetragonal zirconia phase transformation against time for MgO-inhibitive vanadium-induced hot corrosion 8YSZ powder samples at 900^{o}C isothermal heating. (8YSZ) Isothermal heated 8YSZ powder sample, (5MgO(10% V2O5)) 8YSZ sample with M_{MgO}/M_{V2O5}=5, (3MgO(10% V2O5)) 8YSZ sample with M_{MgO}/M_{V2O5}=3, (2MgO(10% V2O5)) 8YSZ sample with M_{MgO}/M_{V2O5}=2, (1MgO(10% V2O5)) 8YSZ sample with M_{MgO}/M_{V2O5}=1, (10% V2O5) 8YSZ+V_2O_5 (10% wt. 8YSZ)

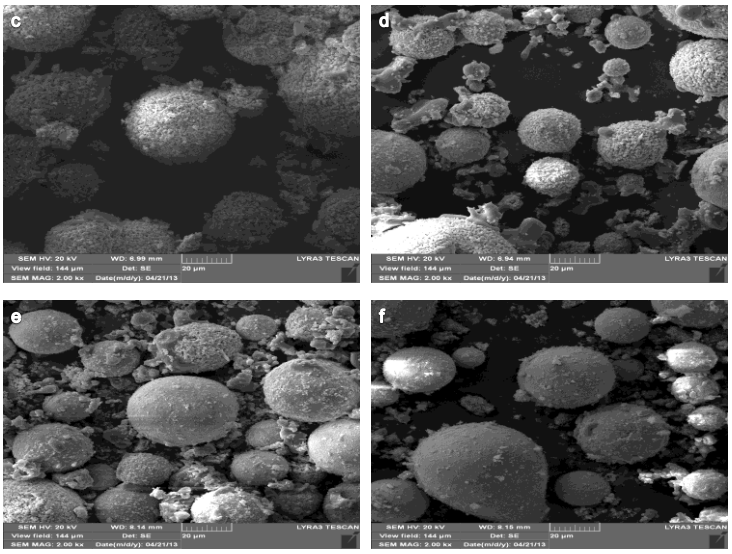

(i)

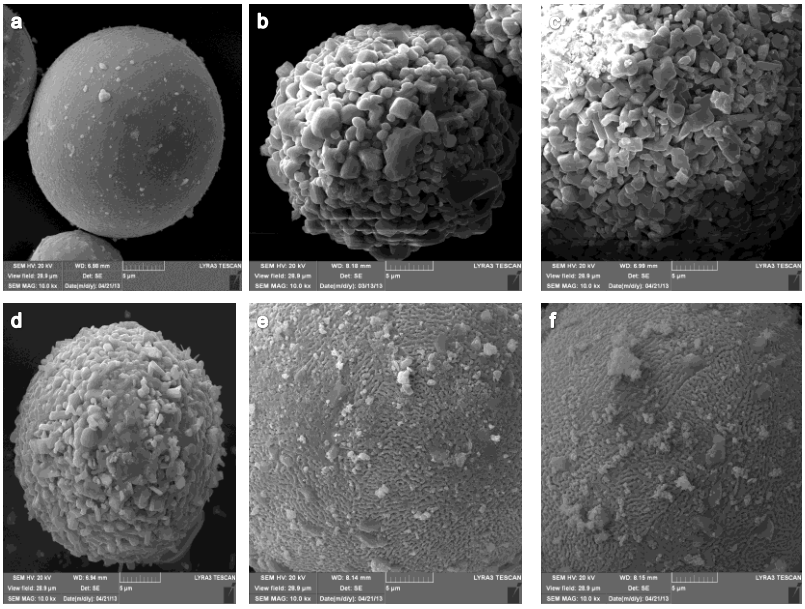

(ii)

Figure 4.13: SEM micrographs of MgO-inhibitive vanadium-induced hot corrosion 8YSZ powder samples with varying MgO/V_2O_5 molar concentration ratio at 100hrs-900^oC isothermal heating. (a) Heated 8YSZ, (b) Vanadium-induced hot corrosion 8YSZ sample (V_2O_5=10% wt. 8YSZ), (c) Sample with M_{MgO}/M_{V2O5} =1, (d) Sample with M_{MgO}/M_{V2O5}=2, (e) Sample with M_{MgO}/M_{V2O5}=3, (f) Sample with M_{MgO}/M_{V2O5}=5

spherical particles as shown in Fig. 4.14 in spectra A and B have large weight composition of zirconium and oxygen elements, but yttrium that is supposed to be distributed along the same trend with the zirconium is absent. The bar structures as seen growing out of the spherical shaped particles is the m-ZrO_2 from t-ZrO_2 transformation due to the reaction of the yttria stabilizer. The spectra C and D in the same Fig. 4.14 indicate large weight composition of vanadium, yttrium and oxygen elements in the irregular shaped structures. These structures can be seen as YVO_4 structures formed from the reaction between the yttria stabilizer and V_2O_5. The lump-like structures show large weight concentration of magnesium, vanadium and oxygen elements as seen in spectra E and F in Fig. 4.14 and spectra B and C in Fig. 4.15 respectively. The lump structures depict magnesium vanadate compounds formed from the reaction between MgO and V_2O_5. The ridge-face spherical shaped particles as shown in the powder samples with M_{MgO}/M_{V2O5} equal 3 and 5 contain large weight composition of zirconium, yttrium and oxygen elements as shown in spectrum A in Fig. 4.15. It indicates the presence of the yttrium element with the zirconium; this portrays these structures as yttria stabilized zirconia phase in line with the XRD analysis for these samples. It is worthy of note that the suggestion of compounds formed based on concentration of elements present in the powder particles is in-line with the XRD analysis were such compound peaks have been identified in the samples.

4.3.5 X-ray mapping analysis

X-ray mapping elemental analysis of the powder particles in MgO-inhibitive hot corrosion samples is shown in Fig. 4.16. It shows elemental distribution in the smooth-face, ridge-surface, rough-face spherical shaped and lump shaped powder particles. Like in the EDS analysis, the lump shaped particles indicate high presence of magnesium, vanadium and oxygen elements as shown in Fig. 4.16. It validates the earlier statement that these structures are magnesium

vanadate compounds formed from the reaction between MgO and V_2O_5. In Fig. 4.16(b), the smooth-face and ridge-face spherical shaped particles depict yttria stabilized zirconia phase due to high evenly distributed concentration of zirconium, yttrium and oxygen elements. The rough-face spherical shaped particles as shown from previous SEM and EDS analysis; mixture of the bar like and irregular shape structures indicate evenly dominance of the Zr, Y, V and O elements. This is shown in Fig. 4.16(a). It depicts the presence of monoclinic zirconia phase with the YVO_4 compound muddle together in the rough-face spherical shaped particles. Like earlier mentioned for the EDS analysis, suggestion of compounds based on elemental distribution is based on the XRD analysis and expected products from such powder samples combination.

4.4 MgO-inhibition of Vanadium-induced Hot Corrosion of 8YSZ powder with lower V_2O_5 concentration (5% wt. 8YSZ)

4.4.1 Colour Spectrum Analysis

Figure 4.17 and Table 4.3 show the colour spectrum analysis of powder particles at 100hrs-900^oC isothermal heating for 8YSZ+V_2O_5(5% wt. 8YSZ)+MgO samples; with MgO-V_2O_5 molar concentration ratios equal 2, 3 and 5 respectively. Figure 4.17(a) represents isothermal heated 8YSZ powder particles showing a whitish colour appearance and the brownish powder particles in Fig. 4.17(b) are vanadium-induced 8YSZ particles with V_2O_5 concentration (5% wt. 8YSZ). The MgO-inhibitive sample of M_{MgO}/M_{V2O5}=5, Fig. 4.17(e) portrays a whitish colour appearance almost similar to the heated 8YSZ powder. However sample of M_{MgO}/M_{V2O5}=3, Fig. 4.17(d) shows a yellowish colour particles and that of sample with M_{MgO}/M_{V2O5}=2, Fig. 4.17(c) appears dark yellowish which is closer in colour to the vanadium-induced 8YSZ sample. Colour scale of the powder samples is shown in Tab. 4.3.

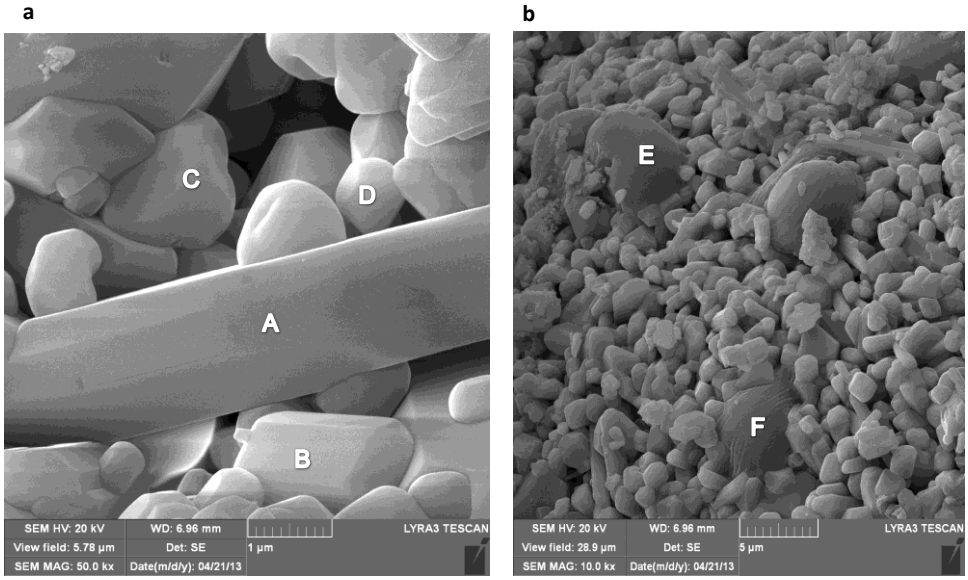

Spectrum	O	Mg	Y	V	Zr	Total
A	26.0	0.0	0.0	1.0	73.0	100.0
B	32.4	0.1	0.0	1.5	66.0	100.0
C	22.3	0.3	28.2	17.2	31.9	100.0
D	16.2	0.0	5.2	3.5	75.1	100.0
E	33.4	29.3	0.0	37.3	0.0	100.0
F	27.7	21.5	0.0	48.1	2.7	100.0

Figure 4.14: EDS analysis of MgO-inhibitive vanadium-induced hot corrosion samples. (a) Rough-face spherical shaped particles, (b) Lump shaped powder particles

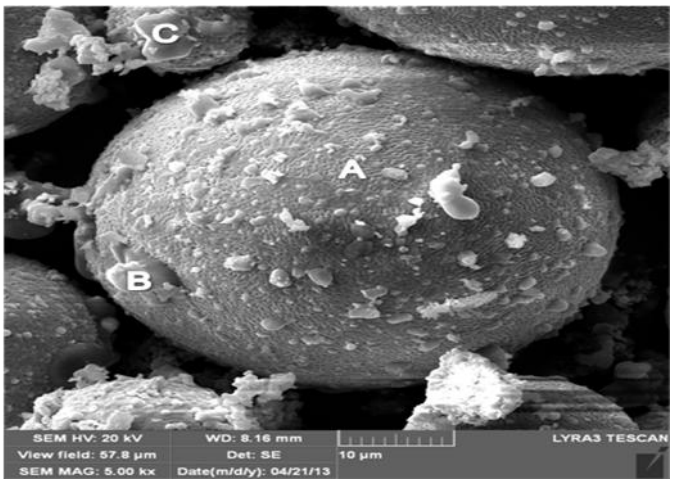

Spectrum	O	Mg	Y	V	Zr	Total
A	39.4	1.2	3.1	0.7	55.7	100.0
B	45.3	30.2	0.0	23.0	1.6	100.0
C	37.5	27.2	0.4	24.8	10.1	100.0

Figure 4.15: EDS analysis of Ridge-face spherical shaped powder particles in MgO-inhibitive vanadium-induced hot corrosion samples

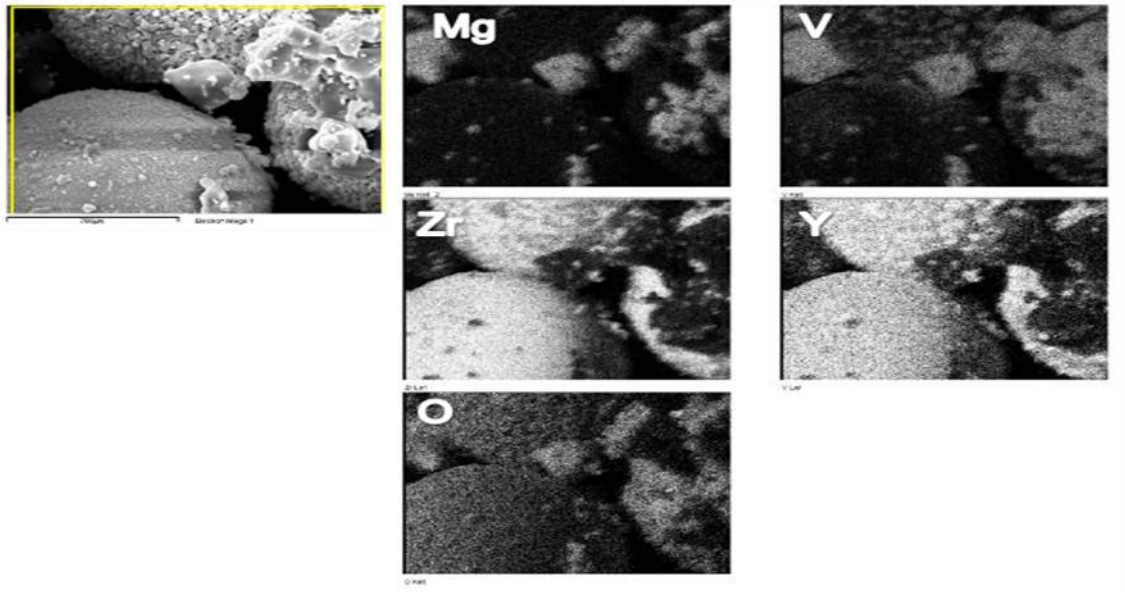

(a)

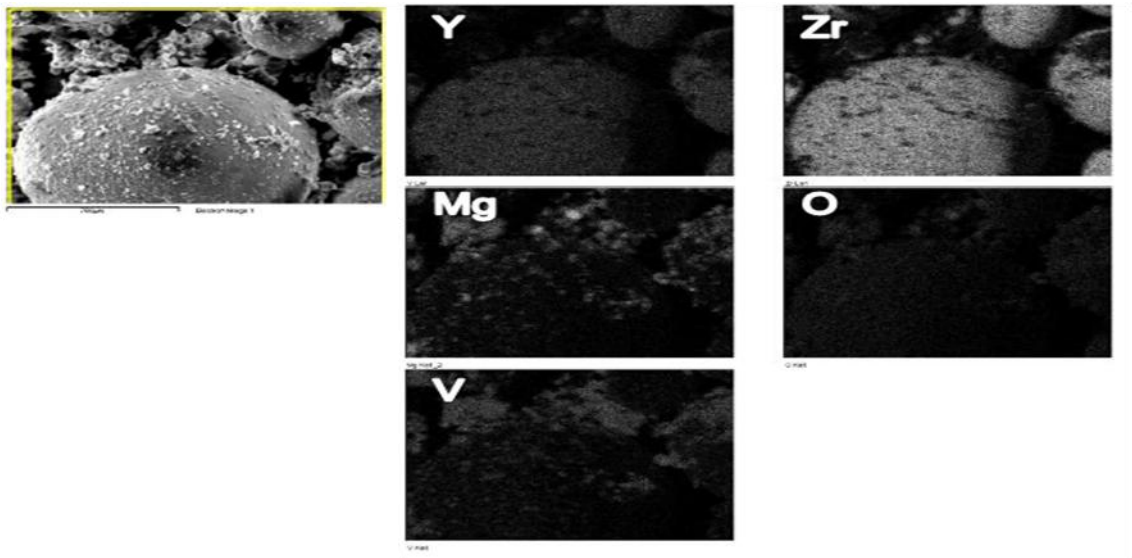

(b)

Figure 4.16: (a) X-ray mapping elemental analysis of MgO-inhibitive vanadium-induced hot corrosion sample (Smooth-face spherical, rough-face spherical and lump shaped particles), (b) X-ray mapping elemental analysis of MgO-inhibitive vanadium-induced hot corrosion sample (Ridge-face spherical shaped and lump shaped particles)

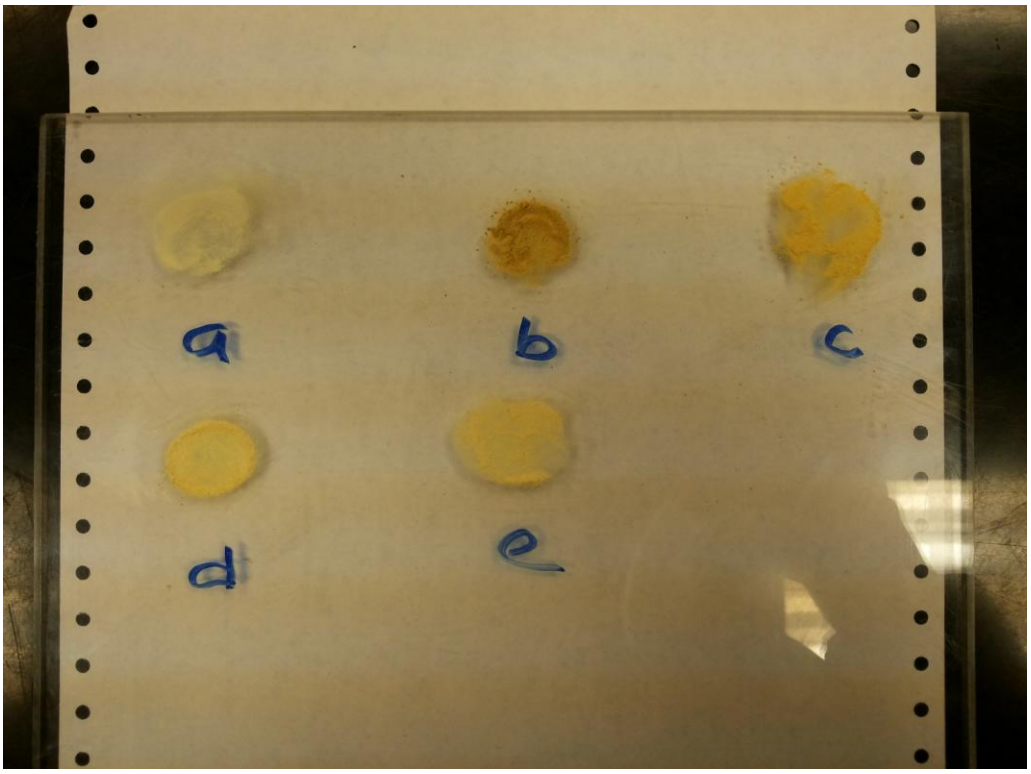

Figure 4.17: Physical colour appearance of powder particles for the MgO-inhibitive hot corrosion samples at 100hrs-900^{o}C isothermal heating. (a) Heated 8YSZ, (b) Vanadium-induced hot corrosion 8YSZ, (c) 8YSZ powder sample (M_{MgO}/M_{V2O5} =2), (d) 8YSZ powder sample (M_{MgO}/M_{V2O5} =3), (e) 8YSZ powder sample (M_{MgO}/M_{V2O5} =5)

Table 4.3: Colour scale of MgO-inhibitive vanadium-induced hot corrosion of 8YSZ+V_2O_5 (5% wt. 8YSZ)+MgO samples with varying M_{MgO}/M_{V2O5}

Powder particles at 100hrs-900^{o}C isothermal heating	L*	a*	b*	dL*	da*	db*
8YSZ	80.72	-2.11	16.63	80.72	-2.11	16.63
8YSZ + V_2O_5 (5% wt. 8YSZ)	60.03	6.23	38.79	-19.83	8.96	25.30
8YSZ + MgO (M_{MgO}/M_{V2O5} =2) + V_2O_5 (5% wt. 8YSZ)	75.16	9.03	41.81	-5.55	11.15	25.18
8YSZ + MgO (M_{MgO}/M_{V2O5} =3) + V_2O_5 (5% wt. 8YSZ)	79.88	3.81	23.37	-0.84	5.92	16.74
8YSZ+MgO (M_{MgO}/M_{V2O5} =5) +V_2O_5(M_{MgO}/M_{V2O5} =5) (5% wt. 8YSZ)	79.27	-1.27	19.90	-1.45	0.84	3.27

Sample of M_{MgO}/M_{V2O5}=5 shows proximity in lightness, greenness and yellowness to the isothermal heated 8YSZ which is the reference sample. Although decrease in M_{MgO}/M_{V2O5} of the MgO-inhibitive samples reduces the lightness, however the redness and yellowness of the samples increases. Hence, sample with M_{MgO}/M_{V2O5}=3 is lighter and of lower redness and yellowness compared to sample with M_{MgO}/M_{V2O5}=2, while the vanadium-induced 8YSZ shows the least lightness and highest redness and yellowness compared to other samples.

4.4.2 XRD Analysis

MgO-inhibition of vanadium-induced hot corrosion of 8YSZ powder in the presence of lower V_2O_5 concentration (5% wt. 8YSZ) portrays the same trend as with that of higher V_2O_5 concentration (10% wt. 8YSZ). This is shown in XRD analysis in Fig. 18. The XRD spectra for sample of M_{MgO}/M_{V2O5}=2, shows the same trend with that of sample with the same M_{MgO}/M_{V2O5} but with different V_2O_5 concentration (10% wt. 8YSZ). The XRD analysis as shown in Fig. 4.18(i) indicates the growth of YVO_4 and new monoclinic zirconia peaks within few minutes of 900^{o}C isothermal heating as shown by the XRD spectra. The XRD spectra also show consequential increase and decrease in the intensities of the monoclinic zirconia; ($\bar{1}$, 1, 1) and (111) planes and tetragonal zirconia; (101) plane peaks respectively. $Mg_2V_2O_7$ peaks also appear in the inhibitive hot corrosion spectra as the expected magnesium vanadate compound. Though the inhibitive samples have the same features, but the magnitude of these features in sample with V_2O_5 concentration (5% wt. 8YSZ), is not as intense compared to that of the sample with V_2O_5 concentration (10% wt. 8YSZ), Fig. 4.10(b) considering the effect of V_2O_5 concentration in hot corrosion of 8YSZ. The XRD spectra of samples with increased M_{MgO}/M_{V2O5} to 3 and 5 are shown in Figure 4.18(ii-iii) respectively. The spectra just like for sample with high V_2O_5

concentration and of the same M_{MgO}/M_{V2O5}, Fig. 11 show constant intensities for the tetragonal and monoclinic zirconia phase peaks for the sample with M_{MgO}/M_{V2O5}=5. Although the sample with M_{MgO}/M_{V2O5}=3 shows minute traces of YVO_4 compound in the inhibitive XRD spectra after several hours of 900^{o}C isothermal heating, however both XRD analyses show the presence of $Mg_3V_2O_8$ peaks in the inhibitive spectra. The amount of tetragonal zirconia transformation plots for the MgO-inhibitive vanadium-induced hot corrosion samples with lower V_2O_5 concentration (5% wt. 8YSZ) using equation 4.1 are shown in Fig. 4.19. The data for the plots are obtained from the XRD spectra in Figs. 4.18, 4.3(i) and 4.4(i). The plots portray the same trend as that of sample with high V_2O_5 concentration; the higher the M_{MgO}/M_{V2O5} in the sample the lower the volume fraction of the monoclinic zirconia in the sample and vice versa. Thus sample with M_{MgO}/M_{V2O5}=5 shows the lowest volume fraction of monoclinic zirconia compared to other inhibitive samples and is next to that of 900^{o}C isothermal heated 8YSZ plot. The sample with M_{MgO}/M_{V2O5}=3 shows lower volume fraction of monoclinic zirconia compared to sample with M_{MgO}/M_{V2O5}=2. The amount of tetragonal zirconia transformation plot for sample with M_{MgO}/M_{V2O5}=2 is closer to that of the vanadium-induce hot corrosion 8YSZ powder sample with V_2O_5 concentration (5% wt. 8YSZ).

4.4.3 SEM Analysis

SEM micrographs of MgO-inhibition of vanadium-induced hot corrosion of 8YSZ powder samples with lower V_2O_5 concentration (5% wt. of 8YSZ) at 100hrs-900^{o}C isothermal heating are shown in Fig. 4.20. Figure 4.20(i) represents the SEM micrographs for sample with M_{MgO}/M_{V2O5}=2, it depicts spectrum of smooth-face and rough-face spherical shaped particles. Figures 4.20(ii-iii) are micrographs for samples with M_{MgO}/M_{V2O5} equal 3 and 5 respectively.

The micrographs for both samples show huge presences of ridge-face spherical shaped powder particles. A comparison of SEM micrographs of the powder particles for MgO-inhibitive vanadium-induced hot corrosion 8YSZ powder samples for both low and high V_2O_5 concentrations (10% and 5% wt. 8YSZ) with the same M_{MgO}/M_{V2O5} are shown in Fig. 4.21. The micrographs show resemblance in the morphology of the powder particles for samples at low and high V_2O_5 concentration with the same the M_{MgO}/M_{V2O5} i.e. Fig. 4.21(i) shows samples with M_{MgO}/M_{V2O5}=2 depicting mixture of smooth-face and rough face spherical shaped particles. Likewise in Figs. 4.21(ii-iii), the micrographs for samples with M_{MgO}/M_{V2O5} equal 3 and 5 respectively shows similarity for both high and low V_2O_5 concentration samples. The micrographs show dominant presence of ridge-face spherical powder particles in all the samples.

4.5 CaO-inhibition of Vanadium-induced Hot Corrosion of 8YSZ powder with V_2O_5 concentration (10% wt. 8YSZ)

4.5.1 Colour Spectrum analysis

Figure 4.22 shows the colour appearance of the powder particles at 100hrs-900^oC isothermal heating for CaO-inhibitive vanadium-induced hot corrosion of 8YSZ powder samples. Fig 4.22(a) shows whitish colour powder particles of the isothermal heated 8YSZ powder sample at 100hrs which is the same colour as the as-received 8YSZ powder. Figs. 4.22(b) and (c) represent vanadium-induced hot corrosion sample at 2hrs and 100hrs respectively; brownish colour particles. The addition of CaO into the hot corrosion sample of 8YSZ+V_2O_5 however changes the colour from brownish to whitish or yellowish colour depending on the CaO/V_2O_5 molar concentration (M_{CaO}/M_{V2O5}).

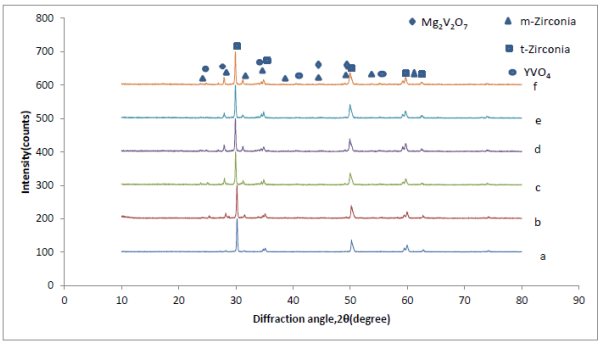

(i)

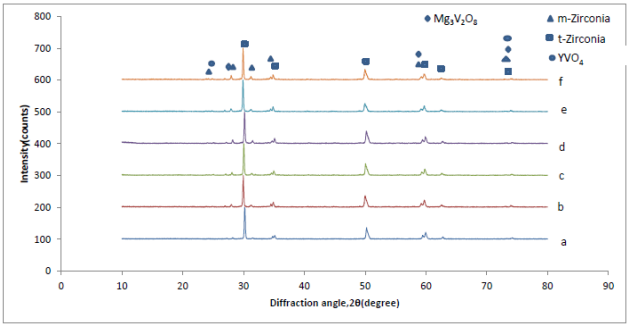

(ii)

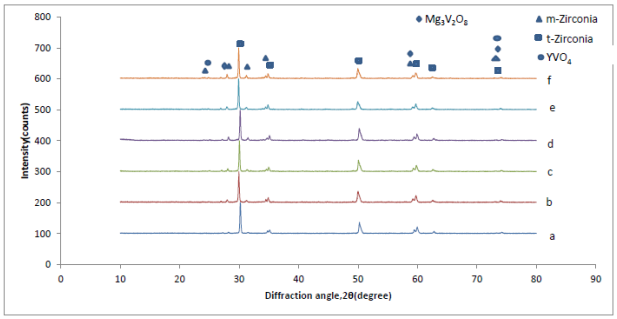

(iii)

Figure 4.18: XRD analysis of MgO-inhibitive vanadium-induced hot corrosion of 8YSZ powder samples with V_2O_5 concentration (5% wt. 8YSZ) and varying MgO/V_2O_5 molar concentration at 900^oC isothermal heating. (i) Sample with M_{MgO}/M_{V2O5}=2, (ii) Sample with M_{MgO}/M_{V2O5}=3, (iii) Sample with M_{MgO}/M_{V2O5}=5. (a) As-received 8YSZ, (b) 2hrs heating, (c) 5hrs heating, (d) 20hrs heating, (e) 50hrs heating, (f)100hrs heating.

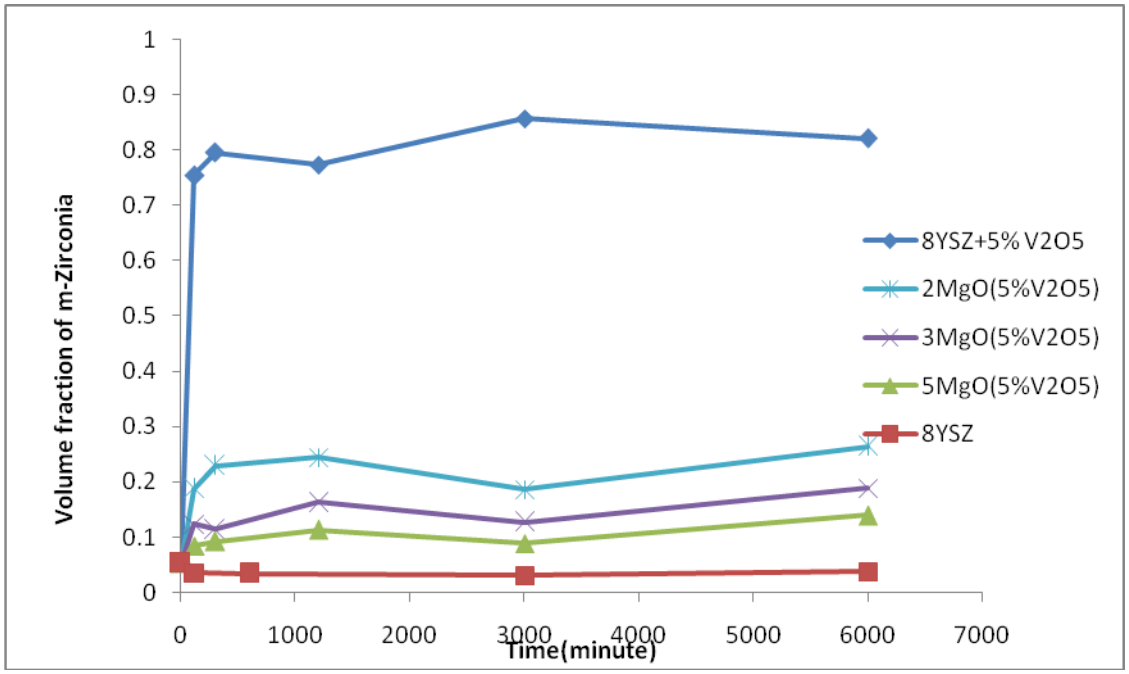

Figure 4.19: Amount of tetragonal zirconia phase transformation for MgO-inhibitive vanadium-induced hot corrosion 8YSZ powder samples at 900°C isothermal heating. (8YSZ) 8YSZ powder, (5MgO(5% V2O5)) 8YSZ sample with M_{MgO}/M_{V2O5}=5, (3MgO(5% V2O5)) 8YSZ sample with M_{MgO}/M_{V2O5}=3, (2MgO(5% V2O5)) 8YSZ sample with M_{MgO}/M_{V2O5}=2, (8YSZ+5% V2O5) 8YSZ + V_2O_5(5% wt. 8YSZ)

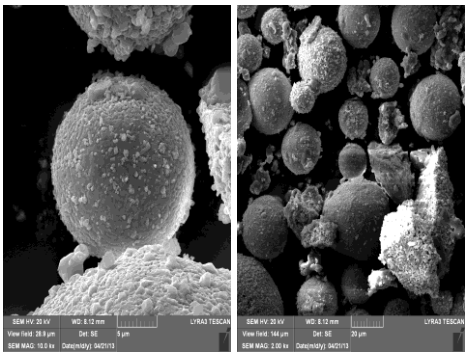

(i)

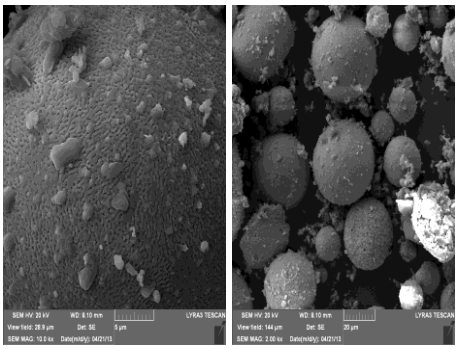

(ii)

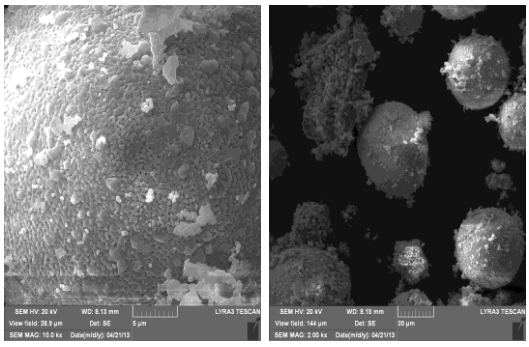

(iii)

Figure 4.20: SEM micrographs of powder particles at 100hrs-900^{o}C isothermal heating for MgO-inhibitive hot corrosion samples of 8YSZ+V_2O_5 (5% wt. 8YSZ)+MgO. (i) Sample with M_{MgO}/M_{V2O5}=2, (ii) Sample with M_{MgO}/M_{V2O5}=3, (iii) Sample with M_{MgO}/M_{V2O5}=5

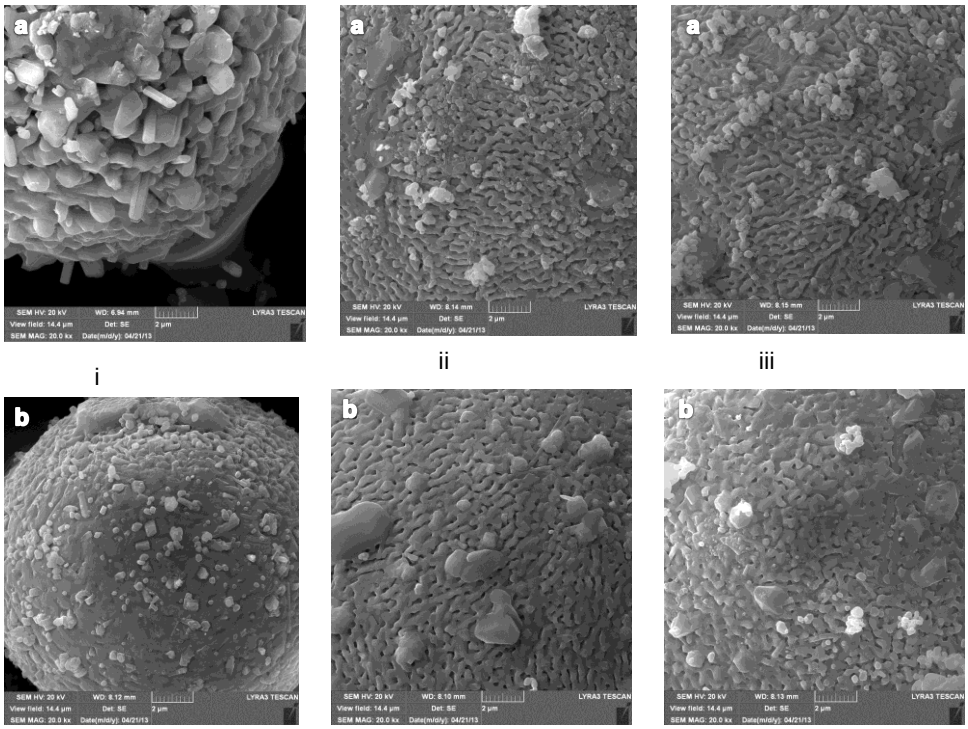

Figure 4.21: SEM micrographs comparison of powder particles at 100hrs-900^{o}C isothermal heating for MgO-inhibitive vanadium-induced hot corrosion 8YSZ powder samples with low and high V_2O_5 concentration (i) Samples with M_{MgO}/M_{V2O5}=2, (ii) Samples with M_{MgO}/M_{V2O5}=3, (iii) Samples with M_{MgO}/M_{V2O5}=5. (a) Samples of V_2O_5 concentration (10% wt. 8YSZ), (b) Samples of V_2O_5 concentration (5% wt. 8YSZ)

The sample of M_{CaO}/M_{V2O5}=1 at 100hrs shows a dark yellowish colour as shown in Fig 4.22(d). The intensity of the yellowness of the samples however reduces with increase in M_{CaO}/M_{V2O5} and ultimately to whitish colour with M_{CaO}/M_{V2O5}=5 as shown in Fig. 4.22(g). Figs. 4.22(e) and (f) represent the samples with M_{CaO}/M_{V2O5} equal 2 and 3 respectively.

The colour scale for the CaO-inhibitive samples shown in Figure 4.22 at 100hrs is shown in Table 4.4. The colour scale was measured with 100hrs-900^{o}C isothermal heated 8YSZ as the reference sample. The colour scale shows that the higher the M_{CaO}/M_{V2O5} in the sample, the closer the colour scale to that of the reference sample. The colour scale value is similar to that of MgO-inhibitive samples were also the higher the M_{MgO}/M_{V2O5} in the sample, the closer the colour scale to that of isothermal heated 8YSZ reference sample. Thus the lightness, greenness and yellowness of sample with M_{CaO}/M_{V2O5}=5 is closer in magnitude to that of the isothermal heated 8YSZ and reduction in M_{CaO}/M_{V2O5} makes the colour scale of the sample farther from the reference sample and closer the vanadium-induced hot corrosion sample. The vanadium-induced hot corrosion 8YSZ sample has the greatest deviation from the reference sample in terms of blackness, redness and yellowness.

4.5.2 XRD Analysis

XRD analyses of using CaO to inhibit vanadium-induced hot corrosion of 8YSZ powder at 900^{o}C isothermal heating are shown in Figs. 4.23-4.24. XRD spectra of CaO-inhibitive sample of M_{CaO}/M_{V2O5}=1 are shown in Fig. 4.23(i). The inhibitive spectra unlike the as-received 8YSZ powder XRD spectrum, Fig. 4.23-i(a) show new peaks indicating monoclinic zirconia, YVO_4 and CaV_2O_6 (PDF card number 00-023-0137) within few minutes of heating as shown in spectrum for 2hrs. CaV_2O_6 is the expected calcium vanadate reaction product with M_{CaO}/M_{V2O5}

equals 1. The sample spectra hence show consequential increase and decrease in the intensities of m-ZrO_2; (111) and ($\bar{1}$, 1, 1) and t-ZrO_2; (101) plane peaks respectively. Although the XRD analysis when compared to that of vanadium-induced 8YSZ sample, Fig. 4.4(ii) depicts reduced rate of change in the intensities of m-ZrO_2; (111) and ($\bar{1}$, 1, 1) and t-ZrO_2; (101) plane peaks, however the degradation of the 8YSZ powder is still obvious despite the presence of CaO. The increase in the presences of CaO in the sample to M_{CaO}/M_{V2O5}=2 further retards the changes in the intensities of the monoclinic and tetragonal peaks as seen in the XRD spectra, Fig. 4.23(i). The sample however still shows minute growth of new peaks corresponding to YVO_4 and monoclinic zirconia as shown in Fig. 4.23(ii). The presence of $Ca_2V_2O_7$ peaks (PDF card number 00-052-1478) as the CaO-V_2O_5 reaction product rather than CaV_2O_6 are also shown in the inhibitive spectra. The inhibitive spectra show resemblance of the as-received 8YSZ spectrum in terms of the intensity and phase peaks for sample with M_{CaO}/M_{V2O5}=3. The presence of $Ca_3V_2O_8$ (PDF card number 01-071-3318) is also shown in the spectra and neither the growth of new peaks indicating YVO_4 nor m-ZrO_2 appear in the spectra as seen in Fig. 4.24(i). With increase in M_{CaO}/M_{V2O5} in the sample to 5 as shown Fig. 4.24(ii), the peaks intensities of monoclinic zirconia and tetragonal zirconia remain constant throughout the inhibitive hot corrosion tests like that of sample with M_{CaO}/M_{V2O5}=3. Also like in sample with M_{CaO}/M_{V2O5}=3, neither YVO_4 peaks nor new peaks corresponding to m-ZrO_2 phase are present. The presence of $Ca_3V_2O_8$ peaks are also shown in the spectra as the expected calcium vanadate compound.

The amount of t-ZrO_2 phase transformation in the 8YSZ powder as a result of isothermal heating, vanadium-induced corrosion and CaO-inhibitive hot corrosion test with 10wt.% V_2O_5 using equation 4.1 is shown in Figure 4.25. The data for the plots are from the XRD spectra in

Figs. 4.23-4.24, 4.3(i) and 4.4(ii). The plots for isothermal exposed 8YSZ sample and the inhibitive samples with M_{CaO}/M_{V2O5} equal 3 and 5 respectively have the least values for volume fraction of m-ZrO_2 and show almost equal values for the selected periods in the test. This is in accordance with the XRD analysis where the inhibitive spectra of the samples show the same trend with that of the as-received 8YSZ spectrum. The plot for sample with M_{CaO}/M_{V2O5}=2 however shows little volume fraction of m-ZrO_2 as compared to the samples with M_{CaO}/M_{V2O5} equal 3 and 5, but lower than that of sample with M_{CaO}/M_{V2O5}=1 and vanadium-induced sample. The plot for sample with M_{CaO}/M_{V2O5}=1 indicates the presence of noticeable amount of volume fraction of the m-zirconia phase as shown in the figure 4.25. The plot for vanadium-induced hot corrosion 8YSZ sample occurs at the other extreme to the isothermal heated 8YSZ sample plot. It shows huge transformation of the tetragonal zirconia with the volume fraction of monoclinic zirconia phase attaining a unit value at 50hrs-900^oC isothermal heating.

4.5.3 SEM Analysis

SEM micrographs of isothermal heated 8YSZ, vanadium-induced 8YSZ and CaO-inhibitive samples particles at 100hrs-900^oC isothermal heating are shown in Figure 4.26. The morphology of isothermal heated 8YSZ sample as shown in previous figures is shown in Figs. 4.26(a); a smooth-face spherical shaped particles which are resemblance of the as-received 8YSZ particles. Likewise the powder particles for vanadium-induced 8YSZ sample with V_2O_5 concentration (10% wt. 8YSZ) are shown in Figure 4.26(b) for ease comparison with that of CaO-inhibitive samples. The vanadium-induced 8YSZ particles depict a rough-face spherical morphology

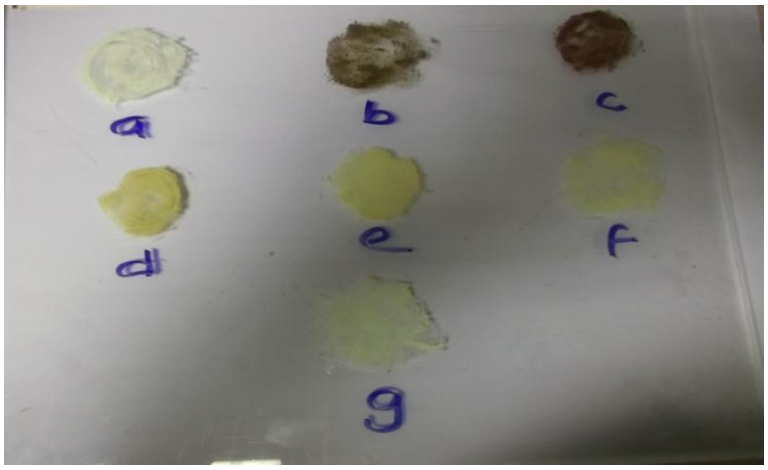

Figure 4.22: CaO-inhibitive vanadium-induced hot corrosion 8YSZ powder samples with varying CaO/V_2O_5 molar concentration (M_{CaO}/M_{V2O5}) colour appearance at 900^oC isothermal heating. (a) Isothermal heated 8YSZ at 100hrs, (b) Vanadium-induced hot corrosion sample at 2hrs, (c) Vanadium-induced hot corrosion sample at 100hrs, (d) Sample with M_{CaO}/M_{V2O5}=1 at 100hrs, (e) Sample with M_{CaO}/M_{V2O5}=2 at 100hrs, (f) Sample with M_{CaO}/M_{V2O5}=3 at 100hrs, (g) Sample with M_{CaO}/M_{V2O5}=5 at 100hrs

Table 4.4: Colour scale of powder particles for CaO-inhibitive hot corrosion samples of 8YSZ+ V_2O_5 (10% wt. 8YSZ)+CaO with varying M_{CaO}/M_{V2O5}

Powder particles at 100hrs	L*	a*	b*	dL*	da*	db*
8YSZ	79.88	-2.66	12.78	79.88	-2.66	12.78
8YSZ + V_2O_5	42.15	17.73	11.41	-37.72	20.39	-1.37
8YSZ + CaO + V_2O_5 (M_{CaO}/M_{V2O5} =1)	69.55	4.37	35.42	-10.33	7.03	22.64
8YSZ + CaO + V_2O_5 (M_{CaO}/M_{V2O5} =2)	74.28	-0.17	35.55	-5.59	2.49	22.76
8YSZ + CaO + V_2O_5 (M_{CaO}/M_{V2O5} =3)	75.41	-2.65	17.48	-4.47	0.01	4.70
8YSZ + CaO + V_2O_5 (M_{CaO}/M_{V2O5} =5)	79.77	-2.07	11.84	-0.11	0.59	-0.95

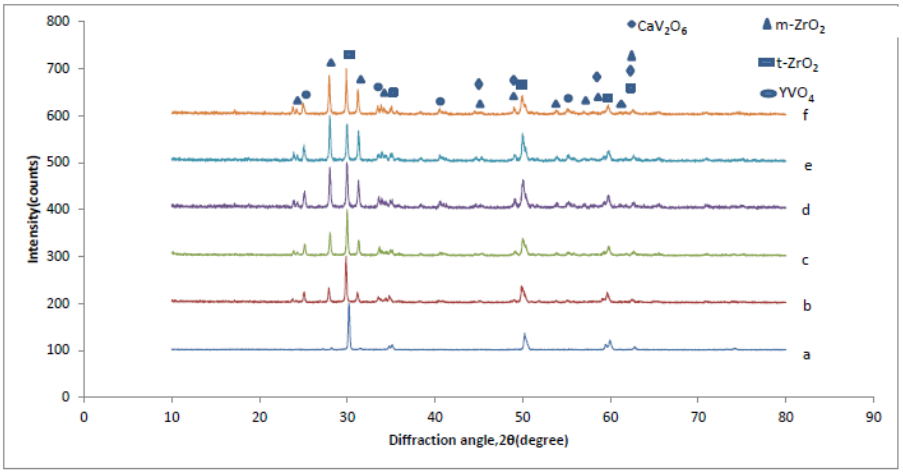

(i)

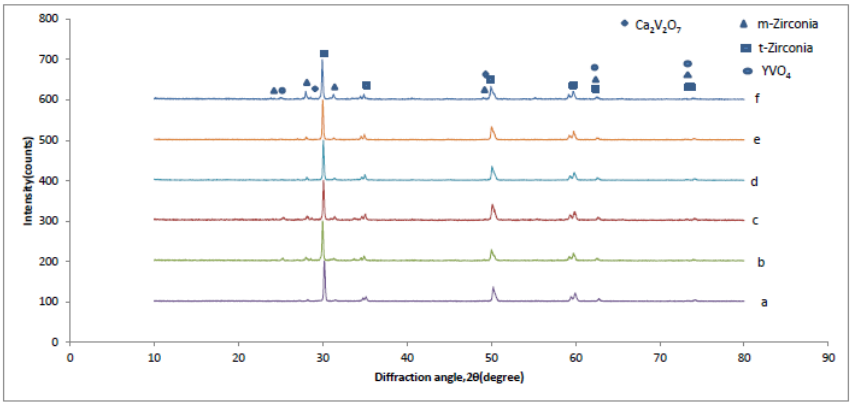

(ii)

Figure 4.23: XRD analysis of CaO-inhibitive vanadium-induced hot corrosion 8YSZ powder samples at 900°C isothermal heating. (i) Sample of M_{CaO}/M_{V2O5}=1, (ii) Sample of M_{CaO}/M_{V2O5}=2. (a) As-received 8YSZ, (b) 2hrs heating, (c) 5hrs heating, (d) 20hrs heating, (e) 50hrs heating, (f) 100hrs heating

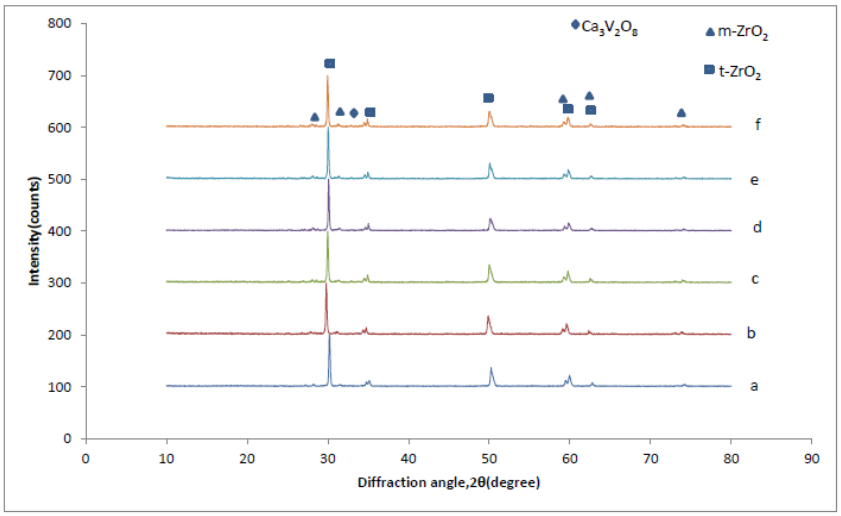

(i)

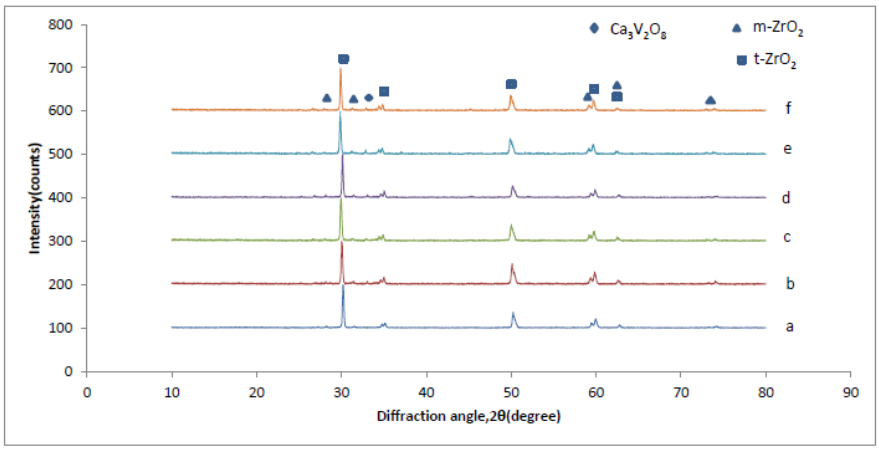

(ii)

Figure 4.24: XRD analysis of CaO-inhibitive vanadium-induced hot corrosion 8YSZ powder samples at 900^{o}C isothermal heating. (i) Sample of M_{CaO}/M_{V2O}=3, (ii) Sample of M_{CaO}/M_{V2O5}=5. (a) As-received 8YSZ, (b) 2hrs heating, (c) 5hrs heating, (d) 20hrs heating, (e) 50hrs heating, (f) 100hrs heating

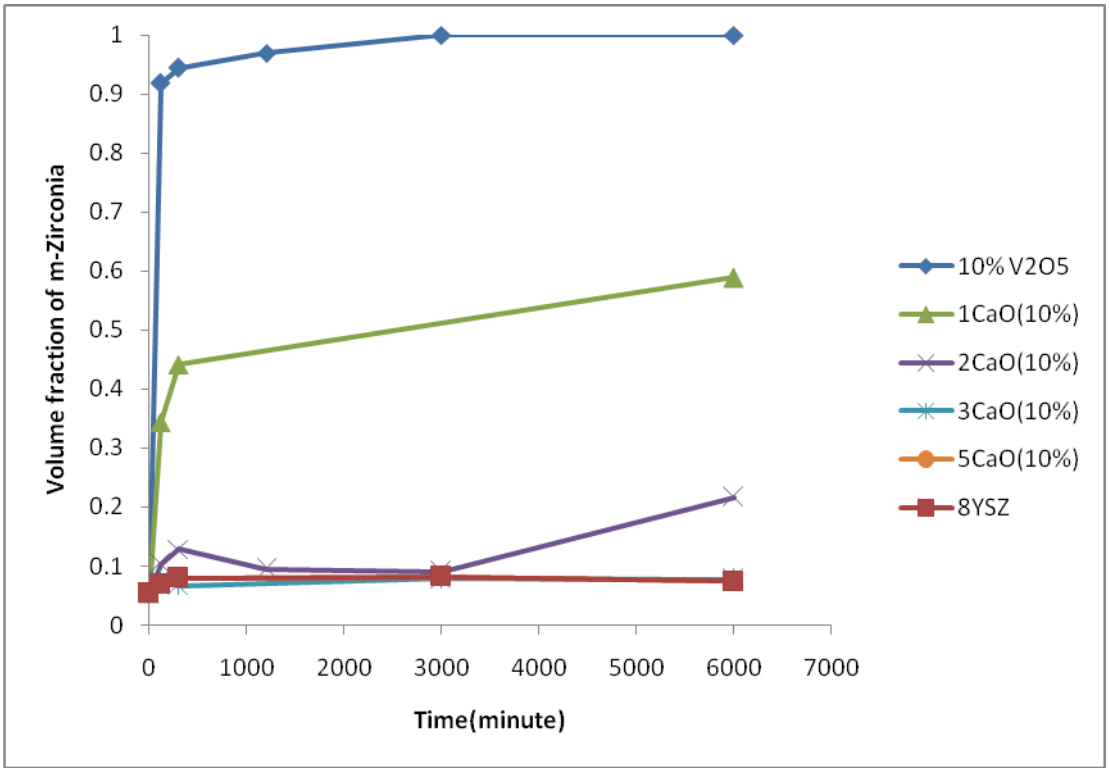

Figure 4.25: Amount of tetragonal zirconia phase transformation against time for CaO-inhibitive vanadium-induced hot corrosion 8YSZ powder samples at 900^{o}C isothermal heating. (8YSZ) 8YSZ powder, (5CaO(10% V2O5)) Sample of M_{CaO}/M_{V2O5}=5, (3CaO(10% V2O5)) Sample of M_{CaO}/M_{V2O5}=3, (2CaO(10% V2O5)) Sample of M_{CaO}/M_{V2O5}=2, (1CaO(10% V2O5)) Sample of M_{CaO}/M_{V2O5}=1, (10% V2O5) 8YSZ+ V_2O_5 (10% wt. 8YSZ)

comprising of facet and irregular structures as shown in previous SEM and EDS analyses. The rough-face spherical shaped particles are also present in CaO-inhibitive sample with M_{CaO}/M_{V2O5} equal 1 and 2 as shown in Fig. 4.26(c-d). However, the rough-face spherical shaped particles unlike that of the vanadium-induced sample comprises of bar structures muddled with irregular structures. The dominance of these irregular spherical particles is more in sample with M_{CaO}/M_{V2O5}=1 compared to that of M_{CaO}/M_{V2O5}=2, but lesser when compared to the vanadium-induced hot corrosion sample. The inhibitive samples with M_{CaO}/M_{V2O5} equal 3 and 5 depict smooth-face spherical shaped particles just like the as-received and the isothermal heated 8YSZ powder; however the particles in sample with M_{CaO}/M_{V2O5}=5 is smoother in appearance compared to that of M_{CaO}/M_{V2O5}=3; these are shown in Figs. 4.26(e-f). Fig. 4.26(d-f) aside showing the presence of an spherical morphology particles, indicate conspicuously the presences of lump-shaped structures attached to the surface of the spherical shaped particles or either as a standing alone structures.

4.5.4 EDS Analysis

EDS analysis of the spherical powder particles found in CaO-inhibitive vanadium-induced hot corrosion 8YSZ powder samples with varying CaO-V_2O_5 molar concentration at 100hrs-900^oC isothermal heating are shown in Figures 4.27-4.28. The elemental distribution analysis of the smooth-face spherical shaped particles is shown in Fig. 4.27. These particles are majorly found in inhibitive samples with M_{CaO}/M_{V2O5} equal 3 and 5 respectively; and few in samples with M_{CaO}/M_{V2O5} equal 2 and 1 respectively as shown in Fig. 4.26. The spectra B, C, D and E in Fig. 4.27 show dominant presences of Zr, Y and O elements that depict these particles as yttria stabilized zirconia. This is in accordance with the XRD spectra for these samples where the

tetragonal zirconia peaks show higher intensity relative to that of monoclinic zirconia. This further demonstrates that the inhibitive samples with M_{CaO}/M_{V2O5} equal 3 and 5 have majorly yttria stabilized zirconia particles in the sample after the inhibitive test. The lump structures show significant presence of Ca, V and O elements as shown in spectra A and F in Figs. 4.27. It portrays these structures as a reaction product between CaO and V_2O_5. These are the expected calcium vanadate compounds in the structures due to acid-base reaction. The bar structures which are common feature in the rough-face spherical shaped particles indicate large presence of Zr and O elements as shown in spectra A,B and C in Fig. 4.28. This portrays these structures as the monoclinic zirconia phase due to the absence of Y element that is supposed to be present with the Zr element. However Y element shows dominant presence with V element in the flake-like structures muddle with these bar structures as shown in spectra D, E and F in Fig. 4.28. This depicts the YVO_4 compound formed due to reaction of the stabilizer with V_2O5. Like earlier mentioned, suggestion of compound is based on correlating the EDS analysis with the XRD analysis of the samples

4.5.5 X-ray Mapping

Elemental distribution of Zr, Ca, Y, V and O elements in CaO- inhibitive sample particles at 100hrs using X-ray mapping analysis is shown Fig. 4.29. The rough-face spherical shaped particles which are present in samples with M_{CaO}/M_{V2O5} equal 1 and 2, show evenly distribution of Zr, Y, V and O in Fig. 4.29(i). This is an indication that the rough surface particles comprises of phases formed from these elements, obviously the monoclinic zirconia and YVO_4 as earlier shown in the XRD and EDS analyses. However unlike the irregular spherical particles, the smooth-face spherical shaped particles indicate even distribution of Zr, Y and O elements as

shown in Fig. 4.29(ii). The presence of Y alongside the Zr element distribution portrays these smooth-face spherical particles as yttria stabilized zirconia. The lump shaped structures as shown in Fig. 4.29, shows evenly distribution of Ca ,O and V elements that portrays it as calcium vanadate compounds.

4.6 CaO-inhibition of Vanadium-induced Hot Corrosion of 8YSZ powder with lower V_2O_5 concentration (2% wt. 8YSZ)

4.6.1 Colour Spectrum Analysis

Physical colour appearance of powder particles of CaO-inhibitive 8YSZ powder samples with V_2O_5 concentration (2% wt. 8YSZ) and varying CaO-V_2O_5 molar concentration ratio is shown in Fig. 4.30. The particles depict the samples at 100hrs-900^oC isothermal heating. Fig. 4.30(a) represents the powder particles of isothermal heated 8YSZ, portraying a whitish colour appearance. The powder particles for the vanadium-induced 8YSZ powder sample with V_2O_5 concentration (2% wt. 8YSZ) is shown in Fig. 4.30(b). It indicates a change in colour of the whitish as-received 8YSZ powder particles to brownish colour particles. Fig. 4.30(c), also brownish in colour like the vanadium-induced 8YSZ powder particles is the sample that contains mixture of 8YSZ, V_2O_5 (2% wt. 8YSZ) and CaO (M_{CaO}/M_{V2O5}=1). Figure 4.30(d) depicts yellowish powder particles for sample with increase in M_{CaO}/M_{V2O5} to 2 and that of sample of M_{CaO}/M_{V2O5}=3 is the light yellowish powder particles shown in Fig. 4.30(e). Colour scale for the samples with isothermal heated 8YSZ as the reference sample is shown in Tab. 4.5. The measured values like those of samples with high V_2O_5 concentration (10% wt. 8YSZ), depict increase in lightness and greenness but decrease in redness with increase in M_{CaO}/M_{V2O5} in the

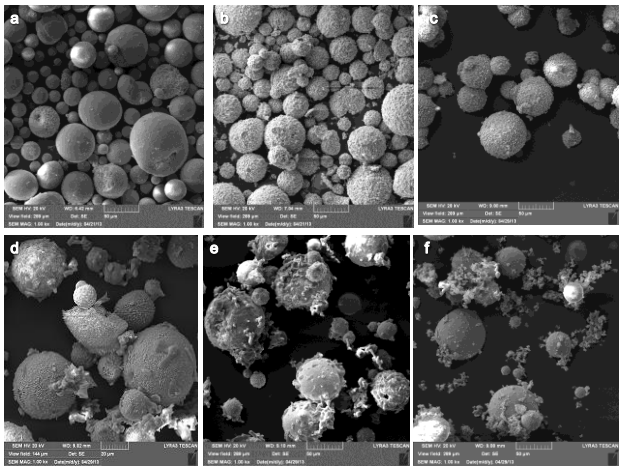

(i)

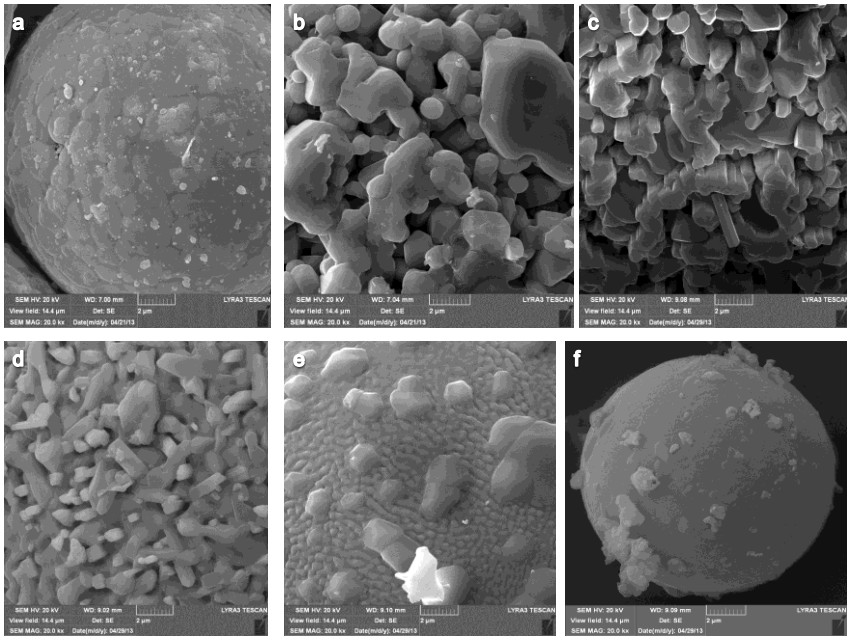

(ii)

Figure 4.26: SEM micrographs of powder particles in CaO-inhibitive vanadium-induced hot corrosion 8YSZ powder samples at 100hrs-900^{o}C isothermal heating. (i) Lower magnification, (ii) Higher Magnification. (a) Isothermal heated 8YSZ, (b) Vanadium-induced hot corrosion 8YSZ , (c) 8YSZ sample with M_{CaO}/M_{V2O5}=1, (d) 8YSZ sample with M_{CaO}/M_{V2O5}=2, (e) 8YSZ sample with M_{CaO}/M_{V2O5}=3, (f) 8YSZ sample with M_{CaO}/M_{V2O5}=5

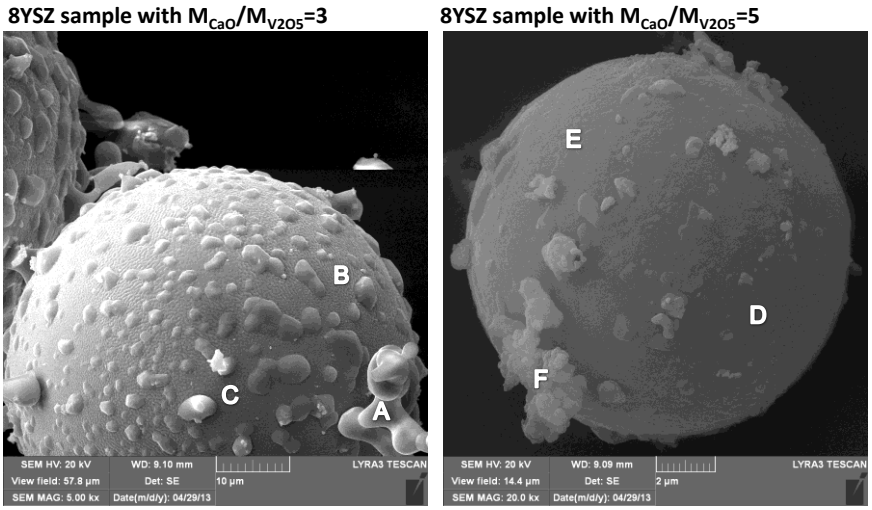

Spectrum	O	Ca	Y	V	Zr	Total
A	42.5	27.8	0.1	25.2	4.4	100.0
B	39.6	1.1	3.8	0.9	54.6	100.0
C	16.6	0.9	4.8	0.5	77.3	100.0
D	26.6	4.5	4.3	1.2	64.4	100.0
E	28.9	4.2	4.9	0.5	61.5	100.0
F	67.5	22.7	0.0	2.7	7.1	100.0

Figure 4.27: EDS analysis of smooth-faced spherical shaped particles at 100hrs-900^{o}C isothermal heating CaO-inhibitive hot corrosion experiment

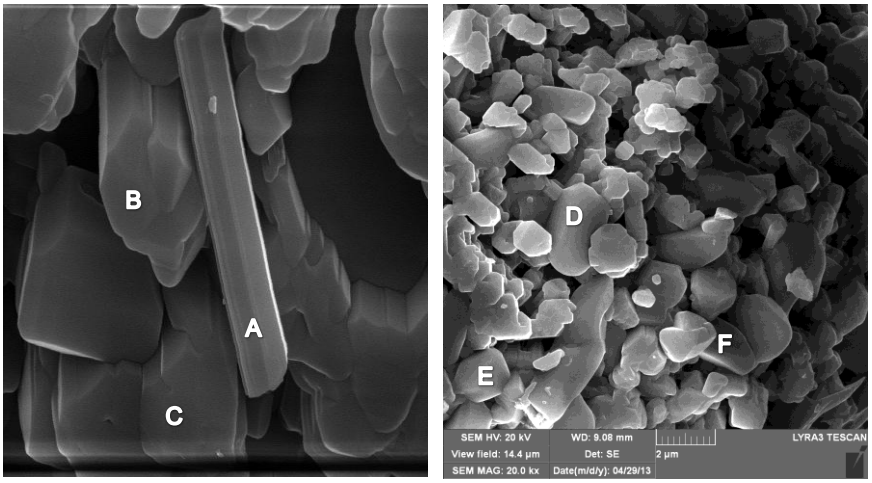

Spectrum	O	Ca	Y	V	Zr	Total
A	20.0	0.7	0.0	2.9	76.4	100.0
B	22.1	0.5	0.0	3.9	73.5	100.0
C	24.4	0.8	0.0	2.4	72.4	100.0
D	29.9	3.1	14.5	13.6	38.9	100.0
E	28.0	1.5	8.6	8.9	53.0	100.0
F	19.3	1.9	7.4	5.6	65.8	100.0

Figure 4.28: EDS analysis of rough-face spherical shaped powder particles at 100hrs-900^{o}C isothermal heating CaO-inhibitive hot corrosion experiment (8YSZ samples with M_{CaO}/M_{V2O5} =1 and 2 respectively)

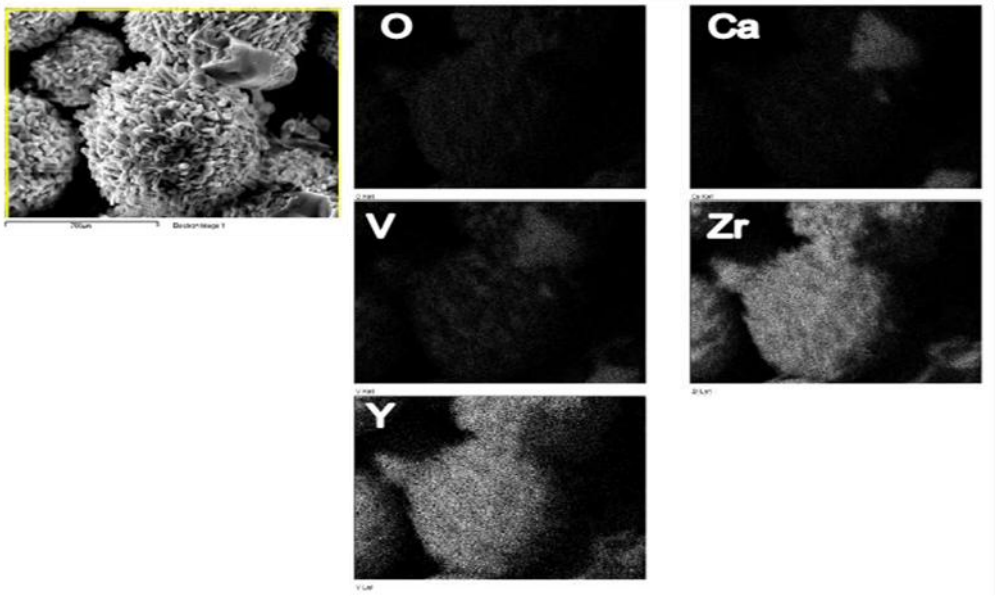

(i)

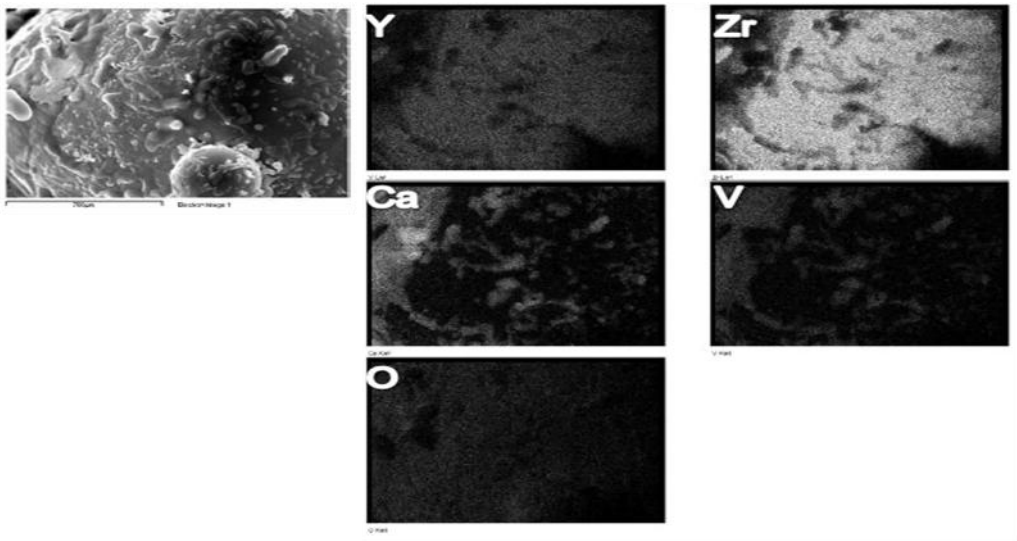

(ii)

Figure 4.29: (i) X-ray mapping analysis of rough-face spherical shaped powder particles at 100hrs-900^{o}C isothermal heating (CaO-inhibitive hot corrosion experiment), (ii) X-ray mapping analysis of smooth-face spherical shaped powder particles at 100hrs-900^{o}C isothermal heating (CaO-inhibitive hot corrosion experiment)

samples. Hence, sample with M_{CaO}/M_{V2O}=1 shows lower L* and a*, but higher b* values compared to the sample with M_{CaO}/M_{V2O5}=2 and the same trend comparing samples with M_{CaO}/M_{V2O5} equal 2 and 3 respectively. The scale shows that the vanadium-induced sample showed the least lightness but the highest degree of redness and yellowness.

4.6.2 XRD Analysis

XRD analysis of inhibiting vanadium-induced hot corrosion of 8YSZ powder with lower V_2O_5 concentration (2% wt. 8YSZ) using CaO as inhibitor is shown in Figures 4.31. Like in samples with high V_2O_5 concentration (10% wt. 8YSZ), the inhibitive XRD spectra for sample with M_{CaO}/M_{V2O5}=1 indicates increase and decrease of monoclinic zirconia (111) and ($\bar{1}$, 1, 1) planes and tetragonal zirconia (101) plane peaks respectively; Fig. 4.31(i). The changes in the intensities of the peaks are however of minute magnitude due to the little intensity of hot corrosion associated with the lower V_2O_5 concentration. Peaks indicating YVO_4 and CaV_2O_6 compound are also present in the inhibitive spectra as compared to the as-received 8YSZ spectrum. Sample of M_{CaO}/M_{V2O5}=2 XRD analysis is shown in Fig. 4.31(ii), the inhibitive spectra show little growth in monoclinic zirconia and decrease in tetragonal zirconia peaks respectively. Minute growth of YVO_4 and $Ca_2V_2O_7$ peaks are also shown in the inhibitive XRD spectra. The sample with M_{CaO}/M_{V2O5}=3 indicates a good inhibitive effect with the intensities of peaks of monoclinic and tetragonal zirconia maintaining constant values through-out the entire isothermal heating period; Fig. 4.31(iii). The presence of $Ca_3V_2O_8$ compound as shown in the inhibitive XRD spectra is the expected calcium vanadate compound. Amount of tetragonal zirconia transformation plots using equation 4.1 with data obtained from Figs. 4.31, 4.3(i) and 4.4(ii) are shown in Figure 4.32. The plots portray the same trend like that of samples with higher V_2O_5

concentration, higher transformation rate is shown by samples with lower CaO-V_2O_5 molar concentration ratio i.e. sample of M_{CaO}/M_{V2O5}=1. However lower monoclinic zirconia volume fraction is shown by samples with higher CaO-V_2O_5 molar concentration ratio i.e. samples with M_{CaO}/M_{V2O5} equal 2 and 3 respectively. The vanadium-induced and the isothermal heated 8YSZ samples are at the two extremes of the plots, with the former showing the highest and the latter showing the least monoclinic zirconia volume fraction.

4.6.3 SEM Analysis

SEM micrographs of powder particles in CaO-inhibitive 8YSZ powder samples with V_2O_5 concentration (2% wt. 8YSZ) and varying CaO-V_2O_5 molar concentration ratio at 100hrs-900^oC isothermal heating are shown Fig. 4.33. It also includes SEM micrographs of isothermal heated 8YSZ and vanadium-induced hot corrosion 8YSZ sample with V_2O_5 concentration (2% wt. 8YSZ), Fig. 4.33(a) and (b) respectively. The particles of the isothermal heated 8YSZ sample depict a smooth-face spherical morphology, a resemblance of the as-received 8YSZ powder particles. The vanadium-induced 8YSZ sample portrays powder particles that show rough-face spherical morphology and as shown in Fig. 4.6, it comprises of monoclinic zirconia irregular structures and facet YVO_4 structures. The inhibitive sample with M_{CaO}/M_{V2O5}=1, Fig. 4.33(c) shows powder particles with rough-face spherical morphology, though not as rough and many when compared to that of sample with high V_2O_5 concentration but of the same CaO-V_2O_5 molar concentration ratio as shown in Fig. 4.34(i). These spherical particles comprise of the bar-shaped and irregular shaped structures which depict monoclinic zirconia and YVO_4 respectively. The inhibitive sample with M_{CaO}/M_{V2O5}=2 is shown in Fig. 4.33(d) and its comparison with that of sample with high V_2O_5 concentration (10% wt. 8YSZ) but of the same CaO-V_2O_5 molar

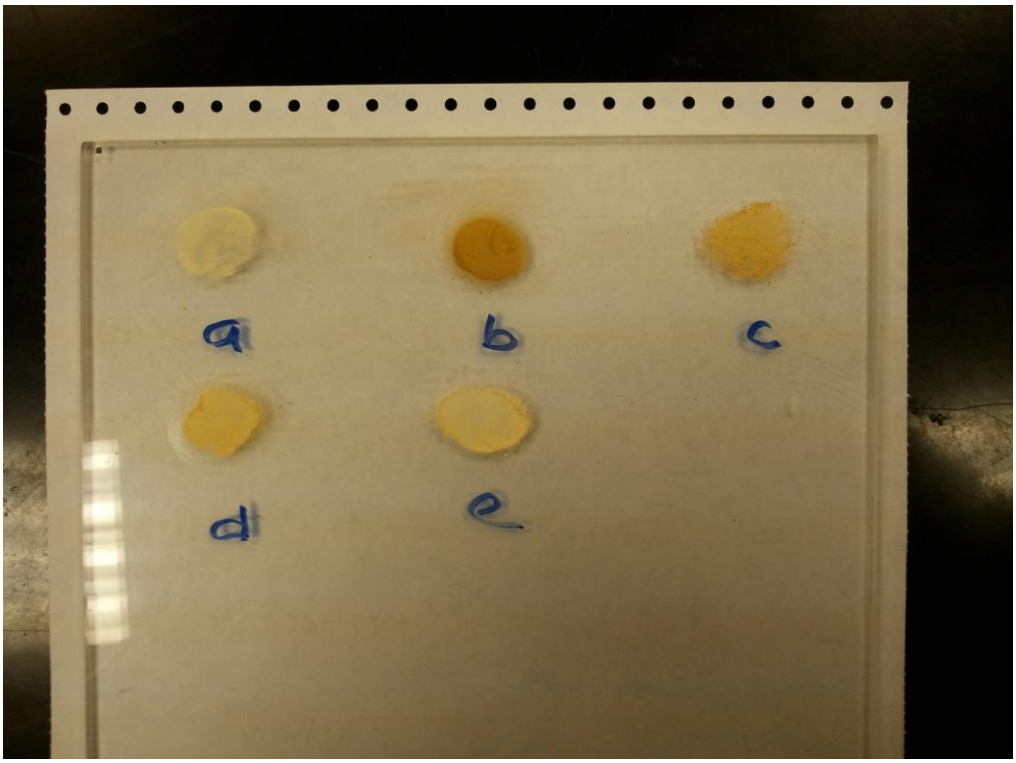

Figure 4.30: Physical colour appearance of powder particles for the CaO-inhibitive vanadium-induced hot corrosion 8YSZ powder samples with V_2O_5 concentration (2% wt. 8YSZ) and varying M_{CaO}/M_{V2O5} at 100hrs-900^oC isothermal heating. (a) Isothermal heated 8YSZ, (b) Vanadium-induced 8YSZ, (c) 8YSZ powder sample (M_{CaO}/M_{V2O5} =1), (d) 8YSZ powder sample (M_{CaO}/M_{V2O5} =2), (e) 8YSZ powder sample (M_{CaO}/M_{V2O5} =3)

Table 4.5: Colour scale of powder particles for the CaO-inhibitive hot corrosion experiments of mixture of 8YSZ, V_2O_5 (2% wt. 8YSZ) and CaO

Powder particles at 100hrs-900^oC isothermal heating	L*	a*	b*	dL*	da*	db*
8YSZ	80.28	-2.05	16.58	80.28	-2.05	16.58
8YSZ + V_2O_5 (2% 8YSZ)	65.61	4.73	39.78	-14.25	7.47	26.29
8YSZ+ CaO (M_{CaO}/M_{V2O5} =2) + V_2O_5 (2% wt. 8YSZ)	54.19	11.51	42.94	-26.09	13.57	20.77
8YSZ+ CaO (M_{CaO}/M_{V2O5} =2) + V_2O_5 (2% wt. 8YSZ)	78.42	0.40	30.44	-1.86	2.46	13.85
8YSZ + CaO (M_{CaO}/M_{V2O5} =3) + V_2O_5 (2% wt. 8YSZ)	80.29	-0.10	27.11	0.01	1.96	10.52

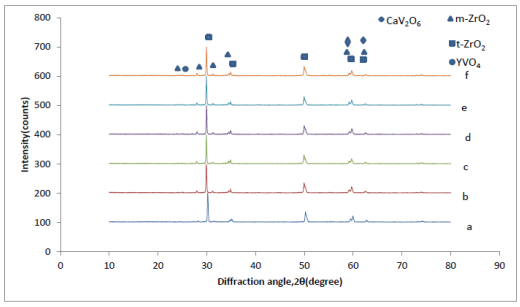

(i)

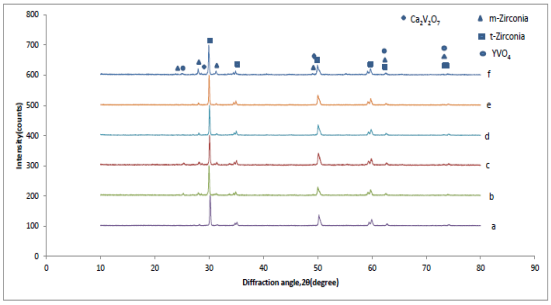

(ii)

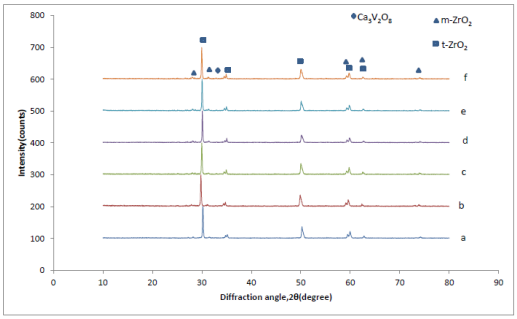

(iii)

Figure 4.31: XRD analysis of CaO-inhibitive vanadium-induced hot corrosion 8YSZ powder samples with V_2O_5 concentration (2% wt. 8YSZ) at 900^{o}C isothermal heating. (i) Sample of M_{CaO}/M_{V2O5}=1, (ii) Sample of M_{CaO}/M_{V2O5}=2, (i) Sampleof M_{CaO}/M_{V2O5}=3. (a) As-received 8YSZ, (b) 2hrs heating, (c) 5hrs heating, (d) 20hrs heating, (e) 50hrs heating, (f) 100hrs heating

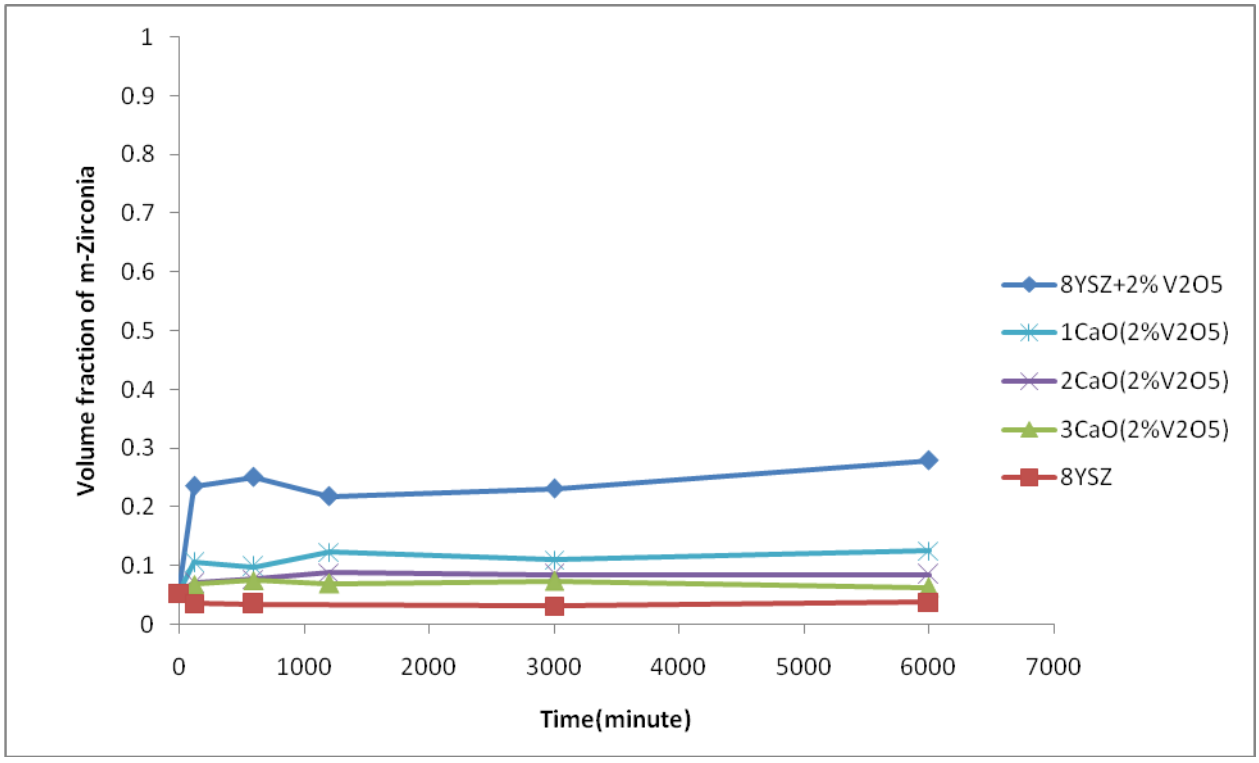

Figure 4.32: Amount of tetragonal zirconia phase transformation against time for CaO-inhibitive vanadium-induced hot corrosion of 8YSZ powder samples with V_2O_5 concentration (2% wt. 8YSZ) at 900^{o}C isothermal heating. (8YSZ) Heated 8YSZ powder, (3CaO(2% V2O5)) Sample with M_{CaO}/M_{V2O5}=3, (2CaO(2% V2O5)) Sample with M_{CaO}/M_{V2O5}=2, (1CaO(2% V2O5)) Sample with M_{CaO}/M_{V2O5}=1, (8YSZ+2% V2O5) 8YSZ+V_2O_5 (2% wt. 8YSZ)

concentration ratio is shown in Fig. 4.34(ii). The sample particles showed smooth-face spherical morphology with lump structures attached to its surface, though not as smooth when compared to the smoothness in particles of as-received 8YSZ powder. The sample of M_{CaO}/M_{V2O5}=3 is shown in Fig. 4.33(e), it comprises of smooth-face spherical shaped powder particles with lump shaped particles scattered on its surface. The smooth-face powder particles like in previous EDS analysis depict tetragonal zirconia phase and the lump shaped structures are the calcium vanadate compounds; CaV_2O_6, $Ca_2V_2O_7$ and $Ca_3V_2O_8$ formed based on the CaO-V_2O_5 molar concentration ratio. The SEM micrograph in Fig. 4.34(iii) is a comparison of samples with CaO/V_2O_5 molar concentration equals 3, but with different V_2O_5 concentration. The two samples show smooth-face spherical shaped particles at 100hrs-900^oC isothermal heating.

4.7 CaO-MgO mixture Inhibition of Vanadium-induced Hot Corrosion of 8YSZ powder with V_2O_5 concentration (10% wt. 8YSZ)

4.7.1 Colour Spectrum Analysis

Physical colour appearance of powder particles using mixture of MgO and CaO to inhibit vanadium-induced hot corrosion of 8YSZ powder sample with V_2O_5 concentration (10% wt. 8YSZ) is shown in Fig. 4.35. Fig. 4.35(d-f) are inhibitive hot corrosion powder samples at 100hrs-900^oC isothermal heating compared to that of isothermal heated 8YSZ; Fig. 4.35(a) and vanadium-induced 8YSZ powder; Fig 4.35(b-c) under the same experimental conditions. Fig. 4.35(d) shows the inhibitive hot corrosion sample with CaO/V_2O_5 and MgO/V_2O_5 molar concentrations equal 1 and 1 respectively. It shows that the powder particles colour after the inhibitive hot corrosion test is dark yellow. Fig. 4.35(e) shows light yellow powder particles for powder sample with CaO/V_2O_5 and MgO/V_2O_5 molar concentrations equal 1 and 2 respectively

and the creamy yellow powder in Fig. 4.35(f); represents the sample with CaO/V_2O_5 and MgO/V_2O_5 molar concentrations equal 2 and 1 respectively. The colour scale analysis of CaO-MgO mixture inhibitive vanadium-induced hot corrosion 8YSZ powder samples with isothermal heated 8YSZ as reference sample at 100hrs-900^oC isothermal heating is shown in Tab. 4.6. The sample with CaO/V_2O_5 and MgO/V_2O_5 molar concentrations equal 2 and 1 respectively shows the highest degree of lightness, but least redness and yellowness out of the inhibitive samples. It is also the closest to the isothermal heated 8YSZ sample in terms of colour scale. The sample with CaO/V_2O_5 and MgO/V_2O_5 molar concentrations equal 1 and 2 respectively colour scale is next to that of sample with CaO/V_2O_5 and MgO/V_2O_5 molar concentrations equal 2 and 1 respectively. The sample with CaO/V_2O_5 and MgO/V_2O_5 molar concentrations equal 1 and 1 respectively however shows the least lightness and highest degree redness and yellowness of the inhibitive samples and is closest to colour scale values of the vanadium-induced sample.

4.7.2 XRD Analysis

XRD analyses of using mixture of CaO and MgO to mitigate 900^oC isothermal heating vanadium-induced hot corrosion of 8YSZ powder with V_2O_5 concentration (10% wt. 8YSZ) are shown in Fig 4.36. Fig. 4.36(i) is that of the sample with CaO/V_2O_5 and MgO/V_2O_5 molar concentrations equal 1 and 1 respectively. The inhibitive spectra show the presence of tetragonal and monoclinic zirconia phase similar to what is in the as-received 8YSZ powder spectrum, Fig. 4.36(i-a); but with some little differences. Unlike the as-received 8YSZ powder spectrum, there is presence of the monoclinic zirconia phase peaks at some new 2θ value in the inhibitive spectra. The inhibitive spectra also depict increase and decrease in the intensities of monoclinic

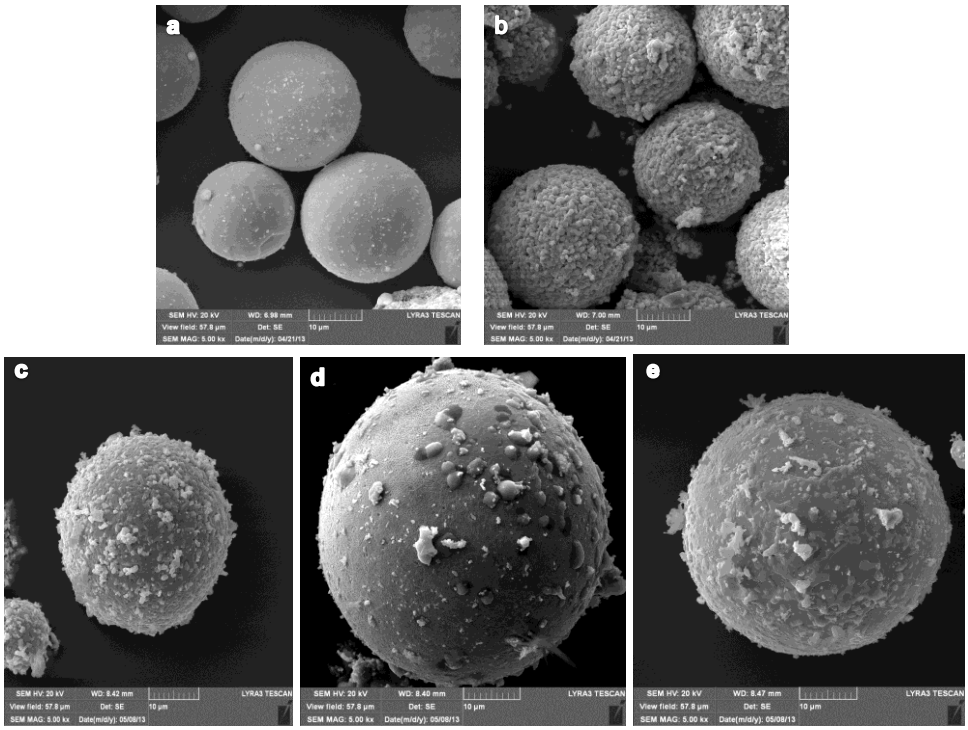

Figure 4.33: SEM micrographs of powder particles at 100hrs-900^{o}C isothermal heating CaO-inhibitive hot corrosion experiments of 8YSZ mixture with V_2O_5 (2% wt. 8YSZ) and CaO with varying CaO-V_2O_5 molar concentration ratio. (a) Isothermal heated 8YSZ, (b) Vanadium-induced hot corrosion 8YSZ, (c) Sample with M_{CaO}/M_{V2O5}=1, (d) Sample with M_{CaO}/M_{V2O5}=2, (e) Sample with M_{CaO}/M_{V2O5}=3

i

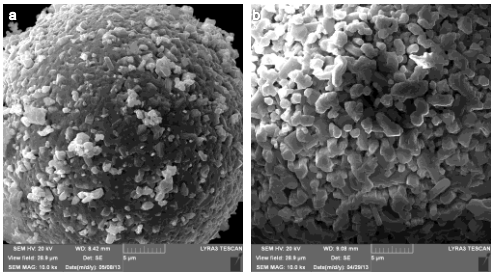

ii

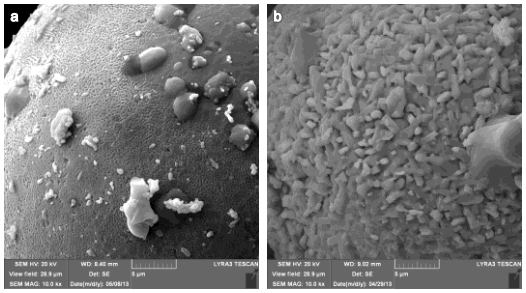

iii

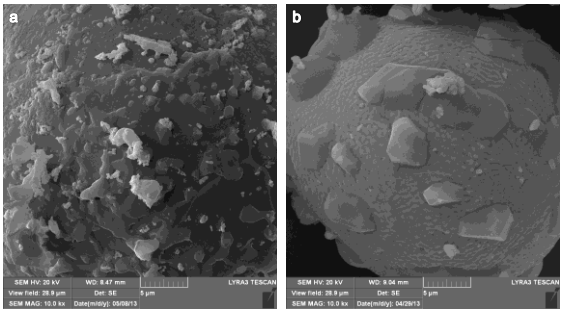

Figure 4.34: SEM micrographs comparison of powder particles at 100hrs-900^{o}C isothermal heating for CaO-inhibitive hot corrosion samples with low and high V_2O_5 concentrations. (i) Samples with M_{CaO}/M_{V2O5}=1, (ii) Samples with M_{CaO}/M_{V2O5}=2, (iii) Samples with M_{CaO}/M_{V2O5}=3. (a) V_2O_5 concentration (10% wt. 8YSZ), (b) V_2O_5 concentration (2% wt. 8YSZ)

zirconia; (111) and ($\bar{1}$, 1, 1) plane and tetragonal zirconia; (101) plane peaks respectively. The inhibitive spectra aside the aforementioned, portray the presence of YVO_4 compound and $CaMgV_2O_7$ compound (PDF card number 01-077-0964). The same XRD inhibitive spectra trend is shown by sample with CaO/V_2O_5 and MgO/V_2O_5 molar concentrations equal 1 and 2 respectively, Fig. 4.36(ii) and also for sample with CaO/V_2O_5 and MgO/V_2O_5 molar concentrations equal 2 and 1 respectively, Fig. 4.36(iii). However unlike the inhibitive spectra in Fig. 4.36(i), the intensities of the YVO_4 compound peaks and the rate of increase of the monoclinic zirconia peaks are minute; the transformation of the tetragonal zirconia phase is minute.

The plots for amount of tetragonal zirconia transformation using equation 4.1 for CaO-MgO mixture inhibitive vanadium-induced hot corrosion 8YSZ powder samples are shown in Fig. 4.37. The data used for the plots are obtained from the XRD spectra in Figs. 4.36, 4.3(i) and 4.4(ii). The plots are in line with the XRD analyses, the plot for sample with CaO/V_2O_5 and MgO/V_2O molar concentrations equal 1 and 1 respectively shows highest volume fraction of monoclinic zirconia compared to other inhibitive samples. It also shows a better inhibition when compared to vanadium-induced sample which has the highest volume fraction of monoclinic zirconia out of all the samples. The sample with CaO/V_2O_5 and MgO/V_2O_5 molar concentrations equal 2 and 1 respectively has lower volume fraction of monoclinic zirconia at 100hrs compared to that of sample with CaO/V_2O_5 and MgO/V_2O_5 molar concentrations equal 1 and 2 respectively. Though the difference is minute, but it further validates that presences of CaO in the inhibitive sample retards the transformation rate of the tetragonal zirconia when compared to MgO of the same molar ratio to V_2O_5.

The bar chart showing comparison between the effectiveness of MgO, CaO and mixture of the two in inhibiting vanadium-induced hot corrosion of 8YSZ powder with V_2O_5 concentration (10% wt. 8YSZ) is shown in Fig. 4.38. The bar chart shows measure of the volume fraction of monoclinic zirconia phase in each of the inhibitive powder sample at 100hrs-900^oC isothermal heating. The chart was obtained using equation 4.1 and data from the XRD spectrum for each inhibitive sample respectively at 100hrs. The isothermal heated 8YSZ shows the least value for the volumetric fraction of monoclinic zirconia, while vanadium-induced 8YSZ sample shows the highest. In all the inhibitive hot corrosion test samples, the sample with CaO-V_2O_5 molar concentration ratio equals 5 shows the least monoclinic zirconia volume fraction which is next to that of the isothermal heated 8YSZ. The highest volume fraction for inhibitive samples is that of the sample with MgO-V_2O_5 molar concentration ratio equals 1 and the other inhibitive samples volume fraction of monoclinic zirconia falls in between these two samples. CaO-inhibitive samples proved better when compared to MgO-inhibitive samples of the same molar concentration ratio to vanadium oxide; that is they have lower volume fraction of monoclinic zirconia when compared to that of MgO-inhibitive samples.

4.7.3 SEM Analysis

SEM micrographs of using CaO-MgO mixture in mitigating vanadium-induced hot corrosion of 8YSZ powder sample with varying CaO/V_2O_5 and MgO/V_2O_5 molar concentrations are shown in Fig. 4.39. The micrographs represent powder particles of the inhibitive samples at 100hrs-900^oC isothermal heating. The smooth-face and rough-face spherical shaped particles as shown in Fig. 4.39(i) depict the particles at 100hrs for inhibitive sample with CaO/V_2O_5 and MgO/V_2O_5 molar concentrations equal 1 and 1 respectively. The rough-face spherical shaped particles comprise of

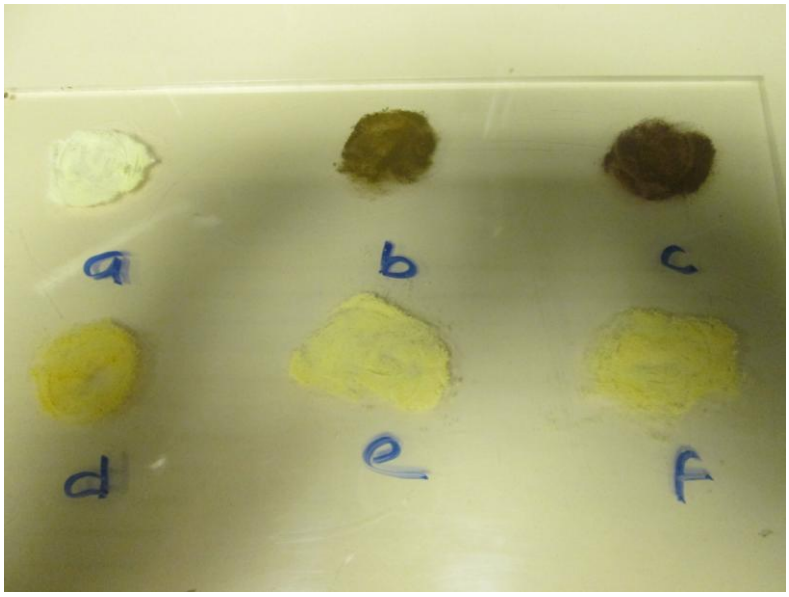

Figure 4.35: CaO-MgO-inhibitive vanadium-induced hot corrosion of 8YSZ powder samples with varying CaO /V_2O_5 and MgO/V_2O_5 molar concentrations colour spectrum at 900^oC isothermal heating. (a) Isothermal heated 8YSZ (100hrs) (b) Vanadium-induced 8YSZ (2hrs), (c) Vanadium-induced 8YSZ (100hrs), (d) 8YSZ sample (M_{CaO}/M_{V2O5} : M_{MgO}/M_{V2O5} =1:1 at 100hrs), (e) 8YSZ sample (M_{CaO}/M_{V2O5} : M_{MgO}/M_{V2O5} =1:2 at 100hrs), (f) 8YSZ sample (M_{CaO}/M_{V2O5} : M_{MgO}/M_{V2O5} =2:1 at 100hrs)

Table 4.6:Colour scale of powder particles for CaO-MgO inhibitive vanadium-induced hot corrosion 8YSZ powder samples

Powder particles at 100hrs-900^oC isothermal heating	L*	a*	b*	dL*	da*	db*
8YSZ	80.11	-1.98	16.45	80.11	-1.98	16.45
8YSZ + V2O5 (10% wt. 8YSZ)	25.15	19.52	34.84	-54.92	21.50	18.39
8YSZ + CaO + MgO + V_2O_5 (M_{CaO}/M_{V2O5} : M_{MgO}/M_{V2O5} =1:1)	65.16	6.99	40.47	-14.95	8.97	24.02
8YSZ + CaO + MgO + V_2O_5 (M_{CaO}/M_{V2O5} : M_{MgO}/M_{V2O5} =1:2)	73.75	1.38	29.00	-6.36	3.36	12.54
8YSZ + CaO + MgO + V_2O_5 (M_{CaO}/M_{V2O5} : M_{MgO}/M_{V2O5} =2:1)	71.54	3.60	34.47	-8.57	5.58	18.01

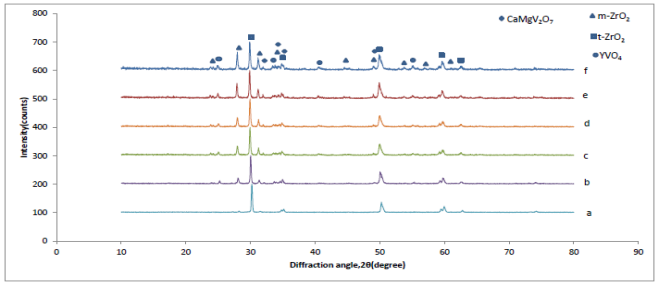

(i)

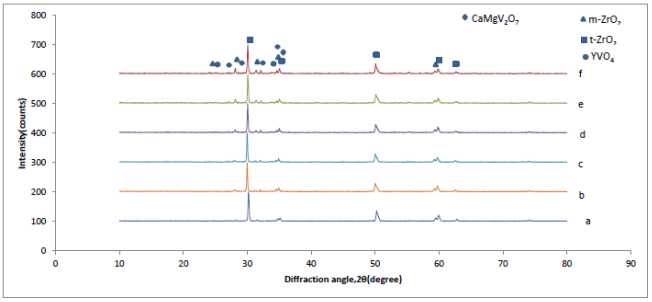

(ii)

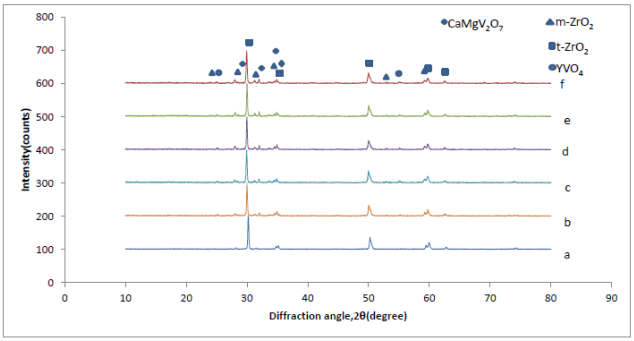

(iii)

Figure 4.36: XRD analysis of CaO-MgO-inhibitive vanadium-induced hot corrosion 8YSZ powder samples with varying CaO/V_2O_5 and MgO/V_2O_5 molar concentrations at 900°C isothermal heating. (i) Sample with M_{CaO}/M_{V2O5} : M_{MgO}/M_{V2O5} =1:1, (ii) Sample mixture with M_{CaO}/M_{V2O5} : M_{MgO}/M_{V2O5} =1:2, (iii) Sample mixture with M_{CaO}/M_{V2O5} : M_{MgO}/M_{V2O5} =2:1. (a) As-received 8YSZ, (b) 2hrs heating, (c) 5hrs heating, (d) 20hrs heating,(e) 50hrs heating, (f)100hrs heating

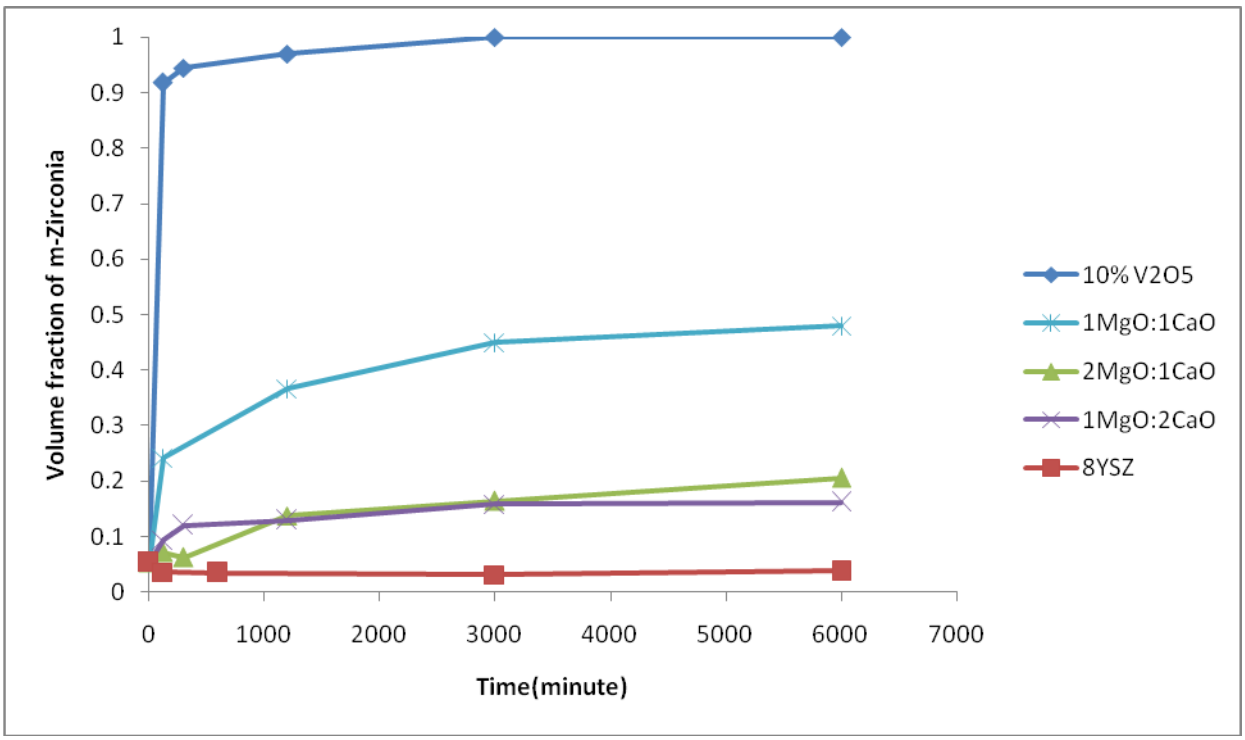

Figure 4.37: Amount of tetragonal zirconia phase transformation against time for CaO-MgO-inhibitive vanadium-induced hot corrosion 8YSZ powder samples at 900°C isothermal heating. (8YSZ) 8YSZ powder, (1MgO:2CaO) Sample with M_{MgO}/M_{V2O5}:M_{CaO}/M_{V2O5}=1:2, (2MgO:1CaO) Sample with M_{MgO}/M_{V2O5}:M_{CaO}/M_{V2O5}=2:1, (1MgO:1CaO) Sample with M_{MgO}/M_{V2O5}:M_{CaO}/M_{V2O5}=1:1, (10% V2O5) 8YSZ+V_2O_5 (10% wt. 8YSZ)

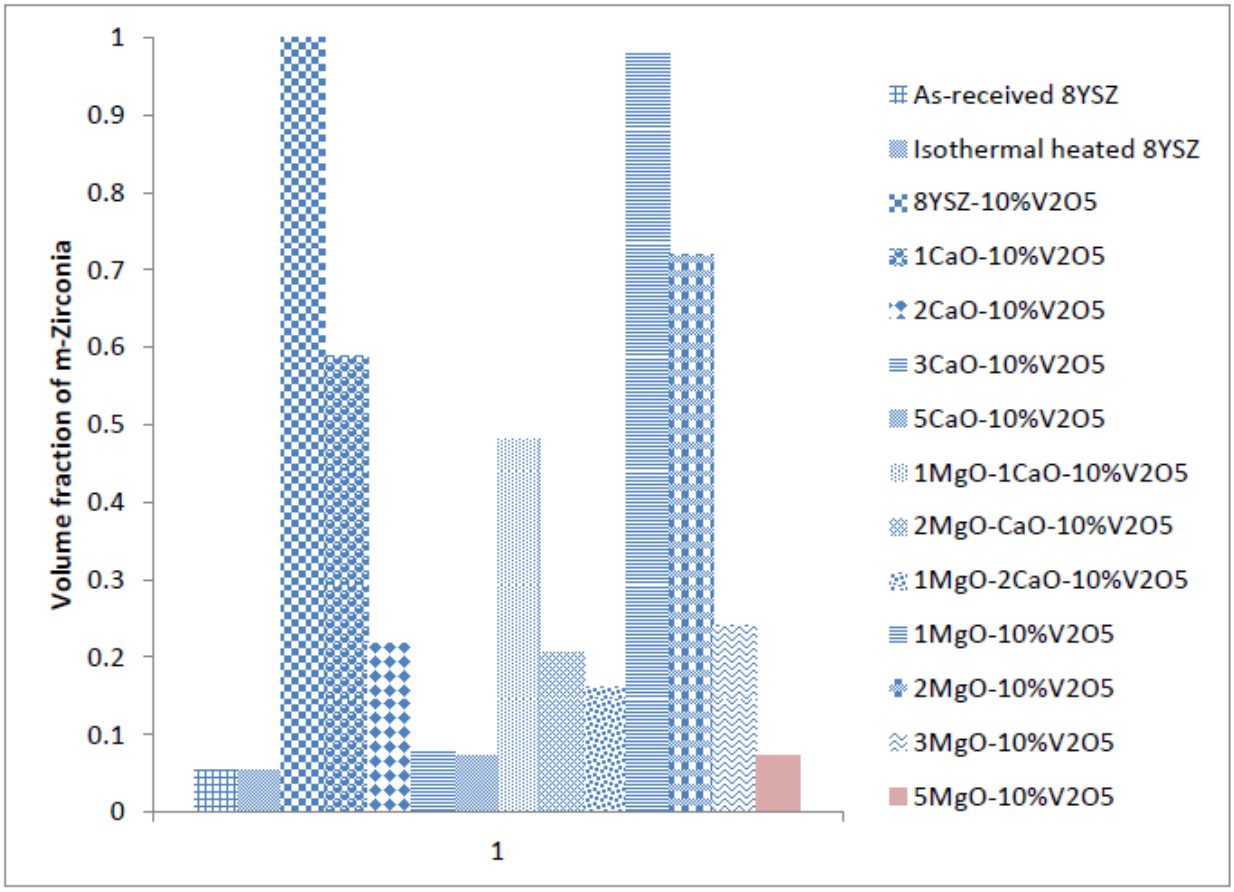

Figure 4.38: Amount of tetragonal zirconia transformation comparison of 8YSZ samples with V_2O_5 conccentration (10% wt. 8YSZ) at 100hrs-900^{o}C isothermal heating in vanadium-induced hot corrosion inhibitive experiments using different inhibitors

bar and irregular shaped structures. 8YSZ sample with CaO/V_2O_5 and MgO/V_2O_5 molar concentrations equal 1 and 2 respectively micrographs are shown in Fig. 4.39(ii). It shows the sample has large presence of the smooth-face and few rough-face spherical shaped particles. The sample with CaO/V_2O_5 and MgO/V_2O_5 molar concentrations equal 2 and 1 respectively also shows similar trait of large presence of smooth-face and few rough-face spherical particles as shown in Fig. 4.39(iii). The presences of lump shaped structures were also seen on the spherical shape particles as shown in Fig. 4.39.

4.7.4 EDS Analysis

EDS analyses of powder particles of samples in vanadium-induced 8YSZ hot corrosion inhibitive tests with CaO-MgO mixture at 100hrs-900^oC isothermal heating are shown in Figs. 4.40-4.42. Fig. 4.44 represents EDS analysis of rough-face spherical shaped particles for sample with CaO/V_2O_5 and MgO/V_2O_5 molar concentrations equal 1 and 1 respectively. These particles are few in other CaO-MgO mixture inhibitive samples. Like in the previous mentioned case of rough-face spherical particles in the inhibitive test samples, that it mainly comprise of the bar-shaped and irregular shaped structures, same is for these spherical shaped particles in CaO-MgO inhibitive sample. The bar shaped structure as shown in spectrum C like in the previous analyses shows zero concentration of yttrium element and large deposition of the zirconium and oxygen elements; it depicts the monoclinic zirconia phase. In spectrum D, that represent the irregular structures; there is large presence of yttrium and vanadium elements that portray these structures as the YVO_4 compound. The lump structures as shown in spectra A and B show dominant presence of oxygen, calcium, magnesium and vanadium which portray it as the calcium-magnesium vanadate compound; $CaMgV_2O_7$ as shown in the XRD spectra. The same elements

concentration is also seen in lump structures shown in Figs. 4.41-4.42 for samples with higher molar concentrations of CaO/V_2O_5 and MgO/V_2O_5 combinations. The smooth-face spherical shaped particles as shown in Fig. 4.42, spectra B and C depict these structures as tetragonal zirconia phase due to large weight concentration of oxygen, yttrium and zirconia elements.

4.8 Air Plasma Sprayed Specimen Inhibitive Hot Corrosion Test

4.8.1 Physical Appearance

The samples which are sample A; isothermal heated APS coupon, sample B; vanadium-induced hot corrosion APS coupon and sample C; APS coupon with slurry mixture of $MgO\text{-}V_2O_5$ powder with $M_{MgO}/M_{V2O5}=3$. The other samples are sample D; APS coupon with slurry mixture of $MgO\text{-}V_2O_5$ powder with $M_{MgO}/M_{V2O5}=5$, sample E; APS coupon with slurry mixture of $CaO\text{-}V_2O_5$ powder with $M_{CaO}/M_{V2O5}=3$ and sample F; APS coupon with slurry mixture of $CaO\text{-}V_2O_5$ powder with $M_{CaO}/M_{V2O5}=5$. Sample B unlike other samples as shown in Fig. 4.47(b) shows total spallation of the TBC coatings from the substrate, while sample C shows little delamination of the ceramic topcoat at one of its edges; Fig. 4.43(c) at 100hrs-900^{o}C isothermal heating. The other samples; A, D, E and F shows neither spallation nor delamination of the TBCs at 100hrs-900^{o}C isothermal heating as shown in Fig. 4.43(a, d, e and f).

4.8.2 XRD Analysis

Figure 4.44 shows the XRD analyses of the TBCs coupon samples at 100hrs-900^{o}C isothermal heating inhibitive-hot corrosion test. The XRD spectrum for sample A as shown in Fig. 4.44(a) shows only peaks for the tetragonal zirconia phase, but sample B aside not showing tetragonal zirconia peaks indicates the presences of the monoclinic zirconia and YVO_4 compounds peaks,

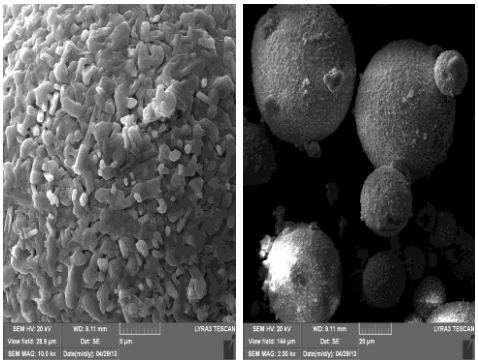

(i)

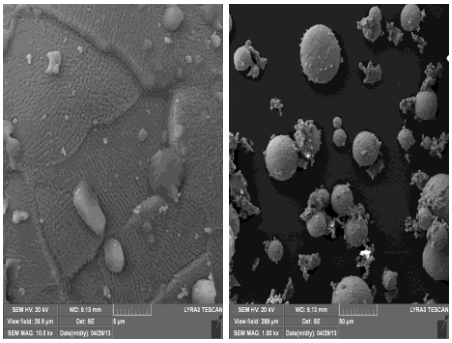

(ii)

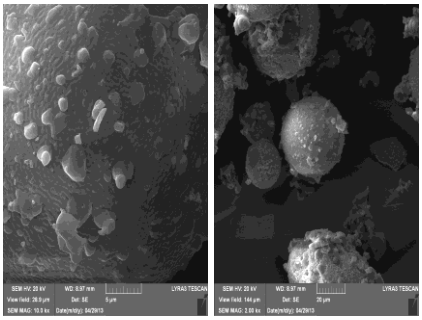

(iii)

Figure 4.39: SEM micrographs of CaO-MgO-inhibitive vanadium-induced hot corrosion 8YSZ powder samples at 100hrs-900^{o}C isothermal heating. (i) Sample with M_{CaO}/M_{V2O5} : M_{MgO}/M_{V2O5} =1:1, (ii) Sample with M_{CaO}/M_{V2O5} : M_{MgO}/M_{V2O5} =1:2, (iii) Sample with M_{CaO}/M_{V2O5} : M_{MgO}/M_{V2O5} =2:1

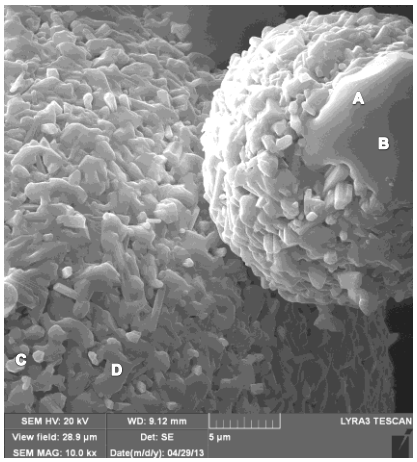

Spectrum	O	Mg	Ca	Y	V	Zr	Total
A	47.5	15.9	13.6	0.0	22.9	0.0	100.0
B	10.2	10.6	28.97	0.0	50.1	0.0	100.0
C	39.0	0.5	0.1	0.0	1.7	58.5	100.0
D	30.5	0.1	2.1	13.5	12.1	41.5	100.0

Figure 4.40: EDS analysis of rough-face spherical shaped powder particles in CaO-MgO-inhibitive vanadium-induced hot corrosion sample (CaO/V_2O_5: MgO/V_2O_5 =1:1)

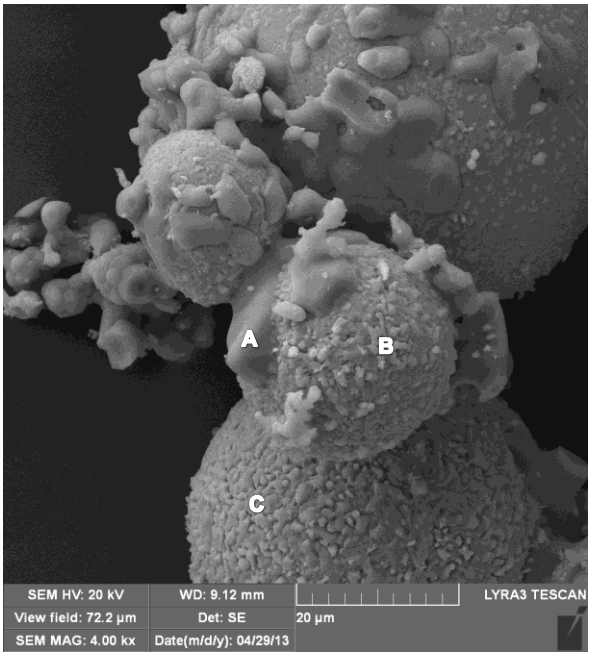

Spectrum	O	Mg	Ca	Y	V	Zr	Total
A	35.2	10.0	8.8	0.3	16.5	28.9	100.0
B	44.4	9.4	5.3	4.7	12.7	23.2	100.0
C	44.7	8.7	4.7	2.1	12.3	27.3	100.0

Figure 4.41: EDS analysis of powder particles in CaO-MgO-inhibitive vanadium-induced hot corrosion sample (CaO/V_2O_5: MgO/V_2O_5 =1:2)

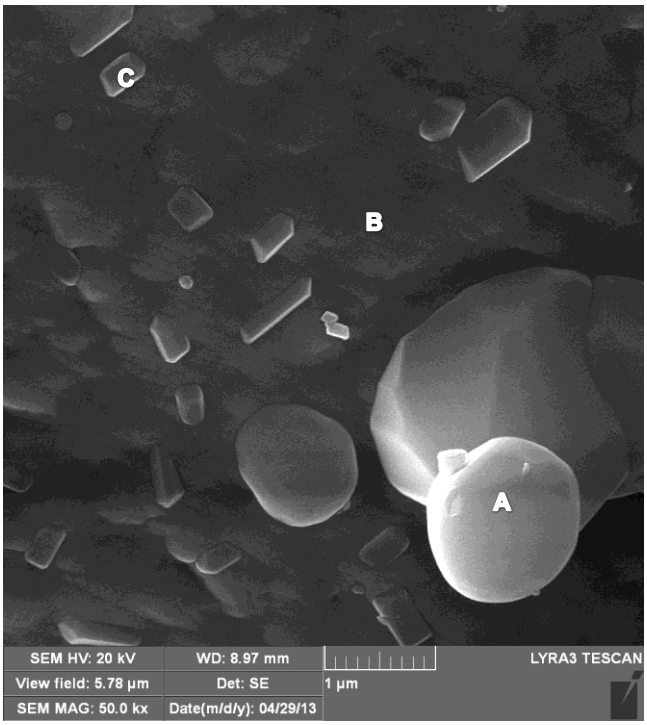

Spectrum	O	Mg	Ca	Y	V	Zr	Total
A	47.1	11.1	14.2	0.0	20.2	7.2	100.0
B	16.0	0.4	0.9	4.5	0.5	77.4	100.0
C	18.7	0.0	1.4	7.4	2.9	69.4	100.0

Figure 4. 42: EDS analysis of powder particles in CaO-MgO-inhibitive vanadium-induced hot corrosion sample (CaO/V_2O_5: MgO/V_2O_5 =2:1)

Fig.4.44(b)**.** Samples E and F like sample A also show only the presences of tetragonal zirconia peaks as shown Fig. 4.44i(c-d), the XRD spectrum of sample D however shows minute trace of peaks corresponding to monoclinic zirconia and YVO_4 but huge presences of the tetragonal zirconia peaks is conspicuously shown. Sample C XRD spectrum as shown in Fig. 4.44(c) shows the presences of monoclinic zirconia, tetragonal zirconia and YVO_4 peaks.

The bar chart showing the amount of tetragonal zirconia phase transformation in each of the sample using equation 4.1 is shown in Fig. 4.45. The samples A, E and F as shown in the chart have zero volume fraction of monoclinic zirconia to show no transformation occurred during the 100hrs inhibitive hot corrosion test. Sample D shows negligible monoclinic zirconia volume fraction as less as 0.09 while that of samples B and C is 1 and 0.37 respectively. The volume fraction of monoclinic zirconia present in sample B; vanadium-induced sample shows that total transformation of the tetragonal zirconia occurred during the test within 100hrs which further validates the earlier results obtained using the powder samples.

Figure 4.46(i) is a comparison of the XRD spectra of solid particles that are present on the TBCs coupon after the CaO-inhibitive test; samples E and F with that of the as received CaO and V_2O_5 powder samples. The spectra obviously show that new compound was formed from the slurry mixture of CaO and V_2O_5, having seen difference in terms of peaks in these solids particles spectra compared to that of the as-received CaO and V_2O_5 XRD spectra. This indicates calcium vanadate compound (PDF card number 01-071-3318) forms during the 100hrs isothermal heating time. Fig. 4.46(ii) though for the MgO-inhibitive test samples, samples C and D shows the same trend; that is the spectra of the solid particles found on these specimens after the test have different peaks as compared to that of the as-received MgO and V_2O_5 powder XRD spectra

peaks. This confirms that during the cause of the inhibitive isothermal heat test, these powder particles in the slurry react to form $Mg_3V_2O_8$ (PDF card number 01-073-0207). It is worthy of note that the availability of these new compound on the samples after the inhibitive hot corrosion tests depends on the new compound melting point because the vanadium-induced sample shows no powder particle on it after the experiment. This is an indication that the V_2O_5 powder particle which melting point is 699^oC must have melt during the test and diffuse into the ceramic coating making it to have disappeared after the test.

4.9 Inhibition Efficiency

The inhibition efficiency of the of using alkaline-earth metal oxides; MgO and CaO in inhibiting vanadium-induced hot corrosion of 8YSZ powder and APS 8YSZ topcoat TBCs coupon has been evaluated using equation 4.2.

$$\varepsilon\% = ((A-B)/A)*100 \qquad (4.2)$$

$\varepsilon\%$ = Inhibition efficiency

A = Volume fraction of monoclinic zirconia in vanadium-induced hot corrosion sample

B = Volume fraction of monoclinic zirconia in the inhibitive samples.

Table 4.7 shows the inhibition efficiency for the powder samples. It shows that with increase in the alkaline-earth metal oxide-vanadium oxide molar concentration ratio, the higher the inhibition efficiency. Thus good inhibition was achieved in sample with M_{MgO}/M_{V2O5}=5 compared to sample of M_{MgO}/M_{V2O5}=3. Likewise an inhibition efficiency of 92.7% was achieved in powder sample with M_{CaO}/M_{V2O5}=5 while inhibition efficiency as less as 52.4% was achieved in sample with M_{CaO}/M_{V2O5}=1 under the same experimental conditions. Fig. 4.47 shows the

inhibition efficiency comparison between MgO and CaO in inhibiting vanadium-induced hot corrosion in powder and APS samples. It shows the superiority of CaO over MgO in inhibiting vanadium-induced hot corrosion phenomenon. It shows higher inhibition efficiency in CaO-inhibitive samples compared to the MgO-inhibitive samples of the same molar concentration ratio to vanadium-oxide. Inhibition efficiency as high as 100% was achieved with CaO inhibitor while the highest achieved with the use of MgO is 92.6%.

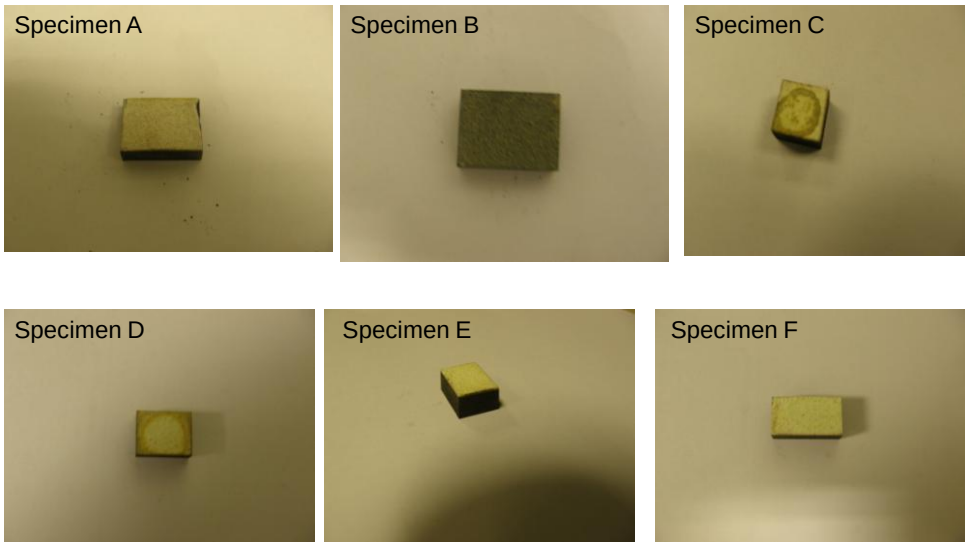

Figure 4.43: Physical appearance of APS samples after 100hrs-900^{o}C isothermal inhibitive hot corrosion test

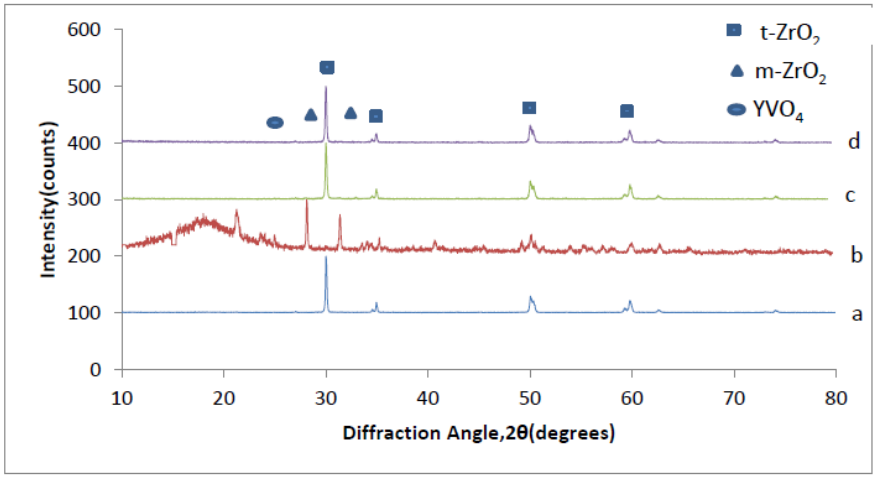

(i)

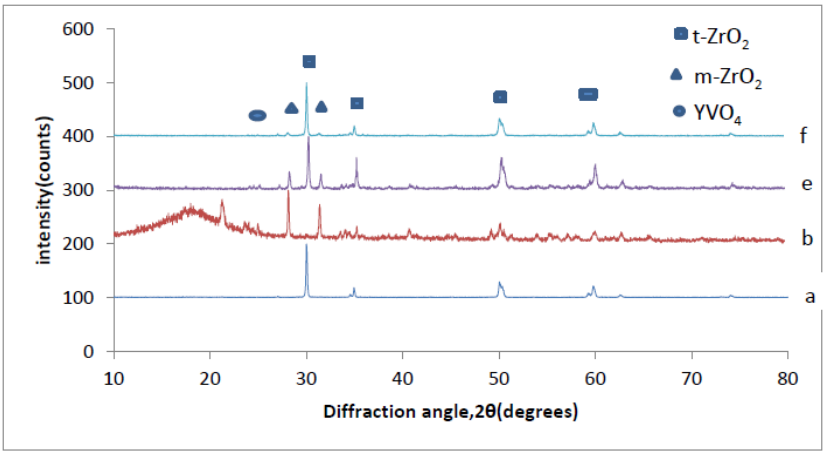

(ii)

Figure 4.44: XRD analysis of APS samples after 100hrs-900^{o}C isothermal heating inhibitive hot corrosion test. (i) CaO-inhibitive test, (ii) MgO-inhibitive test. (a) Sample A, (b) Sample B, (c) Sample E, (d) Sample F, (e) Sample C, (f) Sample D

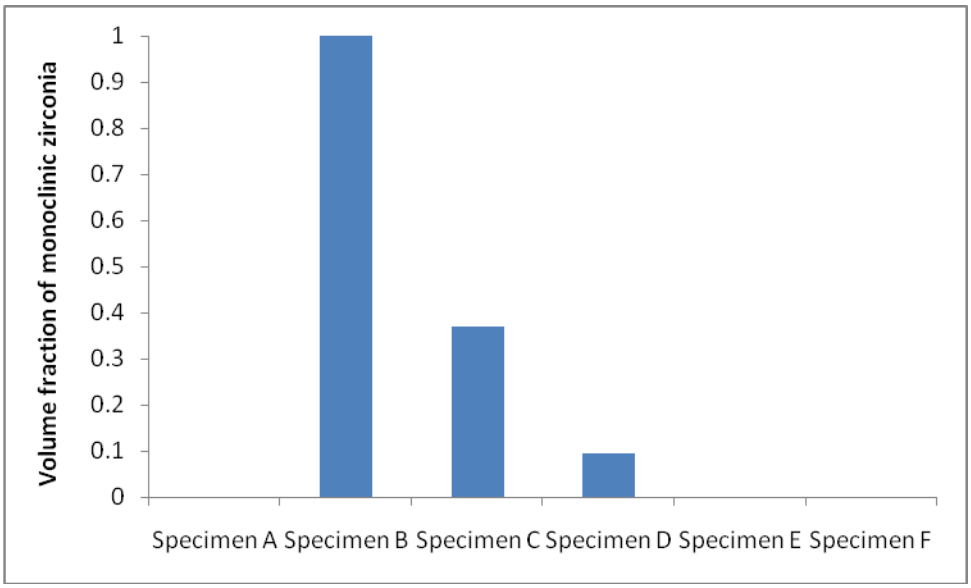

Figure 4.45: Amount of tetragonal zirconia phase transformation in the APS TBCs samples at 100hrs-900^{o}C isothermal heating inhibitive hot corrosion test.

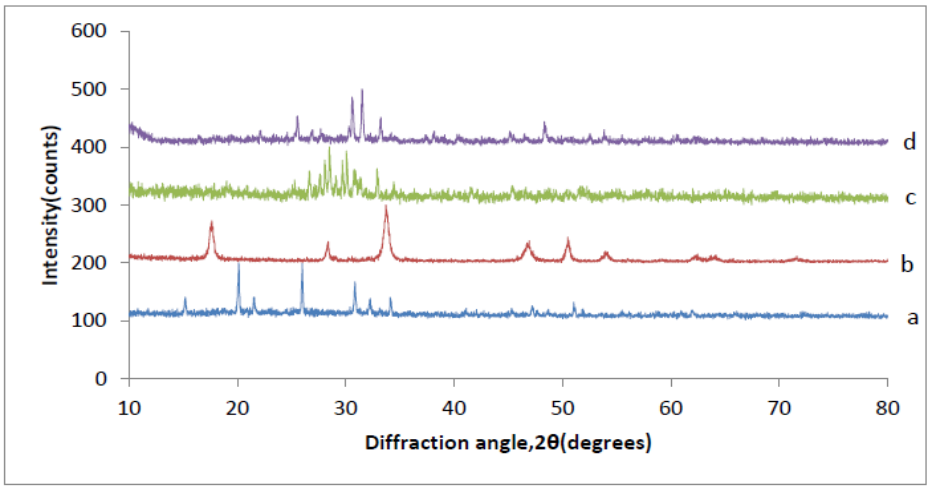

(i)

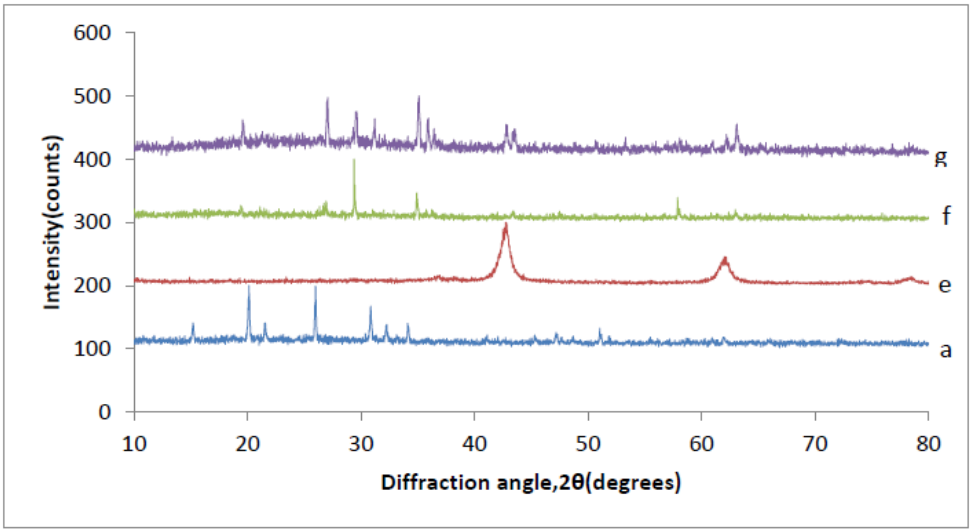

(ii)

Figure 4.46: XRD analysis of as-received powders and slurry powders after inhibitive hot corrosion test. (a) As-received V_2O_5 powder, (b) As received CaO powder, (c) Slurry powder of CaO-V_2O_5 with M_{CaO}/M_{V2O5}=3, (d) Slurry powder of CaO-V_2O_5 with M_{CaO}/M_{V2O5}=5, (e) As receieved MgO powder, (f) Slurry powder of MgO-V_2O_5 with M_{MgO}/M_{V2O5}=3, (g) Slurry powder of MgO-V_2O_5 with M_{MgO}/M_{V2O5}=5

Table 4.7:Inhibition efficiency of using alkaline-earth metal oxides to inhibits vanadium-induced hot corrosion of 8YSZ powder

8YSZ Powder Samples with V_2O_5 concentration (10% wt. 8YSZ)	Inhibition efficiency (%)
Sample with M_{MgO}/M_{V2O5}=1	1.8
Sample with M_{MgO}/M_{V2O5}=2	28.1
Sample with M_{MgO}/M_{V2O5}=3	78.5
Sample with M_{MgO}/M_{V2O5}=5	92.7
Sample with M_{CaO}/M_{V2O5}=1	41.2
Sample with M_{CaO}/M_{V2O5}=2	78.2
Sample with M_{CaO}/M_{V2O5}=3	92.2
Sample with M_{CaO}/M_{V2O5}=5	92.7
Sample with M_{CaO}/M_{V2O5}: M_{MgO}/M_{V2O5} equals 1:1	51.9
Sample with M_{CaO}/M_{V2O5}: M_{MgO}/M_{V2O5} equals 1:2	79.4
Sample with M_{CaO}/M_{V2O5}: M_{MgO}/M_{V2O5} equals 2:1	83.8

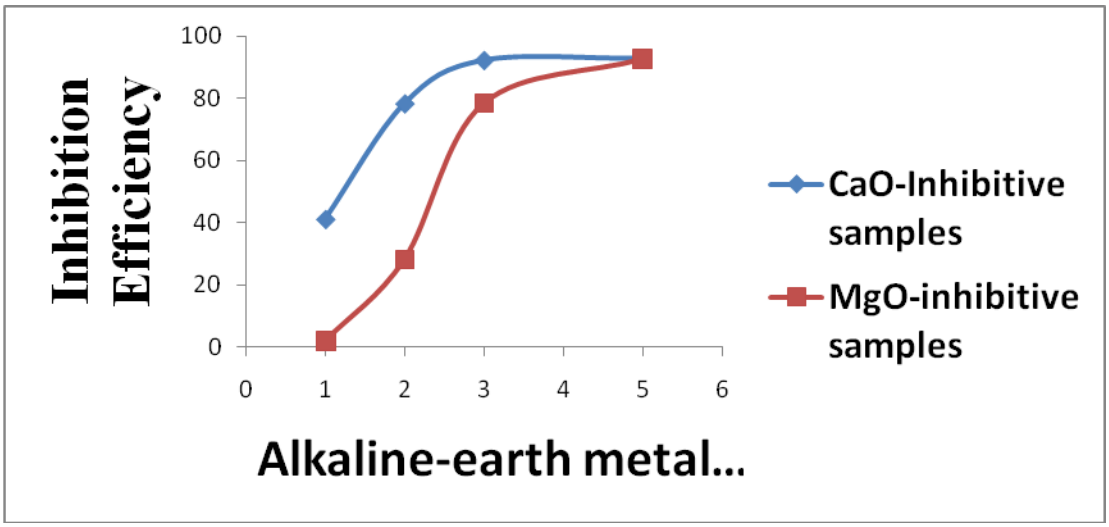

(i)

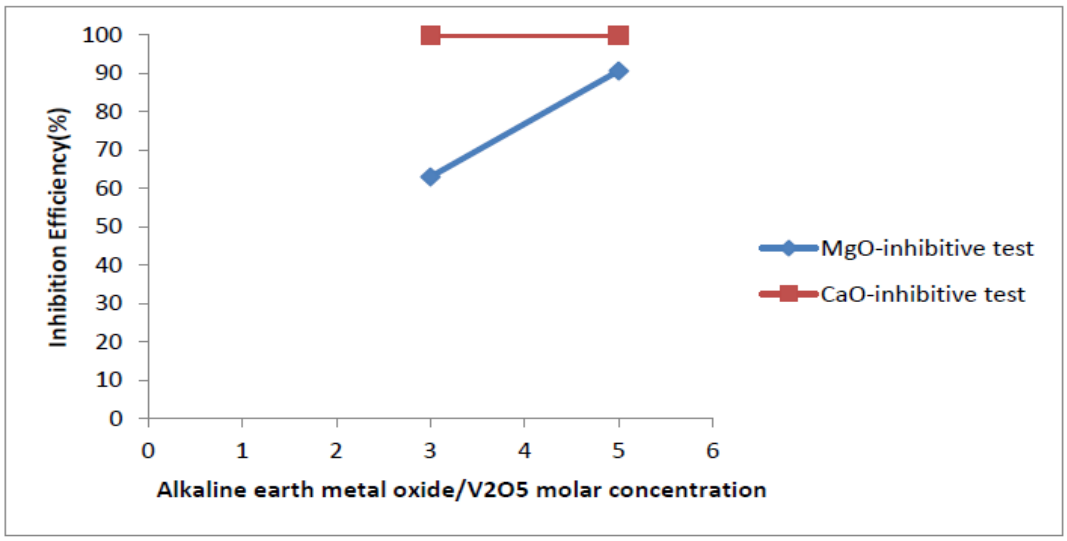

(ii)

Figure 4.47: Comparison of the inhibitive efficiency of alkaline-earth metal oxides in inhibiting vanadium-induced hot corrosion of 8YSZ. (i) Vanadium-induced hot corrosion of 8YSZ powder samples with V_2O_5 concentration (10% wt. 8YSZ), (ii) APS 8YSZ TBC samples

CHAPTER 5

DISCUSSIONS

5.1 The Effect of Isothermal Heating and Cooling

In our study, 2hrs-900^{o}C isothermal heated 8YSZ powder in the absence of V_2O_5 showed the same volume fraction of monoclinic zirconia in the as received 8YSZ powder, laboratory air and furnace cooled samples as shown in Table 5.1. This can be attributed to zirconia phase temperature dependence phenomenon. The presence of yttria stabilizer in the 8YSZ powder stabilized the tetragonal phase of the powder; hence at room temperature which is the final temperature after cooling via furnace and laboratory air showed the same volume fraction of the zirconia phase with that of the as-received powder. The essence of the yttria stabilizer is to stabilize the tetragonal 8YSZ zirconia both at higher temperature and room temperature [29]. This result shows that the degradation of the 8YSZ powder is independent of isothermal heating and cooling, and also effective stabilization of (Y_2O_3) ZrO_2 in the absence of V_2O_5.

Table 5. 1:Comparison of monoclinic zirconia volume fraction of 2hrs-900^{o}C isothermal heated 8YSZ cooled via laboratory air and furnace

Sample	Volume fraction of monoclinic zirconia (%)
As-received 8YSZ powder	3.1
Air cooled 2hrs-900^{o}C Isothermal Heated 8YSZ powder	3.1
Furnace cooled 2hrs-900^{o}C Isothermal Heated 8YSZ powder	3.1

5.2 Vanadium-induced Hot Corrosion of 8YSZ powder

Isothermal hot corrosion reaction of 8YSZ in the presence of V_2O_5 at 900^oC can be rationalized based on Lewis acid mechanism [10, 47]. The mechanism proposes the tendency of a strong base reacting with a strong acid in the presence of other weak acids and bases. V_2O_5 is a strong acid that has great affinity to react with the yttria, a strong base in the stabilized zirconia. Although yttria (Y_2O_3) and zirconia (ZrO_2) are both bases, yttria is of higher basicity [36]; which leads to its accelerated reaction with V_2O_5 to form YVO_4. Figure 5.1 depicts the level of preferential reaction of metal oxides with vanadium compounds based on the degree of basicity and acidity of these compounds. It also suggests the high tendency of Y_2O_3 compared to ZrO_2 in terms of basicity and the tendency of the V_2O_5 to preferentially react with the former compared to the latter. The reaction of the yttria stabilizer with V_2O_5 causes the transformation of the tetragonal zirconia to monoclinic zirconia as it is cooled to room temperature. The essence of the yttria stabilizer is to stabilize the tetragonal 8YSZ zirconia both at higher temperature and room temperature as shown in Figure 1.3. It is also worth of noting that the reaction of yttria stabilizer is due to the molten state of the corrosive vanadium salt at the temperature of hot corrosion test. V_2O_5 melting point is 690^oC [10, 11, 16, 48]. The molten form of the acidic V_2O_5 at 900^oC isothermal heating allows it to react with the yttria stabilizer. This explains the reason why in all the powder samples that have V_2O_5 concentration (2% wt., 5% wt. and 10% wt. of 8YSZ) showed YVO_4 peaks, increased in monoclinic zirconia intensities peaks, decreased in the tetragonal zirconia intensities peaks and transformation from the smooth-face to rough-face powder particles (Figs. 4.3, 4.4 and 4.5). The reaction can be represented as

$$Y_2O_3\,(ZrO_2)_{(s)} + V_2O_{5\,(l)} \longrightarrow 2\,YVO_4 + ZrO_2\,(\text{m-zirconia}) \qquad (5.1)$$

The higher the V_2O_5 concentration the more intense is its reaction with yttria stabilizer. This made the transformation of tetragonal zirconia to monoclinic zirconia more intense in hot corrosion test samples with high vanadium oxide concentration. The increase in rate of transformation of the tetragonal zirconia induced higher volume fraction of the monoclinic zirconia. Thus higher concentrations of V_2O_5 contaminant generated higher volume fraction of monoclinic zirconia phase (Fig. 4.5). This is also shown in Fig. 5.2 where the sample with 2wt.% V_2O_5 shows the least volume fraction as compared to those samples that contain 5wt.% and 10wt.% V_2O_5, respectively. This also explains the reason why we have higher volume fraction of monoclinic zirconia, higher intensity YVO_4 peaks and rough-face spherical powder particles in sample where the V_2O_5 is 10% wt. of 8YSZ as compared to that of 5% wt. of 8YSZ. Fig. 5.2 also shows that the most transformation of the tetragonal zirconia phase occurs within short period of isothermal heating since major transformation occurred within 2hrs isothermal heating for all the samples. The figure portrays negligible differences between monoclinic zirconia volume fractions present after 2hrs and 100hrs isothermal heating in all the samples. The sample with zero concentration of V_2O_5 has the least volume fraction of monoclinic zirconia and higher volume of smooth-face powder particles as compared to other samples (Figs 4.5-4.6).

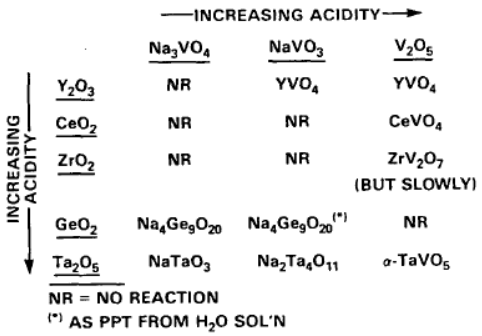

Figure 5.1: Lewis acid-base preferential reactions of compounds [36]

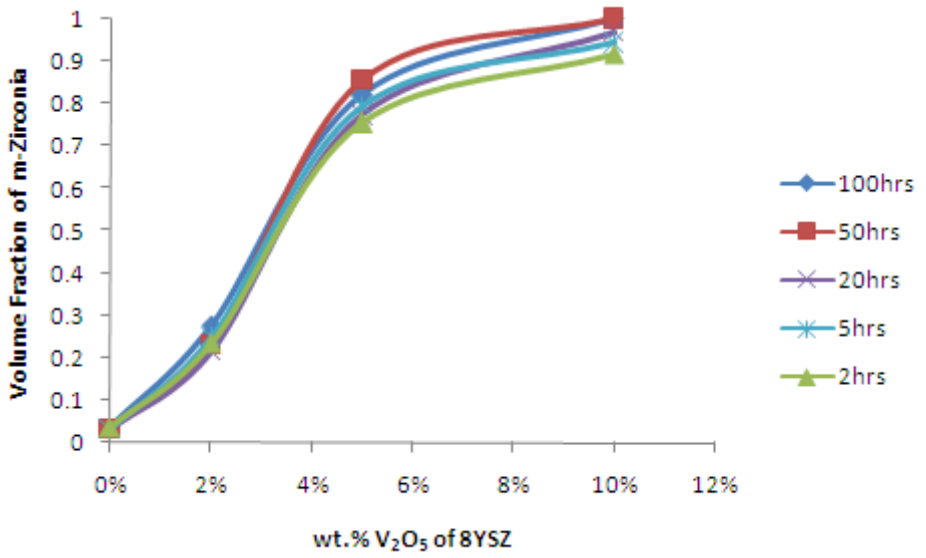

Figure 5.2: Volume fraction of m-ZrO_2 produced in vanadium-induced hot corrosion 8YSZ powder tests as a function of V_2O_5 concentration and time

5.3 MgO-inhibition of Vanadium-induced Hot Corrosion of 8YSZ powder

The presence of MgO in the reacting medium; (8YSZ+10&5wt.%V_2O_5) changed the direction of acid-base reaction based on Lewis acid mechanism. The V_2O_5 particles reacted with the MgO particles and formed magnesium vanadate compounds: MgV_2O_6, $Mg_2V_2O_7$ and $Mg_3V_2O_8$ depending on the molar concentration ratio of the two compounds as shown in the phase diagram, (Fig. 1.11). Magnesium vanadate compounds have different melting points as shown in the phase diagram, (Fig. 1.11) and reproduced in Table 5.2. The use of MgO as inhibitor in the 8YSZ+10 wt.% V_2O_5 sample with M_{MgO}/M_{V2O5}=1 did not produce the desired inhibition effect though it retarded the hot corrosion degradation slightly better compared to MgO-free vanadium-induced hot corrosion sample. This is clearly shown in the magnitude of monoclinic zirconia volume fraction in the two samples, (Fig. 4.12). The reason can be attributed to the formation of MgV_2O_6 from the reaction between MgO and V_2O_5, (Figs. 1.11 and 4.10); which is 100% liquid

phase at the temperature of the hot corrosion test. The molten nature of MgV_2O_6 enabled it to react with the yttria stabilizer to form YVO_4 [10, 11, 16, 48].

Table 5.2:Magnesium vanadate compounds and their melting points

Molar concentration ratio of MgO:V_2O_5	Magnesium Vanadate Compounds	Melting Point	Phase Present and Quantity at 900^oC
1:1	MgV_2O_6	742^oC	Liquid (100%)
2:1	$Mg_2V_2O_7$	980^oC	Liquid (<10%) and Solid (>90%)
3:1	$Mg_3V_2O_8$	1074^oC	Solid (100%)

Thus the sample indicates high volume fraction of monoclinic zirconia, (Fig. 4.12). This also brings about considerable surface roughness to the 8YSZ spherical particles, (Figure 4.13). With increase in molar concentration ratio of MgO-V_2O_5 in the sample to 2; as well as for sample with 8YSZ+5wt.% V_2O_5 of M_{MgO}/M_{V2O5}=2, at 900^oC a solid-liquid phase of $Mg_2V_2O_7$ forms, (Figs. 1.11, 4.10 and 4.18). It showed a better inhibition compared to sample with M_{MgO}/M_{V2O5}=1. The molten phase which was estimated by lever rule to be less than 10% reacted with the yttria stabilizer and caused the formation of YVO_4 and the transformation of the tetragonal zirconia to monoclinic zirconia phase, (Table 5.2, Fig. 4.10 and Fig. 4.18). The solid phase $Mg_2V_2O_7$ didn't take part in the reaction, thus a good inhibition was achieved compared to when entire liquid phase MgV_2O_6 was present. Thus sample of M_{MgO}/M_{V2O5}=2 has lower magnitude of volume fraction of monoclinic zirconia as compared to that of sample with M_{MgO}/M_{V2O5}=1, (Fig. 4.12). The sample also showed lower concentration of the roughened spherical powder particles, (Figs. 4.13 and 4.20). The presence of MgO in the samples with M_{MgO}/M_{V2O5}=3 produced a 100% solid

phase $Mg_3V_2O_8$ at 900^oC as the acid-base reaction product, (Table 5.2). It gave higher inhibition as compared to the earlier mentioned two samples with MgO inhibitor in the vanadium-induced hot corrosion 8YSZ sample, (Figs. 4.12, 4.19 and 4.47). The reason can be linked to the fact that, the solid $Mg_3V_2O_8$ didn't react with yttria stabilizer. Hence the sample showed high concentration of ridge-face spherical tetragonal zirconia powder particles and low volume fraction of monoclinic zirconia phase, (Figs 4.12, 4.13, 4.19 and 4.20). However the traces of YVO_4 after like 50hrs isothermal heating and consequential minute transformation of the zirconia phase, (Fig. 4.11) can be linked to incomplete reaction between the acid and base which took sometime before it manifested in the inhibitive hot corrosion experiment. With increase in M_{MgO}/M_{V2O5} in the sample to 5, it did not only produced 100% solid phase $Mg_3V_2O_8$ but the presence of excess MgO, (Figs. 4.11 and 4.20); made the inhibition of vanadium-induce hot corrosion of the powder sample the most effective, (Table 4.7 and Fig. 4.47). The excess MgO ensured total reaction with the V_2O_5 compound eliminating any possibility of V_2O_5 reacting with Y_2O_3. Thus the sample showed neither YVO_4 nor zirconia transformation during cooling for the entire 100hrs isothermal heating inhibitive test as seen in the XRD spectra, (Figs 4.11 and 4.18). The sample showed the least volume fraction of monoclinic zirconia, almost of the same magnitude with that of the isothermal heated 8YSZ powder and large presence of the ridge-face powder particles, (Figs. 4.12, 4.13, 4.19 and 4.20). In summary, the type of magnesium vanadate compound forming in MgO-inhibitive vanadium-induced hot corrosion 8YSZ sample influenced the vanadium-induced hot corrosion rate, (Fig. 5.3(i)). Fig. 5.5 shows a schematic flowchart of the effectiveness of using MgO to inhibit vanadium-induced hot corrosion of 8YSZ powder.

5.4 CaO-inhibition of Vanadium-induced Hot Corrosion of 8YSZ powder

CaO similar to MgO is an alkaline-earth metal oxide which is of high basicity compared to Y_2O_3 and ZrO_2. The V_2O_5 compound reacts with CaO compound to form various calcium vanadate compounds. The CaO-V_2O_5 phase diagram shown in Fig. 1.12 indicates the formation of various calcium vanadate compounds depending on the molar concentration ratios of the reacting constituents. The phase diagram indicates the formation of CaV_2O_6, $Ca_2V_2O_7$ and $Ca_3V_2O_8$ with CaO-V_2O_5 molar concentration ratios (M_{CaO}/M_{V2O5}) of 1, 2 and 3, respectively. Table 5.3 lists the possible calcium vanadate compounds forming and the melting point of each as well as fraction of the compound existing in the liquid phase at 900^{o}C estimated by lever rule.

Table 5.3:Calcium vanadate compounds and their meltings

Molar concentration ratio of CaO:V_2O_5	Calcium Vanadate Compounds	Melting Point	Phase Present and Quantity at 900^{o}C
1:1	CaV_2O_6	778^{o}C	Liquid (100%)
2:1	$Ca_2V_2O_7$	1015^{o}C	Liquid (<10%) and Solid (>90%)
3:1	$Ca_3V_2O_8$	1380^{o}C	Solid (100%)

The presence of CaO powder in vanadium-induced hot corrosion 8YSZ-V_2O_5 samples with M_{CaO}/M_{V2O5}=1 produced CaV_2O_6 compound which is 100% in the liquid phase at 900^{o}C. The molten state of CaV_2O_6 at 900^{o}C isothermal heating temperature reacted with the yttria stabilizer (Y_2O_3) to form YVO_4 during the test, (Figs 4.23 and 4.31). This led to destabilization of tetragonal zirconia to monoclinic zirconia during cooling of the 8YSZ sample to room temperature as shown in the XRD spectra, (Figs. 4.23 and 4.31). Thus this sample showed

appreciable volume fraction of monoclinic zirconia and rough surface morphology spherical powder particles, (Figs. 4.25, 4.26, 4.32 and 4.33). Although effective inhibition was not achieved in this sample, the presence of CaO retarded the hot corrosion slightly better compared to the un-inhibited vanadium-induced hot corrosion sample, (Figs. 4.25, 4.33 and 4.47). The sample with $M_{CaO}/M_{V2O5}=2$ produced $Ca_2V_2O_7$; a solid-liquid mixture phase at 900^oC as shown in Table 5.3, (Figs. 1.12, 4.23 and 4.31). The formation of $Ca_2V_2O_7$ produced a better inhibitive effect compared to that of sample with $M_{CaO}/M_{V2O5}=1$ based on comparing the volume fractions of monoclinic zirconia of the samples, (Figs. 4.25 and 4.32) and the inhibition efficiency, (Fig. 4.47). The molten phase fraction of $Ca_2V_2O_7$ at 900^oC estimated to be less than 10% reacted with the yttria stabilizer and formed YVO_4 and consequently caused the transformation of the tetragonal zirconia to monoclinic zirconia phase, (Figs. 4.23 and 4.31). The solid phase $Ca_2V_2O_7$ didn't take part in the reaction, thus giving the sample better inhibition compared to sample where entire liquid phase CaV_2O_6 was formed. This led to lower concentration of rough surface spherical particles when compared to that of vanadium-induced and $M_{CaO}/M_{V2O5}=1$ samples, (Figs. 4.26 and 4.33). The sample with $M_{CaO}/M_{V2O5}=3$ is expected to form $Ca_3V_2O_8$ from acid-base reaction. $Ca_3V_2O_8$ is 100% in solid phase at 900^oC as inferred from the phase diagram, (Fig 1.12). The elimination of molten salt gave rise to effective inhibition, (Fig. 4.47) accompanied with lower volume fraction of monoclinic zirconia, (Figs 4.25 and 4.32) and the smooth surfaces of powder particles similar to the as-received 8YSZ powder particles, (Figs 4.26 and 4.33).

Increasing the amount of added inhibitor to $M_{CaO}/M_{V2O5}=5$, produced 100% solid phase of $Ca_3V_2O_8$ and resulted in very effective inhibition, (Table. 4.7 and Fig. 4.47). The excess CaO also ensured total reaction with the V_2O_5 compound and hence least volume fraction of monoclinic zirconia and high concentration of smooth particles, (Figs 4.25 and 4.26). Similar to

MgO, the type of calcium vanadate compound forming depending on the CaO/V_2O_5 molar concentration in a CaO-inhibitive vanadium-induced hot corrosion 8YSZ sample influenced the hot corrosion rate, (Fig. 5.3(ii)). Fig. 5.5 also shows a schematic flowchart of the effectiveness of using CaO to mitigate vanadium-induced hot corrosion of 8YSZ powder.

5.5 CaO-MgO-inhibition of Vanadium-induced Hot Corrosion of 8YSZ powder

Mixture of CaO and MgO was prepared as a mixed inhibitor for vanadium-induced hot corrosion of 8YSZ powder. The mixed inhibitor appears to react with V_2O_5 and formed $CaMgV_2O_7$, a vanadate compound with melting point of 788^oC [PDF card number 01-077-0964]. The mixed inhibitor sample with $M_{CaO}/M_{V2O5}=1$ and $M_{MgO}/M_{V2O5}=1$ formed $CaMgV_2O_7$ according to reaction 5.2 and Fig. 4.36. $CaMgV_2O_7$ is expected to be 100% molten phase at 900^oC. The molten $CaMgV_2O_7$ reacted with yttria stabilizer and formed YVO_4, (Fig. 4.36). This led to appreciable volume fraction of monoclinic zirconia and rough surface particles in the sample, (Figs. 4.37 and 4.39). It is worth noting that $CaMgV_2O_7$ caused a better inhibition compared to CaV_2O_6 and MgV_2O_6, (Fig. 4.38). Firstly, $CaMgV_2O_7$ has the highest melting point out of the three compounds which determines the effectiveness of a compound in inhibiting vanadium-induced hot corrosion. The higher the melting point of the vanadate compound the better is the inhibition effect. Although the mixed inhibitor produced a better inhibition when compared to the use of MgO of the same molar concentration to the vanadium oxide ($M_{MgO}/M_{V2O5}=2$), the inhibition efficiency is however lower to that of using CaO alone of the same molar concentration to V_2O_5 as inhibitor, (Fig. 4.38). The sample with $M_{CaO}/M_{V2O5}=1$ and $M_{MgO}/M_{V2O5}=2$ aside forming the $CaMgV_2O_7$ compound; has excess MgO that further retarded the hot corrosion effect as shown in reaction 5.3. This sample produced better inhibition

compared to the aforementioned CaO-MgO mixed inhibitive sample based on the presence of the excess MgO, though the molten $CaMgV_2O_7$ still induced the hot corrosion products of YVO_4 and zirconia transformation, (Fig. 4.36). This is shown in the volume fraction of monoclinic zirconia and volume of rough surface particles in this sample, (Figs. 4.37 and 4.41). The same trend occurred for sample of $M_{CaO}/M_{V2O5}=2$ and $M_{MgO}/M_{V2O5}=1$, $CaMgV_2O_7$ and CaO formed as shown in reaction 5.4 and Fig. 4.36. The excess CaO further retarded the rate of hot corrosion of the sample. However at 100hrs, this sample showed lower volume fraction of monoclinic zirconia compared to the mixed inhibitive sample with excess MgO, (Figs. 4.37 and 4.38). This can be attributed to the high reactivity of CaO with V_2O_5 and its ability to form high melting point vanadate compounds when compared to MgO of the same molar concentration ratio with V_2O_5. CaO is of high basicity compared to MgO inferring from the positions of calcium and magnesium elements in the periodic table and their pKa values, [49]. This is also the reason why the CaO-inhibitive samples showed better inhibition compared to the MgO-inhibitive samples of the same molar concentration to V_2O_5, (Fig. 4.47).

$$CaO + MgO + V_2O_5 \longrightarrow CaMgV_2O_7 \qquad (5.2)$$

$$CaO + 2MgO + V_2O_5 \longrightarrow CaMgV_2O_7 + MgO \qquad (5.3)$$

$$2CaO + MgO + V_2O_5 \longrightarrow CaMgV_2O_7 + CaO \qquad (5.4)$$

The mixed-inhibitive samples produced a better inhibition compared to MgO-inhibitive samples of the same molar ratio to vanadium oxide but lesser when compared to that of CaO-inhibitive samples. Fig. 5.4 shows XRD comparison of the mixed-inhibitive samples.

5.6 APS Specimen

Sample A like the isothermal heated 8YSZ powder showed neither formation of YVO_4 nor tetragonal zirconia transformation due to absence of the molten acidic V_2O_5 to elicit such hot corrosion products. Thus after 100hrs of isothermal heating, it showed zero magnitude monoclinic zirconia volume fraction and absence of monoclinic zirconia peaks in the XRD spectrum, (Fig. 4.44 and 4.45). Sample B; the vanadium-induced hot corrosion sample exihibited tetragonal zirconia transformation due to reaction of the yttria stabilizer in the topcoat with the molten V_2O_5 based on Lewis acid mechanism as shown in reaction 5.1. The transformation of tetragonal zirconia to monoclinic zirconia during cooling caused the spallation of the topcoat, (Fig. 4.44). The transformation of tetragonal zirconia to monoclinic zirconia is accompanied with 3-5% increase in volume of the zirconia phase [8]; hence the stress which arose initiated the degradation and spallation of the topcoat. Sample C which is the specimen that has the slurry mixture of MgO and V_2O_5 (M_{MgO}/M_{V2O5}=3), though showed the formation of 100% solid phase $Mg_3V_2O_8$, (Fig. 4.46); but the presence of YVO_4 and approximately 40% monoclinic volume fraction could have been due to incomplete reaction of MgO with V_2O_5, (Fig. 4.44). This led to little degradation at the edges of the topcoat, (Figs. 4.43 and 4.45). Sample D though showed minute intensity YVO_4 peaks and minute volume fraction of monoclinic zirconia but no obvious degradation like that of sample C, (Figs 4.43-4.45). The same reasons applies, 100% solid phase $Mg_3V_2O_8$ was formed from the slurry of V_2O_5 and MgO during the inhibitive test but the presence of minute V_2O_5 due to incomplete reaction induced those hot corrosion features, (Fig. 4.46). The presence of more MgO in slurry of sample D compared to that of specimen C gave it better inhibition in terms of reduced amount of YVO_4 and zirconia transformation, (Fig. 4.44). Thus it showed lower volume fraction of monoclinic zirconia out of the two samples, (Fig. 4.45).

Samples E and F like sample A showed the same trend; neither YVO_4 growth nor zirconia transformation due to the absence of molten reactive salt, (Figs. 4.44 and 4.46). The slurries mixture of CaO and V_2O_5 (M_{CaO}/M_{V2O5}=3 and 5, respectively) on the specimens reacted together and formed 100% solid phase $Ca_3V_2O_8$ as shown in the XRD spectra of the solid slurries after the test, (Fig. 4.46). The solid calcium vanadate compound caused neither the growth of YVO_4 nor consequential tetragonal zirconia transformation due to its 100% solid phase at 900^oC, (Table 5.3 and Fig. 1.12). Thus these samples; sample E and F also showed zero volume fraction of the monoclinic zirconia phase, (Fig. 4.45). The high inhibition efficiency displayed by the CaO-inhibitive samples compared to the MgO-inhibitive samples, (4.47) can also be linked to the higher reactivity of CaO with V_2O_5 compared to MgO and formation of higher melting point calcium vanadate compound. Table 5.4 gives a summary of hot corrosion and inhibitive hot corrosion of the coated samples.

Table 5.4:Physical appearance of 8YSZ-APS of the coated samples at 100hrs

Samples	Slurries on the coated samples	Physical Appearance at 100hrs-900^{o}C isothermal heating
Sample A	N/A	Stable 8YSZ-APS
Sample B	V_2O_5	Spallation of 8YSZ-APS
Sample C	MgO and V_2O_5 (M_{MgO}/M_{V2O5}=3)	Little degradation of the 8YSZ-APS
Sample D	MgO and V_2O_5 (M_{MgO}/M_{V2O5}=5)	Stable 8YSZ-APS
Sample E	CaO and V_2O_5 (M_{CaO}/M_{V2O5}=3)	Stable 8YSZ-APS
Sample F	CaO and V_2O_5 (M_{CaO}/M_{V2O5}=5)	Stable 8YSZ-APS

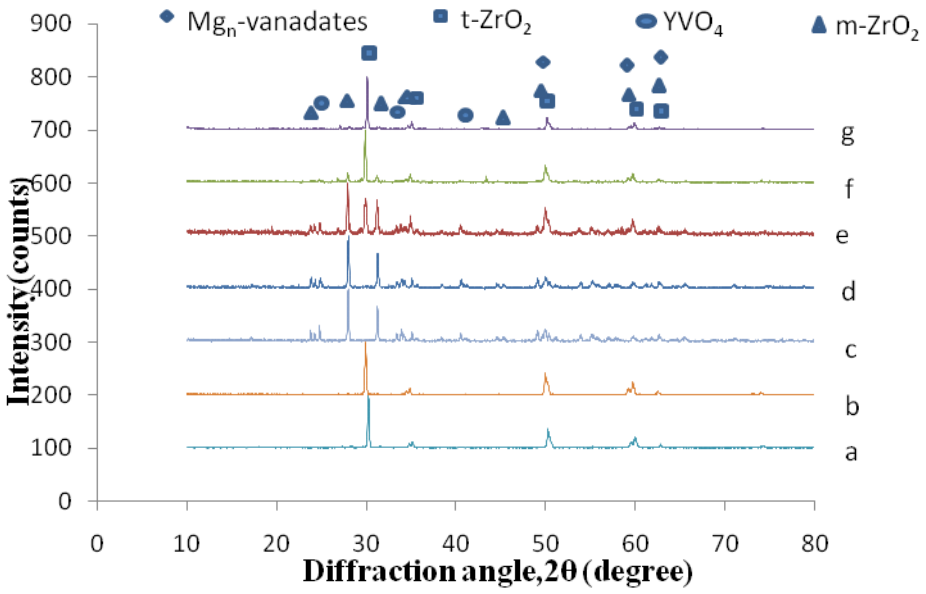

(i)

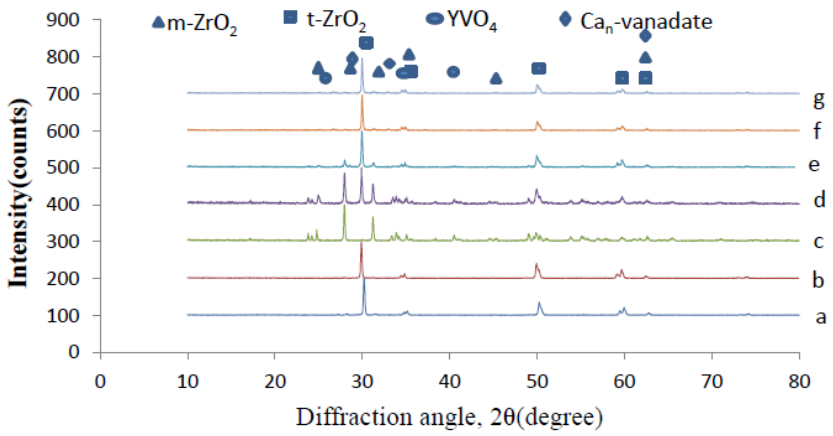

(ii)

Figure 5.3: (i) MgO-inhibitive experiment , (ii) CaO-inhbitive experiment. (a) As-received 8YSZ powder, (b) Isothermal heated 8YSZ powder, (c) Vanadium-induced hot corrosion sample, (d) Sample of $M_{(\text{alkaline earth metal oxide/vanadium oxide})}$=1, (e) Sample of $M_{(\text{alkaline earth metal oxide/vanadium oxide})}$=2, (f) Sample of $M_{(\text{alkaline earth metal oxide/vanadium oxide})}$=3, (g) Sample of $M_{(\text{alkaline earth metal oxide/vanadium oxide})}$=5.

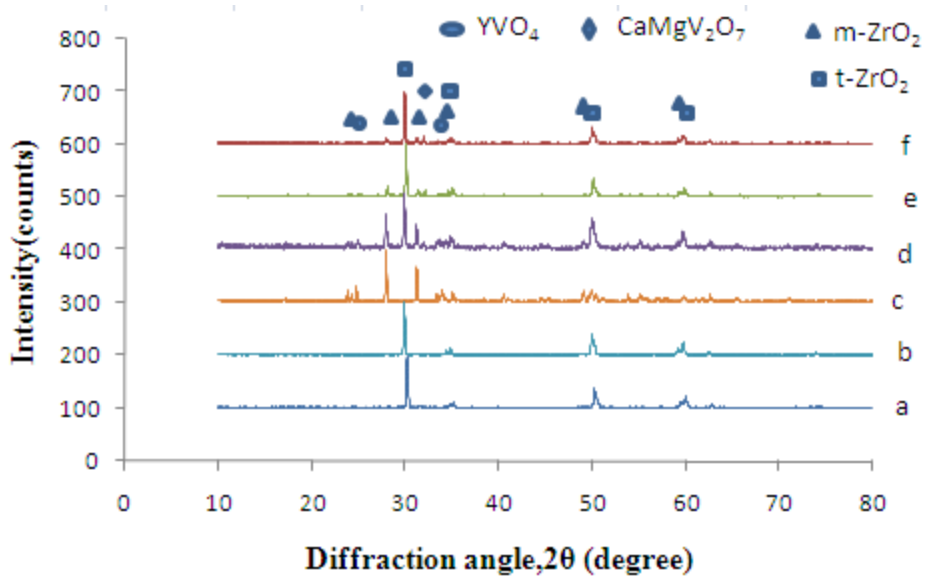

Figure 5.4: CaO-MgO inhibitive experiment (a) As-received 8YSZ, (b) Isothermal heated 8YSZ, (c) Vanadium-induced hot corrosion 8YSZ, (d) Sample with M_{CaO}/M_{V2O5} : M_{MgO}/M_{V2O5} =1:1, (e) Sample with M_{CaO}/M_{V2O5} : M_{MgO}/M_{V2O5} =1:2, (f) Sample with M_{CaO}/M_{V2O5} : M_{MgO}/M_{V2O5} =2:1

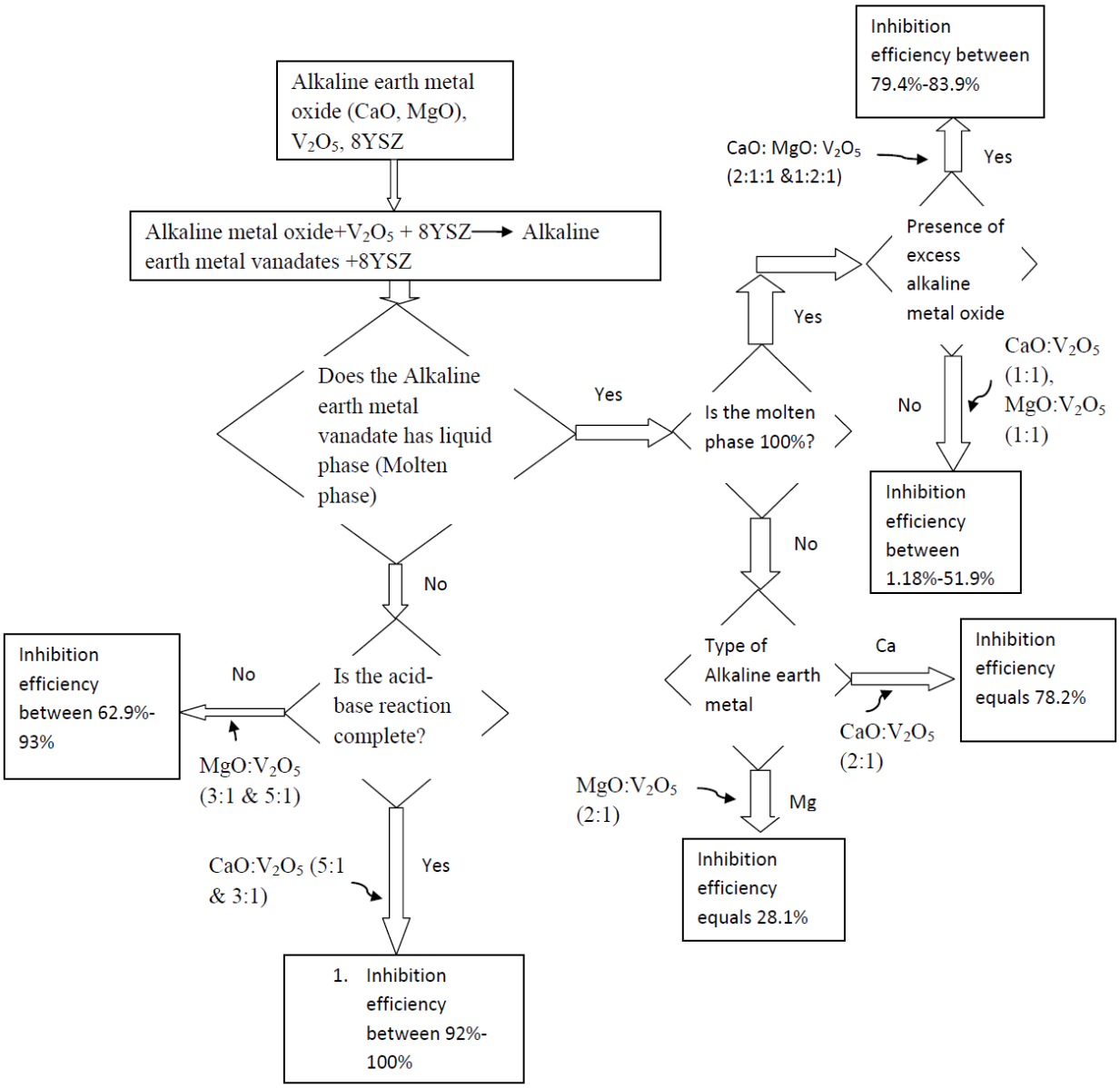

Figure 5.5: Flow chart on the use of alkaline-earth metal oxides to inhibit vanadium-induced hot corrosion of 8YSZ

CHAPTER 6

CONCLUSIONS

Based on the experimental results using 8wt.% Y_2O_3-stabilized ZrO_2 (8YSZ) powder and air plasma coated 8YSZ (8YSZ-APS) samples, the following conclusions can be drawn:

1. The addition of vanadium oxide in the amount between 2-10wt.% of 8YSZ powder caused hot corrosion degradation of the 8YSZ powder with the formation of YVO_4 and transformation of tetragonal zirconia to monoclinic zirconia phase.

2. The higher the concentration of the vanadium oxide the higher was the extent of degradation in the 8YSZ powder samples.

3. The extent of molten vanadate-induced hot corrosion of the 8YSZ powder was a rapid process and reached full damage within 1-2 hours and further degradation was sluggish.

4. The addition of MgO to 8YSZ+10wt.% V_2O_5 and 8YSZ+5wt.% V_2O_5 mixture powder samples, respectively inhibited vanadium-induced hot corrosion. Higher molar concentration ratio of MgO/V_2O_5 generated higher effective inhibition of vanadium-induced hot corrosion of 8YSZ powders. MgO/V_2O_5 molar concentration ratio of 5 showed effective inhibition.

5. The incorporation of CaO to 8YSZ+10wt.% V_2O_5 and 8YSZ+2wt.% V_2O_5 mixture powder samples, respectively inhibited vanadium-induced hot corrosion. Higher molar concentration ratio of CaO/V_2O_5 generated higher inhibition of vanadium-induced hot corrosion of 8YSZ powders. CaO/V_2O_5 molar concentration ratios of 3 and 5 showed effective inhibition.

6. Spraying 8YSZ-APS coated samples with slurry of V_2O_5 solution in the concentration of 20mg/cm^2 caused degradation of the 8YSZ-APS with formation of YVO_4, transformation of the tetragonal zirconia to monoclinic zirconia phase and full spallation of the 8YSZ-APS after 100 h isothermal heating at 900^{o}C.

7. Slurry mixture of MgO+V_2O_5 with MgO/V_2O_5 molar concentration ratios of 3 and 5 sprayed on 8YSZ-APS coated samples in the concentration range of 70-100 mg/cm^2, mitigated vanadium-induced hot corrosion of 8YSZ-APS as compared to the un-inhibited samples after 100 h of isothermal heating at 900^{o}C.

8. Slurry mixture of CaO+V_2O_5 with CaO/V_2O_5 molar concentration ratios of 3 and 5 sprayed on 8YSZ-APS coated samples in the concentration range of 70-100 mg/cm^2, inhibited vanadium-induced hot corrosion of 8YSZ-APS as compared to the un-inhibited samples after 100 h of isothermal heating at 900^{o}C.

9. The use of CaO showed better inhibition effect when compared to MgO of the same molar concentration ratio to V_2O_5 in inhibiting vanadium-induced hot corrosion of 8YSZ powder and 8YSZ-APS.

10. Vanadium-induced hot corrosion of 8YSZ powder and 8YSZ-APS; and its inhibition with MgO and CaO at 900^{o}C isothermal heating is strongly dependent on the fraction of molten salt present and the acidity of the molten salt (Lewis acid mechanism).

REFERENCES

1. Birks, N., Meier, G.H. and Pettit, F.S., *Introduction to the high temperature oxidation of metals*. Cambridge University Press, 2006.
2. Khanna, A.S., *Introduction to high temperature oxidation and corrosion*. ASM International, 2002.
3. Roberge, P., *Corrosion engineering: principles and practice*. McGraw-Hill Professional, 2008.
4. Tool, I.-u.h., *Advance Corrosion Lecture Note (ME 575).* King Fahd University of Petroleum and Minerals, Saudi-Arabia, 2012
5. Bacos, M.P., Dorvaux, J.M., Lavigne, O., Mevrel, R.,Poulain, M., Rio C. and Vidal-Setif, M.H., *Performance and Degradation Mechanisms of Thermal Barrier Coatings for Turbine Blades: a Review of Onera Activities.* Aerospace Lab: The ONERA Journal, 2011.
6. Habibi, M.H., Wang, L. and Guo, S.M., *Evolution of hot corrosion resistance of YSZ, $Gd_2Zr_2O_7$, and $Gd_2Zr_2O_7$+YSZ composite thermal barrier coatings in $Na_2SO_4+V_2O_5$ at 1050°C.* Journal of the European Ceramic Society. 2012, **32**(8): p. 1635-1642.
7. Padture, N.P., Gell, M., and Jordan, E.H., *Thermal barrier coatings for gas-turbine engine applications.* Science, 2002, **296**(5566): p. 280-284.
8. Khalid, A. and Gasem, Z.M., *Effect of Vanadium Contaminated Fuel on Bond Coat and Bond Coat/Top Coat Interface of Thermal Barrier Coatings.* Applied Mechanics and Materials. 2011, **110**: p. 886-891.

9. Afrasiabi, A., Saremi, M. and Kobayashi, A., *A comparative study on hot corrosion resistance of three types of thermal barrier coatings: YSZ, YSZ+ Al_2O_3 and YSZ/Al_2O_3.* Materials Science and Engineering, 2008, **478**(1): p. 264-269.

10. Chen, Z., Speakman, S., Howe J., Wang, H., Porter, W. and Trice, R., *Investigation of reactions between vanadium oxide and plasma-sprayed yttria-stabilized zirconia coatings.* Journal of the European Ceramic Society, 2009, **29**(8): p. 1403-1411.

11. Chen, Z., Mabon, J., Wen, J. and Trice, R., *Degradation of plasma-sprayed yttria-stabilized zirconia coatings via ingress of vanadium oxide.* Journal of the European Ceramic Society, 2009, **29**(9): p. 1647-1656.

12. Lai, G.Y., *High-temperature corrosion and materials applications*. ASM International, 2007.

13. Jones, R.L., *Some aspects of the hot corrosion of thermal barrier coatings.* Journal of Thermal Spray Technology, 1997, **6**(1): p. 77-84.

14. Eliaz, N., G. Shemesh, and R.M. Latanision, *Hot corrosion in gas turbine components.* Engineering Failure Analysis, 2002, **9**(1): p. 31-43.

15. Rocca, E., Aranda, L., Moliere, M. and Steinmetz, P., *Nickel oxide as a new inhibitor of vanadium-induced hot corrosion of superalloys comparison to MgO-based inhibitor.* Journal of Materials Chemistry, 2002, **12**(12): p. 3766-3772.

16. Mohan, P., Yuan, P., Patterson, T., Desai, V.H. and Sohn, Y.H., *Degradation of Yttria□Stabilized Zirconia Thermal Barrier Coatings by Vanadium Pentoxide, Phosphorous Pentoxide, and Sodium Sulfate.* Journal of the American Ceramic Society, 2007, **90**(11): p. 3601-3607.

17. Rhys-Jones, T.N., Nicholls, J.R. and Hancock, P., *Effects of SO_2/SO_2 on the efficiency with which MgO inhibits vanadic corrosion in residual fuel fired gas turbines.* Corrosion Science, 1983, **23**(2): p. 139-149.

18. Singh, H., Gitanjaly, Singh, S. and Prakash, S., *High temperature corrosion behavior of some Fe,Co and Ni-base superalloys in the presence of Y_2O_3 as inhibitors.* Applied Surface Science, 2009.

19. Jones, R.E., *Corrosion Inhibition in High Temperature Environment*. D.O.T.N.W. DC, Editor, 1993.

20. Jones, R.L., *Scandia-stabilized zirconia for resistance to molten vanadate-sulfate corrosion.* Surface and Coatings Technology, 1989, **39**: p. 89-96.

21. Nakahira, H., Harada, Y., Mifune, N. and Doi, T., *Hot Corrosion Behavior of Plasma Sprayed Thermal Barrier Coatings and Acoustic Emission Response to Corrosion Monitoring.* Journal of the Society of Materials Science, Japan(Japan), 1991, **40**(455): p. 989-995.

22. Scott, H.G., *Phase relationships in the zirconia-yttria system.* Journal of Materials Science,1975, **10**(9): p. 1527-1535.

23. Mohan, P., *Environmental degradation of oxidation resistant and thermal barrier coatings for fuel-flexible gas turbine applications*. NASA, 2010.

24. Yugeswaran, S., Kobayashi, A. and Ananthapadmanabhan, P.V., *Hot corrosion behaviors of gas tunnel type plasma sprayed $La_2Zr_2O_7$ thermal barrier coatings.* Journal of the European Ceramic Society. 2012, **32**(4): p. 823-834.

25. Ahmaniemi, S., Tuominen, J., vuoristo, P. and Mantyla, T., *Sealing procedures for thick thermal barrier coatings.* Journal of Thermal Spray Technology, 2002, **11**(3): p. 320-332.

26. Fan, X., *The Fates of Vanadium and Sulfur Introduced with Petcoke to Lime Kilns*. University of Toronto, 2010.

27. Kondos, K.G., *X-Ray Diffraction and Electron Microscope Studies of Yttria Stabilized Zirconia (YSZ) Ceramic Coatings Exposed to Vanadia*. DTIC Document, 1992.

28. Clark, G.M. and Morley, R., *A study of the MgO-V_2O_5 system.* Journal of Solid State Chemistry, 1976, **16**(3): p. 429-435.

29. Miyauchi, A. and Okabe, T.H., *Production of Metallic Vanadium by Preform Reduction Process.* Materials Transactions. 2010, **51**(6): p. 1102-1108.

30. Said, A.A. and Abd El-Wahab, M.M.M., *Structures accompanying the solid-solid interactions in the V_2O_5-MgO system.* Thermochimica acta, 1995, **249**: p. 313-323.

31. Raghavan, S. and Mayo, M.J., *The hot corrosion resistance of 20 mol% $YTaO_4$ stabilized tetragonal zirconia and 14 mol% Ta_2O_5 stabilized orthorhombic zirconia for thermal barrier coating applications.* Surface & Coatings Technology, 2002, **160**(2-3): p. 187-196.

32. Jones, R.L., *Thermogravimetric Study of the 800°C Reaction of Zirconia Stabilizing Oxides with SO_3-$NaVO_3$.* Journal of the Electrochemical Society, 1992, **139**(10): p. 2794-2799.

33. Park, S.Y., Kim, J.H., Kim, M.C., Song, H.S. and Park, C.G., *Microscopic observation of degradation behavior in yttria and ceria stabilized zirconia thermal barrier coatings under hot corrosion.* Surface and Coatings Technology, 2005, **190**(2): p. 357-365.

34. Muqtader, S.A., and Sidhu, R.K.., *Destabilization behaviour of ceria-stabilized tetragonal zirconia polycrystals by sodium sulphate and vanadium oxide melts.* Journal of materials science letters, 1993, **12**(11): p. 831-833.

35. Ahmadi-Pidani, R., Shoja-Razavi, R., Mozafarinia, R. and Jamali, H., *Evaluation of Hot Corrosion Behavior of Plasma Sprayed Ceria and Yttria Stabilized Zirconia Thermal Barrier Coatings in the Presence of $Na_2SO_4+V_2O_5$ Molten Salt.* Ceramics International, 2012.

36. Jones, R.L., *Experiences in Seeking Stabilizers for Zirconia Having Hot Corrosion-Resistance and High Temperature Tetragonal (t') Stability*. DTIC Document, 1996.

37. Li, S., Liu, Z.G. and Ouyang, J.H., *Hot corrosion behaviour of $Yb_2Zr_2O_7$ ceramic coated with V_2O_5 at temperatures of 600-800°C in air.* Corrosion Science. 2010, **52**(10): p. 3568-3572.

38. Chen, X., Zhao, Y., Gu, L., Zou, B., Wang, Y. and Cao, X., *Hot corrosion behaviour of plasma sprayed YSZ/$LaMgAl_{11}O_{19}$ composite coatings in molten sulfate-vanadate salt.* Corrosion Science. 2011, **53**(6): p. 2335-2343.

39. Daroonparvar, M., Yajid, M.A.M., Noordin, M.Y. and Hussain, M.S., *The role of nanostructured Al_2O_3 layer in reduction of hot corrosion products in normal YSZ layer.* Journal of Nanomaterial, 2013.

40. Wu, N., Chen, Z. and Mao, S.X., *Hot Corrosion Mechanism of Composite Alumina/Yttria□Stabilized Zirconia Coating in Molten Sulfate-Vanadate Salt.* Journal of the American Ceramic Society, 2005, **88**(3): p. 675-682.

41. Ramachandra, C., Lee, K.N. and Tewari, S.N., *Durability of TBCs with a surface environmental barrier layer under thermal cycling in air and in molten salt.* Surface and Coatings Technology, 2003, **172**(2): p. 150-157.

42. Batista, C., Portinha, A., Ribeiro, R.M., Teixeira, V. and Oliveira, R.C., *Evaluation of laser-glazed plasma-sprayed thermal barrier coatings under high temperature exposure to molten salts.* Surface and Coatings Technology, 2006, **200**(24): p. 6783-6791.

43. Barbooti, M.M., Al-Niaimi, S. and Al-Sultani, K.F., *The inhibitive action of magnesium hydroxide on hot ash corrosion of stainless steel in a kerosine fired furnace*.Diyala journal of Engineering Science,2010.

44. Barbooti, M.M., Al-Niaimi, S.A. and Al-Sultani, K.F., *Dynamic studies on the inhibitive action of magnesium stearate on hot corrosion in a kerosene fired Furnace*.JMES,2012.

45. Chassagneux, E. and Thomas, G., *Studies on V_2O_5 induced hot corrosion.* Materials chemistry and physics, 1987, **17**(3): p. 273-284.

46. Matta, J., Lamonier, J.F., Abi-Aad, E., Zhilinskaya, A. and Aboukais, A., *Transformation of tetragonal zirconia phase to monoclinic phase in the presence of Fe^{3+} ions as probes: an EPR study.* PCCP, 1999, **1**(21): p. 4975-4980.

47. Jones, R.L. and Williams, C.E., *Hot corrosion studies of zirconia ceramics.* Surface and Coatings Technology, 1987. **32**(1): p. 349-358.

48. Mohan, P., Petterson, A., Yao, B. and Sohn, Y., *Degradation of thermal barrier coatings by fuel impurities and CMAS: thermochemical interactions and mitigation approaches.* Journal of Thermal Spray Technology, 2010, **19**(1-2): p. 156-167.

49 Encyclopedia, http://en.wikipedia.org/wiki/

VITAE

Name: Gbadamosi, Aliyu Arisekola

Date of Birth: 30th March, 1980

Nationality: Nigeria

Permanenet address: 26, Niyi Oloyede Str., Alakia-Isebo, Ibadan, Oyo-State, Nigeria

Telephone: +2348065378979, +966532358096

Email Address: arisebadmus80@yahoo.com

Educational Qualification: 1. BSc. Mechanical Engineering (2006),

Obafemi Awolowo Univeristy, Ile-Ife, Nigeria.

2. National Diploma-Mechanical Engineering (2000)

The Polytechnic Ibadan, Oyo-State, Nigeria

Workshops: 1. 10th Workshop on Clean Water and Clean Energy. June, 2013 (Member of KFUM Research Group working with MIT Group on Hot Corrosion in Gas Turbine Engines)

2. 9th Workshop on Clean Water and Clean Energy. January, 2013 (Member of KFUM Research Group working with MIT Group on Hot Corrosion in Gas Turbine Engines)